UNIVERSITÀ
DEGLI STUDI
DI PADOVA

UNIVERSITY OF PADOVA

DEPARTMENT OF CHEMICAL SCIENCES

DOCTORAL SCHOOL IN MOLECULAR SCIENCES

PHARMACEUTICAL SCIENCES CURRICULUM

XXXII CYCLE

TARGETING DENDRITIC CELLS WITH MANNOSYLATED CATIONIC GLYCOPOLYMERS FOR NUCLEIC ACID-MEDIATED CANCER IMMUNOTHERAPY

School Coordinator: Ch.mo Prof. Leonard Jan Prins

Supervisor: Ch.mo Prof. Stefano Salmaso

Co-supervisor: Dr. Francesca Mastrotto

Ph.D. Student: Federica Bellato

UNIVERSITÀ
DEGLI STUDI
DI PADOVA

UNIVERSITA' DEGLI STUDI DI PADOVA

DIPARTIMENTO DI SCIENZE CHIMICHE

CORSO DI DOTTORATO DI RICERCA IN SCIENZE MOLECOLARI
CURRICULUM SCIENZE FARMACEUTICHE
XXXII CICLO

GLICOPOLIMERI CATIONICI MANNOSILATI DIREZIONATI ALLE CELLULE DENDRITICHE PER L'IMMUNOTERAPIA ANTICANCRO A BASE DI ACIDI NUCLEICI

Coordinatore: Ch.mo Prof. Leonard Jan Prins

Supervisore: Ch.mo Prof. Stefano Salmaso

Co-supervisore: Dott.ssa Francesca Mastrotto

Dottorando: Federica Bellato

Alla mia famiglia

Look in the air 'n catch that boomerang
can't fall anywhere else but in your own hand.
(Elisa)

List of content

ABBREVIATIONS

ACK	Ammonium-chloride-potassium buffer
Agm	Agmatine monomer, agmatine unit
APC	Antigen Presenting Cell
Ar	Argon
BF_3Et_2O	Boron trifluoride diethyl etherate
But	Butyl monomer, butyl unit
$CHCl_3$	Chloroform
CH_3OH	Methanol
CHO	Wild type Chinese Hamster Ovary cell
CHO-MR^+	Mannose receptor expressing Chinese Hamster Ovary cell
CO_2	Carbon Dioxide
CTA	Chain Transfer Agent
CTLD	C-type lectin-like domain
Cy-3, Cy-5	Cyanine-3, Cyanine-5
Đ	Polydispersity Index
D_2O	Deuterium oxide
Da	Dalton
DAPI	4',6-diamino-2-phenylindole
DC	Dendritic cell
DC2.4	Immortalized murine Dendritic Cell Line DC2.4
DCM	Dichloromethane
DDS	Drug Delivery System
DI water	Deionized water
DLS	Dynamic Light Scattering
DMEM	Dulbecco's Modified Eagle Medium
DMSO	Dimethyl sulfoxide
DMSO-d_6	Hexadeuterodimethyl sulfoxide

DP	Degree of Polymerization
EDTA	Ethylendiaminetetraacetic acid
EGFP	Enhanced Green Fluorescence Protein
EPR	Enhanced Permeability and Retention
ESI-TOF	Electrospray ionization time-of-flight mass spectrometry
Et_2O	Diethyl ether
EtOAc	Ethyl Acetate
FBS	Fetal Bovine Serum
GM-CSF	Granulocyte-macrophage colony-stimulating factor
GPC	Gel Permeation Chromatography
GPP	Glycopolyplex
HEPES	4-(2-hydroxyethyl)-piperazine ethanesulfonic acid
hpt	Hours post transfection
iPrOH	Isopropanol
IU	International Units
JAWSII	Immature murine dendritic cell line JAWSII
K_2CO_3	Potassium carbonate
KOH	Potassium hydroxide
FT-IR	Fourier Transform Infrared Spectroscopy
IFN-γ	Interferon- γ
Man	Mannose monomer, mannose unit
MeCN	Acetonitrile
MEHQ	Hydroquinone monomethylether
MFI	Mean Fluorescence Intensity
$MgSO_4$	Magnesium sulfate
MHC	Major histocompatibility complex
MR, CD206	Mannose receptor
MTT	3-(4,5-dimethylthiazol-2yl)-2,5-diphenyltetrazolium
MW	Molecular weight
MWCO	Molecular weight cut-off
NaCl	Sodium chloride
$NaHCO_3$	Sodium bicarbonate

NaOH	Sodium hydroxide
NMR	Nuclear Magnetic Resonance
N/P ratio	Nitrogen/Phosphate molar ratio
ON	Oligonucleotide
OVA	Ovalbumin
PBS	Phosphate Buffered Saline
pDNA	Plasmid DNA
PFA	Paraformaldehyde
PDI	PolyDispersity Index
PEI	Polyethylenimine
RAFT	Reversible Addition-Fragmentation chain Transfer
RBC	Red Blood Cell
RPM	Revolution per minute
RPMI 1640	Roswell Park Memorial Institute medium
RT	Room temperature
s.c.	Subcutaneous injection
SiO_2	Silicon dioxide
ssDNA	Single strand DNA
TAA	Tumor Associated Antigen
TAE	Tris-Ammonium-EDTA
TBE	Tris-Borate-EDTA
TEM	Transmission Electron Microscopy
TLC	Thin Layer Chromatography
Tris HCl	Tris(hydroxymethyl)amminomethane chloride
VA-044	2,2'-Azobis[2-(2-imidazolin-2-yl)propane]dihydrochloride

ABSTRACT

Tumour immunology has been changing the landscape of modern medicine and anticancer therapy, by developing a variety of tumor antigenic peptide-based and nucleic acid-based treatments. Among the several nucleic acid-based therapeutics developed so far, short single-stranded synthetic DNA (ssDNA) molecules, known as CpG oligodeoxynucleotides (ODNs), was found to stimulate B cells and plasmacytoid dendritic cells (pDCs) and activate both innate and adaptative immune responses, thus raising interest for infectious diseases, cancers, and allergy treatment.[1] Furthermore, delivery of pDNA or mRNA encoding Tumor Associated Antigens (TAAs) to Dendritic Cells (DCs) is an emerging and promising alternative to the delivery of the parent antigenic peptide for antitumor vaccination, because they have shown to be safer and to provide a higher protein expression upon internalization by Antigen Presenting Cells (APCs).[2] Nucleic acids uptake by APCs results in the translation in antigens that are presented through the Major Histocompatibility Complex (MHC) to the immune system cells. This strategy allows to trigger both a direct immune response and a long-term memory against cancer cells. To date, lipid-based systems and viral vectors have dominated the nucleic acid delivery scenario. However, recently synthetic positively charged polymeric carriers have drawn increasing attention, since they provide opportunities for improved safety, greater flexibility and more facile manufacturing while preventing the enzymatic degradation of genetic material and mediating its cellular uptake. The specific term "polyplex" has been coined to identify the supramolecular structures derived from the electrostatic interactions between those polymers and nucleic acids.

In this PhD project, Reversible Addition Fragmentation chain Transfer (RAFT) polymerization[3] has been exploited for the synthesis of two generations of diblock and triblock copolymers designed to deliver pDNA encoding TAAs to antigen presenting cells and to trigger the direct immune response and a long-term memory against cancer. The 1st generation of these novel materials was designed with a poly-cationic agmatine acrylamide block to condense oligonucleotides, and with a mannosylated block to actively and selectively target Mannose Receptor (MR)[4] expressed on DCs. Furthermore, a 2nd generation of polymers was further engineered by adding a butyl acrylate-based hydrophobic block with the aim of

enhancing the endosomal escape properties of this family of carriers. A small library of three cationic di-block copolymers (Man_{15}-*b*-Agm_{12}, Man_{29}-*b*-Agm_{25} and Man_{58}-*b*-Agm_{45}) and two tri-block copolymers (Man_{29}-*b*-Agm_{29}-*b*-But_{9} and Man_{62}-*b*-Agm_{52}-*b*-But_{32}) was obtained via fast RAFT polymerization using D-Mannose acrylamide (Man), Agmatine acrylamide (Agm), and butyl acrylate (But) as monomers. Polymers were generated using identical monomer feed ratios but increasing total monomers units (corresponding to different final polymer molecular weights) to elucidate the effect of the polymer length on nucleic acids complexation and delivery to cells, and glycopolyplexes (GPPs) stability.

Initially, a short single strand DNA (ssDNA, 19 bases) as model for CpG ODN, was used to generate the GPPs. The optimum nitrogen to phosphate (N/P) ratio to achieve complete ssDNA complexation was evaluated by gel electrophoresis. Furthermore, DLS and TEM characterization confirmed the assembly and the narrow size distribution in the range of 25-55 nm, which was maintained over time also in the presence of serum proteins. The strong electrostatic interactions between polymers and ssDNA were confirmed by the Zeta potential reduction of 4-11 mV for 1st generation and of 11-18 mV for the 2nd generation polymers after ssDNA complexation. The association strength and the stability of polymers/ssDNA glycopolyplexes was investigated by the heparin displacement assay. All tested systems required a concentration of heparin at least 6-fold higher than its physiological concentration in the blood (0.15 IU/mL) to induce total ssDNA displacement, with di-block co-polymers retaining ssDNA more strongly as compared to the tri-blocks. Furthermore, polymers ability to cause red blood cells lysis *ex vivo* was correlated with their potential to induce endosomal membrane disruption. Particularly, the capacity of the butyl acrylate-based hydrophobic portion to induce endosomolysis under early endosomes mimicking conditions (pH 6) was confirmed by the higher percentage of induced hemolysis for Man_{29}-*b*-Agm_{29}-*b*-But_{9} and Man_{62}-*b*-Agm_{52}-*b*-But_{32} respect to 1st generation polymers. However, a good compromise between biocompatibility and endosomolytic activity of our systems was confirmed by *in vitro* viability assay performed with the polyplexes in the polymer concentrations range 0.005-0.2 mg/mL. *In vitro* uptake studies were performed either on model cell lines CHO (Chinese hamster ovary cells, wild type) and CHO-MR^{+} (Mannose Receptor expressing CHO cells) or on immortalized dendritic cells DC2.4. The internalization of glycopolyplexes loaded with Cy3-ssDNA was evaluated by flow cytometry after 30 minutes or 1 hour of incubation with cells. As expected, a certain degree of selectivity in the recognition of mannose receptor-

expressing cells by the GPPs was observed after 30 minutes of incubation, with the 1st generation low molecular weights polymers outperforming (around 4.5-fold increase in the uptake with respect to free ssDNA) the high molecular weight (2.5-fold increase in the uptake with respect to free ssDNA) and the butyl block-bearing polymers (1.5-fold increase in the uptake with respect to free ssDNA).

The successful complexation and delivery of high molecular weight nucleic acid by the glycopolymers was a key for transfection capabilities. 1st and 2nd generation glycopolymers were used to complex a model plasmid DNA encoding Enhanced Green Fluorescent Protein (pEGFP, 4759 bp). Agarose gel electrophoresis showed that all glycopolymers form stable complexes with pEGFP at relatively low N/P ratios of 5 for Man_{15}-*b*-Agm_{12}/pEGFP and Man_{29}-*b*-Agm_{25}/pEGFP, and 2.5 for Man_{58}-*b*-Agm_{45}/pEGFP, Man_{29}-*b*-Agm_{29}-*b*-But_{9}/pEGFP and Man_{62}-*b*-Agm_{52}-*b*-But_{32}/pEGFP. The stability of the systems in presence of poly-anionic competitive agents was also investigated, showing the release of pDNA at 1 IU/mL heparin concentration, which is 6-fold above its physiological concentration. The DLS and TEM analysis of the resulting GPPs showed the presence of mixed rod- and toroidal- shaped complexes with a size in the range 100-1000 nm. Moreover, *in vitro* transfection efficiency was evaluated on both CHO/CHO-MR^+ and immortalized dendritic cell lines at a selected nitrogen to phosphorous ratio for each polymer. Flow cytometry and confocal microscopy pointed out that Man_{29}-*b*-Agm_{29}-*b*-But_{9}/pEGFP, Man_{62}-*b*-Agm_{52}-*b*-But_{32}/pEGFP and Man_{58}-*b*-Agm_{45}/pEGFP complexes yielded the best transfection performance. In light of these evidences, these materials were selected for further investigation on dendritic cells, using plasmid encoding full-length ovalbumin (pOVA), a well-known immunogenic protein, to trigger an *in vitro* immune response against it. The immunological studies highlighted that the expression on DCs of the costimulatory clusters of differentiation CD86, necessary for T cell activation, was increased by cell incubation with Man_{58}-*b*-Agm_{45}/pOVA and Man_{62}-*b*-Agm_{52}-*b*-But_{32}/pOVA GPPs. Furthermore, these two GPPs were found to induce a slightly higher presentation of the SIINFEKL ovalbumin antigenic epitope by MHC I complex with respect to free pOVA and Man_{29}-*b*-Agm_{29}-*b*-But_{9}/pOVA. Finally, these two polymeric platforms were tested *in vivo* on C57BL/6 mice bearing B16-OVA melanoma tumor to investigate the applicability of these novel systems in the anticancer immunotherapy field. Both prophylactic and therapeutic approaches showed a higher efficacy of Man_{58}-*b*-Agm_{45}/pOVA in comparison to Man_{62}-*b*-Agm_{52}-*b*-But_{32}/pOVA GPPs in controlling the tumor growth or reducing the

tumor volume. In addition, immunological analysis on tumor and spleen samples showed a high level of specific activation of T cells against SIINFEKL antigenic peptide only in samples derived from mice treated with Man_{58}-*b*-Agm_{45}/pOVA, confirming it as a promising candidate for cancer vaccination.

RIASSUNTO

Negli ultimi anni l'immunologia sta cambiando lo scenario della medicina moderna e della terapia anticancro, con terapie che spaziano dall'utilizzo di peptidi antigenici tumorali all'uso di acidi nucleici. Tra le varie terapie a base di acidi nucleici che sono state sviluppate finora, corte sequenze di DNA a singolo filamento (ssDNA) note come CpG oligodesossinucleotidi (ODNs) sono state studiate per la loro capacità di stimolare le cellule B e le cellule dendritiche plasmacitoidi (pDC) e attivare la risposta immunitaria sia innata sia adattativa. Per questa ragione i CpG ODNs hanno acquisito importanza nel trattamento di malattie infettive, cancro e allergie. Inoltre, il direzionamento alle cellule dendritiche (DCs) di pDNA o mRNA che codifichino per antigeni tumorali (TAAs) costituisce un'alternativa emergente e promettente all'utilizzo degli antigeni peptidici in quanto tali per la vaccinazione anticancro, in quanto gli acidi nucleici hanno mostrato di essere più sicuri e di indurre un'espressione proteica più elevata una volta internalizzati dalle cellule presentanti l'antigene (APCs). L'internalizzazione degli acidi nucleici dalle APCs determina la traduzione nel corrispondente antigene, che è così presentato in associazione al complesso maggiore di istocompatibilità (MHC) alle cellule del sistema immunitario. Questa strategia permette di attivare sia una risposta immunitaria veloce sia una memoria anticancro a lungo termine. Ad oggi sistemi lipidici e vettori virali dominano il campo della terapia genica, ma anche polimeri cationici stanno ricevendo sempre maggior attenzione, dal momento che garantiscono un adeguato livello di sicurezza, una migliore flessibilità e una semplice produzione. In questo scenario, ci si riferisce al termine "poliplessi" per indicare le strutture sopramolecolari generate dall'interazione elettrostatica tra i polimeri e i nucleotidi, che previene la degradazione enzimatica del materiale genetico e ne media l'internalizzazione cellulare.

In questo lavoro, il metodo di polimerizzazione RAFT (Reversible Addition Fragmentation chain Transfer) è stato utilizzato per la sintesi di due famiglie di copolimeri a due o tre blocchi pensati per il direzionamento alle cellule presentanti l'antigene di DNA plasmidico codificante per antigeni tumorali al fine di innescare una risposta immunitaria diretta e una memoria a lungo termine anticancro. La prima generazione di questi nuovi materiali è stata progettata con un blocco policationico di agmatina per la condensazione di nucleotidi e con

un blocco di unità di mannosio per il direzionamento attivo e selettivo al recettore del mannosio (MR) espresso sulle cellule dendritiche. Inoltre, una seconda generazione di polimeri è stata disegnata aggiungendo un blocco idrofobico a base di butile acrilato con lo scopo di aumentare il rilascio endosomiale dei poliplessi dopo l'internalizzazione. Una piccola libreria di copolimeri cationici a due blocchi (Man_{15}-*b*-Agm_{12}, Man_{29}-*b*-Agm_{25} e Man_{58}-*b*-Agm_{45}) e a tre blocchi (Man_{29}-*b*-Agm_{29}-*b*-But_{9} e Man_{62}-*b*-Agm_{52}-*b*-But_{32}) è stata ottenuta attraverso la polimerizzazione RAFT, usando agmatina acrilamide (Agm), D-Mannosio acrilamide (Man) e butile acrilato (But) come monomeri. I polimeri sono stati generati usando gli stessi rapporti molari tra i monomeri, ma aumentando le unità totali di monomeri, e quindi il peso molecolare finale dei polimeri, per verificare l'influenza della lunghezza del polimero sulla complessazione e sul direzionamento degli acidi nucleici e sulla stabilità dei poliplessi.

Per lo screening i poliplessi sono stati generati utilizzando una corta sequenza oligonucleotidica (ssDNA, 19 basi), come modello per gli oligodesossinucleotidi CpG. Il rapporto molare ottimale azoti/fosfati (rapporto N/P) per garantire la completa complessazione del DNA è stato valutato per gel elettroforesi. Inoltre, la caratterizzazione dimensionale mediante DLS e TEM ha confermato la formazione di nanocomplessi con una dimensione definita e nel range 25-55 nm, stabile nel tempo anche in presenza di proteine del siero. Le forti interazioni elettrostatiche polimeri/ssDNA sono state confermate anche dalla riduzione del potenziale Z di 4-11 mV per i poliplessi di prima generazione e di 11-18 mV per quelli di seconda generazione. La forza e la stabilità dei glicopoliplessi è stata confermata anche dal test di competizione con eparina e per entrambe le generazioni di polimeri è stata necessaria una concentrazione di eparina almeno 6 volte superiore quella fisiologica (0.15 IU/mL) per avere lo spiazzamento del DNA dal complesso; i polimeri a due blocchi hanno dimostrato una migliore abilità nel trattenere il ssDNA in presenza di molecole anioniche competitive rispetto a quelli a tre blocchi. La capacità dei polimeri di causare lisi dei globuli rossi *ex vivo* è stata correlata alla loro abilità nel destabilizzare le membrane endosomiali. In particolare, la capacità di indure endosomolisi della porzione idrofobica di butile acrilato in condizioni simulanti l'ambiente endosomiale (pH 6) è stata confermata dalla percentuale più elevata di emolisi indotta da Man_{29}-*b*-Agm_{29}-*b*-But_{9} e Man_{62}-*b*-Agm_{52}-*b*-But_{32} rispetto ai polimeri di prima generazione. Una buona compatibilità dei nostri sistemi è stata comunque confermata dagli studi di vitalità cellulare *in vitro* eseguiti a concentrazioni di polimero nel

range 0.005-0.2 mg/mL. Infine, studi preliminari *in vitro* su cellule modello CHO (Chinese hamster ovary cells, wild type) e CHO-MR (cellule CHO esprimenti il recettore del mannosio MR) o su cellule dendritiche immortalizzate DC2.4 sono stati effettuati tramite citofluorimetria per valutare l'internalizzazione di poliplessi marcati dopo 30 minuti o un'ora di incubazione. Come previsto, gli studi di citofluorimetria hanno rivelato un certo grado di selettività da parte dei poliplessi nel riconoscimento di cellule esprimenti il recettore del mannosio, con una diminuita selettività all'aumentare del peso molecolare dei polimeri o per polimeri contenenti il blocco idrofobico.

Parallelamente si è valutata la capacità dei glicopolimeri di complessare e veicolare acidi nucleici ad elevato peso molecolare, quali pDNA e mRNA. A questo scopo, glicopolimeri di prima e seconda generazione sono stati complessati con pDNA modello codificante per la proteina EGFP (Enhanced Green Fluorescent Protein) (pEGFP, 4759 bp) e tramite elettroforesi su gel di agarosio si è verificata la formazione di complessi stabili a rapporti N/P relativamente bassi, ossia a N/P 5 per Man_{15}-*b*-Agm_{12} e Man_{29}-*b*-Agm_{25}, o a N/P 2.5, per Man_{58}-*b*-Agm_{45}, Man_{29}-*b*-Agm_{29}-*b*-But_{9} e Man_{62}-*b*-Agm_{52}-*b*-But_{32}. La dimensione e la morfologia dei poliplessi è stata analizzata tramite DLS e TEM, che hanno mostrato la coesistenza di complessi a toroide e a bastoncello con una dimensione nel range 100-1000 nm. Per quanto riguarda gli studi *in vitro*, l'efficienza di trasfezione dei nostri sistemi è stata valutata utilizzando pEGFP sia su cellule modello CHO/ CHO-MR^{+} sia su cellule dendritiche immortalizzate a rapporti N/P selezionati. I risultati ottenuti dalla citofluorimetria a flusso e dalla microscopia confocale hanno mostrato delle migliori performance da parte dei complessi Man_{29}-*b*-Agm_{29}-*b*-But_{9}/pEGFP, Man_{62}-*b*-Agm_{52}-*b*-But_{32}/pEGFP e Man_{58}-*b*-Agm_{45}/pEGFP, che sono quindi stati selezionati per gli studi successivi con il DNA plasmidico codificante per la proteina antigenica ovalbumina (pOVA). Questi studi immunologici hanno evidenziato come l'espressione sulle cellule dendritiche della molecola costimolatoria CD86, necessaria per l'attivazione delle cellule T, risulti aumentata dal trattamento delle DC con Man_{58}-*b*-Agm_{45}/pOVA and Man_{62}-*b*-Agm_{52}-*b*-But_{32} /pOVA. Inoltre, questi due poliplessi si è visto che sono in grado di indurre un più elevato livello di espressione dell'epitopo antigenico dell'ovalbumina, ossia il peptide SIINFEKL, come associato al complesso maggiore di istocompatibilità di tipo I. Alla luce di questi risultati, queste due più promettenti piattaforme sono state testate *in vivo* su topi C57BL/6 con melanoma B16-OVA al fine di chiarire le possibilità di utilizzo dei nostri sistemi innovativi nel campo dell'immunoterapia anticancro.

In particolare, sia nell'approccio profilattico che in quello terapeutico si è vista una maggiore efficacia del sistema di prima generazione Man_{58}-*b*-Agm_{45}/pOVA rispetto a Man_{62}-*b*-Agm_{52}-*b*-But_{32}/pOVA nel controllo della crescita tumorale o nella riduzione del volume tumorale. In aggiunta, le analisi immunologiche sui campioni di tumore e di milza espiantati dagli animali hanno mostrato un livello elevato di attivazione specifica delle cellule T contro il peptide antigenico SIINFEKL solo nei campioni derivanti dagli animali trattati con Man_{58}-*b*-Agm_{45}/pOVA, confermando così la sua applicabilità per la vaccinazione genetica anticancro.

INTRODUCTION

The "magic bullet" concept, envisioned in 1906 by Paul Ehrlich, has underlined the key role of the specific and targeted delivery of drugs to their molecular target for an efficient therapy. Over the years, the nanotechnology field has focused its attention on the design and development of nano- and micro-sized Drug Delivery Systems (DDSs) able to improve the physico-chemical characteristics, the pharmacokinetic and the site-specific release of loaded therapeutics. Nanotechnology brings together scientists and engineers from many different fields with the common goal of studying, designing and developing systems with a size in between 1 and 100 nm. Broadly, the term “nanomedicine” refers to engineered nanoscale systems with dimension below the micrometer, whose nanostructure confers unique advantageous therapeutic properties. Nanomedicines include nanopharmaceuticals, representing 75% of the market of approved nanomedicine, nanodiagnostics, nanotheranostics, and nanobiomaterials.[5] Initially, DDSs were developed to enhance the solubility and alter the biodistribution of small molecules, ultimately delivering drug more efficiently at the site of action while reducing toxicity to other organs. Aiming at a safe and efficient administration, DDSs must possess defined structural characteristics in term of size, surface charge, shape, molecular architecture and hydrophobic/hydrophilic balance which affect the drug release profile, the formulation biocompatibility and its bioelimination. Considering all these features, several drug delivery systems have been developed in the last decades such as micelles, liposomes, dendrimers, polymer therapeutics and inorganic nanoparticles, and some of those systems have been approved by the US Food and Drug Administration (FDA) and European Medicines Agency (EMA) for a variety of therapeutic indications (Figure 1). The liposomal formulation of doxorubicin (Doxil®) was the first nanocarrier to reach the market in the United States in 1995, followed by various other liposomal formulations. Then about ten years occurred to achieve the market approval of non lipid-based DDSs, including Abraxane (albumin-paclitaxel NPs) and Feraheme (superparamagnetic iron oxide nanoparticles for iron deficiency in anemic patient).

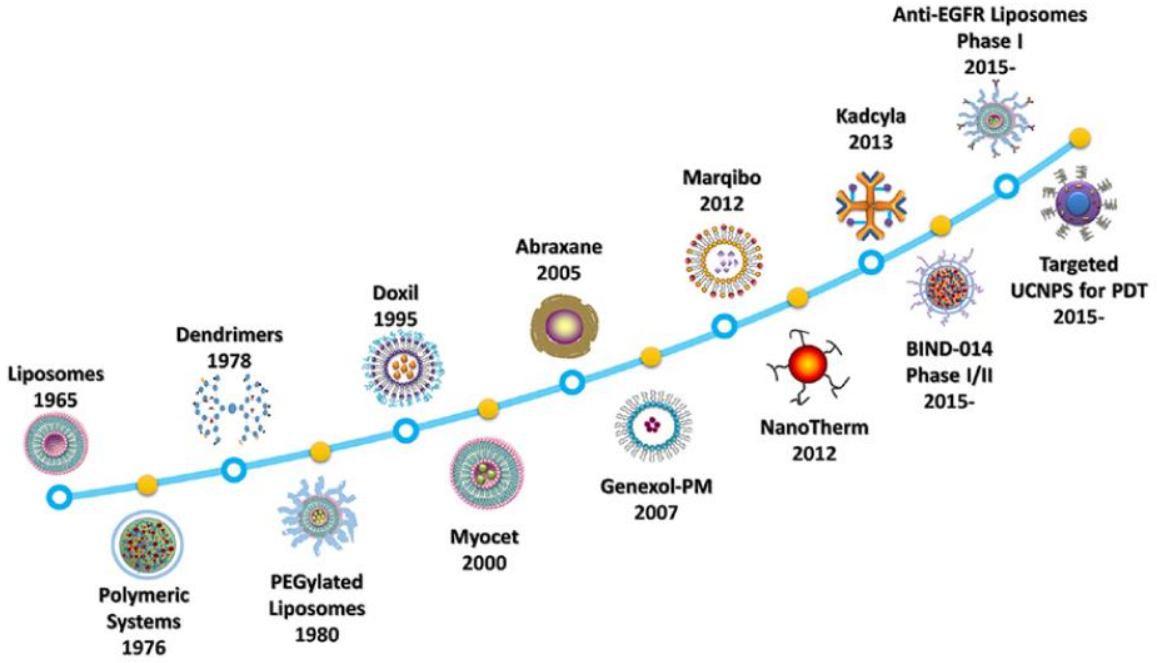

Figure 1. *Timeline of nanomedicine development and approval.*[6]

More recently, new classes of therapeutic biomolecules have emerged (e.g. nucleic acids, proteins) with high therapeutic potential, however they are affected by limiting drawbacks such as fast degradation and/or low ability to cross the cell membrane. Therefore, the design of effective delivery systems able either to protect biotherapeutics from enzymatic degradation or to enhance their cell entry is crucial to achieve efficacy. Particularly, drug delivery systems represent a great promise in the gene therapy field, whose goal is to introduce genetic material into cells to compensate for abnormal gene expression or to make a missing functional protein, thus treating several pathologies such as cancers and hereditary or infectious diseases. To this aim, cationic nanocarriers are capable to complex nucleic acids (e.g. ODN, siRNA, pDNA, mRNA, etc.) exceeding the limits of these macromolecules and increasing their blood half-life, intracellular uptake and efficacy. Moreover, cationic materials can be designed for tailored purposes and endowed with targeting capacities or features and nucleic acids complexing properties.

1.1 Overview on cancer

Cancer is the second leading cause of death worldwide following cardiovascular disease, accounting for an estimated 9.6 million death in 2018 (World Health Organization). The term cancer refers to a wide group of diseases that can affect several tissues of the body, and that arise from the transformation from normal to tumor cells in a complex multistage process. The disease usually progresses from a pre-cancerous lesion to a malignant tumor.

1.1.1 Cancer hallmarks

Malignant cancer cells can invade other tissues and organs by migration from the native tissue through the fast-growing blood and lymphatic vessels, bypassing the immune system recognition. Despite differences between tumor types, during its onset and progression all cancer cells gain distinctive biological abilities enabling their survival, proliferation and metastatic dissemination. Initially, six main cancer hallmarks were described to identify the steps of conversion of normal cells into malignant ones.[7] More recently, two more cancer traits were enumerated, encompassing the contributions of the tumor microenvironment to tumorigenesis.[8]

Cancer hallmarks are represented in Figure 2 and may be summarized as follow:

- Sustaining proliferative signal. Compared to healthy cells, cancer cells sustain chronic proliferation by deregulating the production and release of growth-promoting signals, thus ensuring the abnormal cell growth and cell division. A number of alternative ways to sustain proliferative signaling are exploited, from auto-production of growth factor and overexpression of membrane growth factor receptors to constitutive activation of signaling pathways operating downstream of these receptors. Somatic mutations on cancer cell genome are involved in the constitutive activation of signaling circuit and in the disruptions of negative-feedback mechanisms that in normal condition attenuate proliferative signaling.
- Evading growth suppressors. Cancer cells can circumvent mechanisms that negatively regulate cell proliferation by lacking in tumor suppressors expression, such as RB (retinoblastoma-associated) and TP53 proteins, that in healthy cells integrate signals from extracellular and intracellular sources to decide whether or not permit further cell-cycle progression. In addition, the cell contact inhibition mechanisms, which normally counterbalance the proliferative signals, are defective.

- Resisting cell death. Apoptosis is a physiological programmed cell death triggered in response to various physiological stresses, such as elevated levels of oncogene signaling or DNA damage associated with hyperproliferation. Tumor cells display many strategies to corrupt the apoptotic machinery by deregulating the balance between pro- and antiapoptotic members of the Bcl-2 family of regulatory proteins, by increasing the expression of anti-apoptotic proteins or of survival signals, by eliminating damage sensors from the apoptotic-inducing circuitry.
- Enabling replicative immortality. Differently from normal cells, tumor cells acquire unlimited replicative potential, thus generating macroscopic tumoral masses. Indeed, malignant cells can circumvent either senescence, an irreversible non-proliferative but viable status, or crisis, having the cell death as end point, thus reaching a new status called "immortalization". Multiple lines of evidence indicate that this capacity is related to the expression at functionally significant levels in cancer cells of telomerase, the specialized DNA polymerase that adds telomere repeat segments extending telomeric DNA.
- Inducing angiogenesis. In the adult, angiogenesis is a quiescent process, that is turned on only transiently in defined processes. In tumor tissues an "angiogenic switch" is almost always activated, enabling the creation of new vessels necessary to obtain oxygen and nutrients to endorse the fast and uncontrolled cell growth. The tumor vasculature produced by chronically activated angiogenesis and an unbalanced mix of proangiogenic signals is typically aberrant, with excessive vessel branching, distorted and enlarged vessels, and large-fenestrated and leaky vasculature.
- Activating invasion and metastasis. During the growth progression, tumor cells activate the invasion-metastasis cascade, i.e. a multistep process that begins with a local invasion of tumor cells, followed by the intravasation of the cancer cells in the blood and lymphatic system, then the extravasation in the parenchyma of distant tissues, creating new macroscopic tumors.
- Emerging hallmark: Reprogramming energy metabolism. The reprogramming of cellular energy metabolism enables to support continuous cell growth and proliferation. Particularly, either in presence of oxygen or under the hypoxic conditions that operate within many tumors, cancer cells can switch their energy production, limiting their

energy metabolism largely to glycolysis, leading to a state referred as "aerobic glycolysis".

- Emerging hallmark: Evading immune system. The immune system has dichotomous roles in cancer, both antagonizing and enhancing tumor development and progression. Indeed, the tumor-associated inflammatory response, triggered by immune cell infiltration, can have the paradoxical effect of enhancing tumorigenesis and progression. On the other hand, immune surveillance constantly monitors cells and tissues, recognizing and eliminating the vast majority of incipient cancer cells and thus nascent tumors. A characteristic trait of cancer cells is the evasion from this immune surveillance, hampering their attack and elimination by immune cells. The important role of the immune system in cancer will be deeply discussed in the next paragraph.

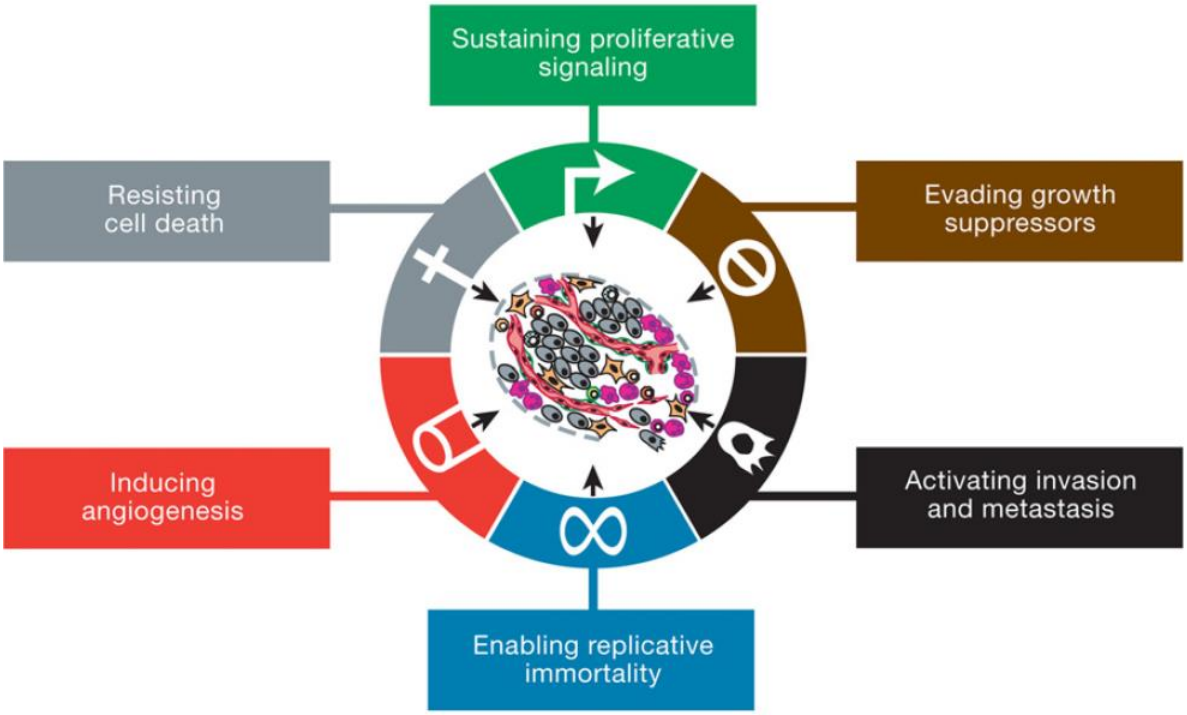

Figure 2. *Representation of the six hallmarks of cancer as originally proposed in 2000 by Weinberg R. A. and Douglas Hanahan.*[7]

1.1.2 Immune system: the double-crosser in cancer development

In the early stage of tumor growth, the innate and adaptive immune responses could identify and eliminate transformed cells, eradicating the tumor, as well as the tumor could develop mutations which allow it to escape immune detection and elimination, resulting in

tumor progression. The generation of an efficient anticancer immune response is dependent on a stepwise process, namely the "cancer immunity cycle" (Figure 3), that can be modulated by stimulatory and inhibitory factors.[9] Briefly, tumor specific surface markers, referred as antigens or tumor associated antigens (TAAs), are expressed or overexpressed on cancer cells. After their release, TAAs can be captured by antigen presenting cells (APCs), that are the connection between innate and adaptive immune systems and represent the interface between the peripheral tissues and the lymphoid organs that stimulate T-cell responses.[10] Indeed, after antigen sequestration and processing, immature dendritic cells (iDCs) undergo an activation and maturation process, which is associated with the upregulation of co-stimulatory molecules on cell surface and with cytokine production, necessary for an efficient subsequent antigen presentation to the T cells. Mature dendritic cells (mDCs) can migrate to the draining lymph nodes and subsequently present antigenic peptides complexed with major histocompatibility complex (MHC) molecules on their membrane, triggering an antigen-specific immune response. Indeed, MHC I- and MHC II-antigen complexes are then presented to naïve $CD8^+$ and $CD4^+$ T-cells, respectively. In this scenario, cancer antigen-specific T cells are activated and, in particular, effector $CD8^+$ cytotoxic T lymphocytes (CTLs) can traffic to the tumor and infiltrate it, subsequently recognizing the specific antigenic epitope and killing the cancer cells. Furthermore, a subset of antigen-specific T cells differentiates into long-lived memory cells, guaranteeing for long term cancer eradication.

To efficiently activate naïve T-cells, the synergy between three signals is required. Firstly, as mentioned above antigens must be presented on DCs surface associated with MHC complexes in order to be recognized by T-cell receptors (TCR). Furthermore, antigen presentation must occur in a condition of immune activation, thus co-stimulatory molecules such as CD80/CD86 and CD40 should be expressed on DCs to allow the interaction with the corresponding receptors expressed on T-cells (CD28 and CD40L, respectively). Finally, DCs release cytokines (interleukin, IL-12, IL-4) and chemokines (interferon IFN-γ) that directly polarize the development of $CD4^+$ T helper cells towards T helper Th1 or Th2 cells. Particularly, Th1 cells usually secrete IFN-γ and tumor necrosis factor (TNF-α) as a response to inflammatory signals from DCs (IL-12) and intracellular pathogens, while Th2 cells protect the organism mainly from extracellular pathogens by secreting IL-4, IL-5, IL-10 and IL-13, in turn stimulating B-cells to produce antibodies against extracellular pathogens and toxins.

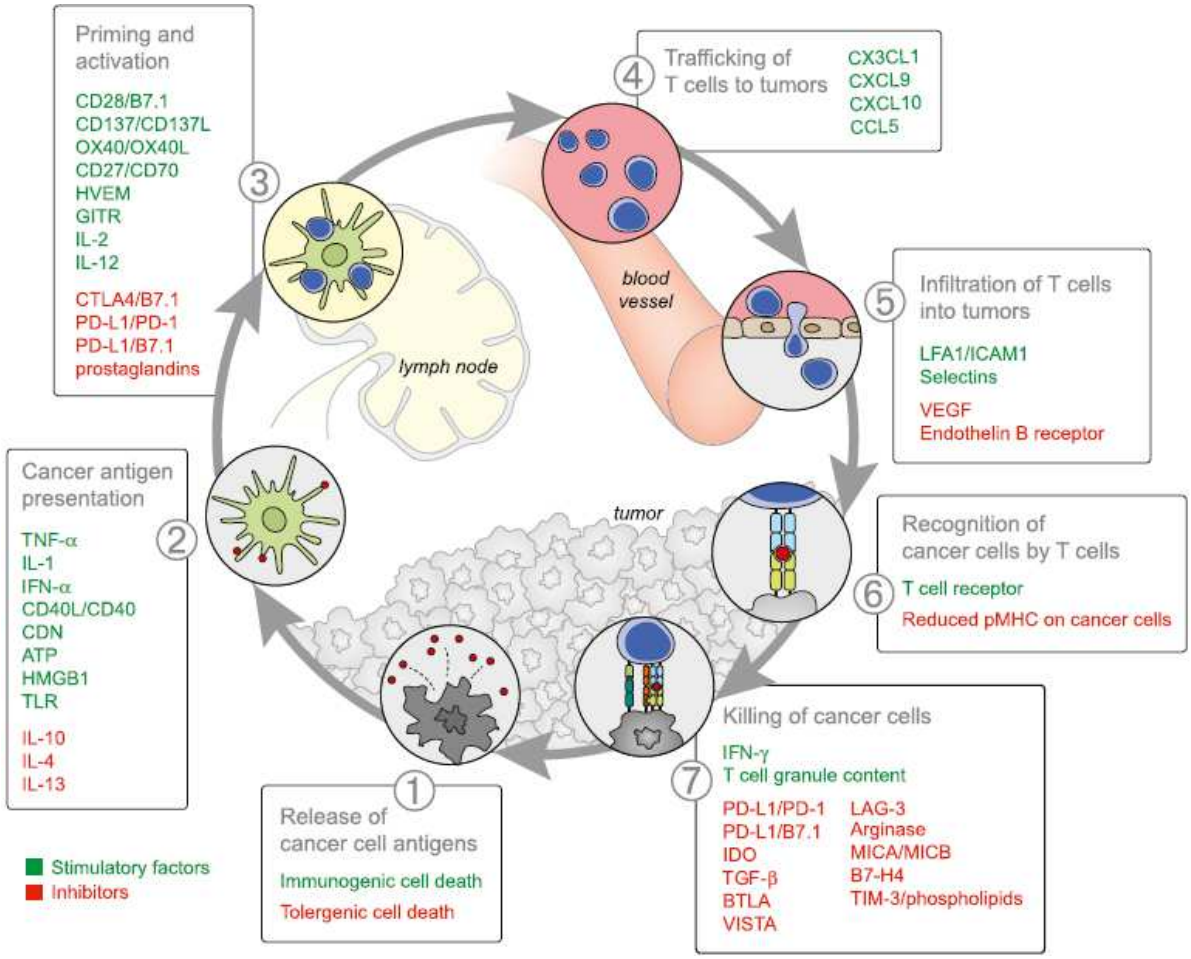

Figure 3. *Diagram illustrating the seven major steps involved in the cancer-immunity cycle and the stimulatory (green, promote immunity) and inhibitory (red, reduce immune activity and/or prevent autoimmunity) factors that act in each step of the cycle.*[9]

In cancer patients, the cancer-immunity cycle is blocked at one or more of these steps, dampening the anti-cancer immune response and allowing for immune escape. Indeed, cancer cells develop mutation that allow them to escape the immune recognition, by inducing loss of tumor antigen expression or by downregulating MHC molecules, by inducing immune cell exhaustion through persistent activation (tolerogenic mechanism) or by expressing ligands for co-inhibitory receptors. Furthermore, tumor infiltrating regulatory T cells (T_{reg}) are a heterogeneous population of immunosuppressive lymphocytes that maintain immune homeostasis and self-tolerance. These cells either secrete immunosuppressive cytokines or sequester IL-2 required for T cells survival and function.

Understanding the different steps at which and the different mechanisms through which cancer cells can escape immune eradication has bring to new way to treat cancer, the cancer immunotherapy.

1.2 Cancer immunotherapy: moving beyond conventional treatments

The three main approaches in cancer patients are the surgical resection of the tumor mass, the radiotherapy and the use of chemotherapeutic drugs. Particularly, the latter are in general the first-line treatment in late stages of the disease or in leukemia. Traditional anticancer drugs are small molecules that interfere with the regular cell cycle of rapidly proliferating cells by inducing nucleus damage, inhibition of cellular replication, or promoting apoptotic pathways. Paclitaxel, doxorubicin, daunorubicin, cisplatin, and docetaxel are just few examples of classic therapeutics in oncology. Despite the antiproliferative effect on tumoral cells, chemotherapeutic agents exhibit a narrow therapeutic index, a wide and non-specific toxicity and deleterious effects also on fast replicating healthy cells.

During the past two decades, the cancer therapy approaches have evolved from the use of relatively nonspecific cytotoxic agents to selective, mechanism-based therapeutics.[11]

In this scenario, drug delivery systems have emerged as a promising strategy to overcome chemotherapeutics drawbacks, either exceeding the pharmacokinetic constraints of traditional formulations or even directing drugs to the desired disease site by nanocarriers decoration with different targeting molecules. Doxil®, a pegylated liposomal form of doxorubicin, was the first FDA-approved DDS in 1995 developed by Gabizon and Barenholtz; its stealth properties result in a prolonged pharmacokinetic and a reduced toxicity, thus enabling the use for Kaposi's sarcoma, ovarian cancer and multiple myeloma treatment with minor side effects on patients in comparison to the free drug.[12] Ten years later also Abraxane®, the physically encapsulated paclitaxel to human albumin, received the clinical approval for the treatment of advanced and metastatic prostate and breast cancer. Since 1995, more than 50 nanopharmaceuticals have received FDA approval and are currently available for clinical use. Furthermore, there are plenty of next generation DDSs in clinical trial that additionally exploit the active targeting approach. As an example, BIND-014 is a docetaxel polymeric nanoparticle targeting Prostate-Specific Membrane Antigen (PSMA) in phase II clinical trial for patients with metastatic prostate cancer.[13]

On the other hand, the recent progress in understanding the basic mechanisms of the immune system and its correlation with cancer resulted in an increasingly available and vital cancer treatment option: the cancer immunotherapy. Immunotherapy marks an entirely different way of treating cancer by generating or boosting an immune response against it, thus targeting the immune system, not the tumor itself.[14] Already in the 1890s, William Coley

began to treat cancer patients with bacterial extracts to activate general systemic immunity.[15] Nevertheless, cancer immunotherapy has only in the past decade been shown, with phase III clinical trials of Nivolumab (anti PD-1 monoclonal antibody, paragraph 1.2.2) and Sipuleucel-T (cell based cancer immunotherapy for prostate cancer), to consistently improve the overall survival of patients with advanced-stage cancer.[16] Considering how refractory cancer is to standard therapy, efforts to develop different immunotherapeutic strategies and to achieve immune control of this disease are well justified. In this realm, natural or synthetic materials can also contribute to overcome some of the limitations of current cancer immunotherapy approaches, and could allow for the development of more effective and more efficient immunotherapies.[17]

A deep investigation on the broad spectrum of anticancer immune-based approaches is reported below.

1.2.1 Monoclonal antibodies (mAbs)

In cancer immunotherapy, monoclonal antibodies are exploited to recognize and bind a specific tumor associated antigen or protein. Once attached to TAAs, they can recruit other components of the immune system to destroy the cells that present that specific antigen on the surface, thus destroying cancer cells in this specific context. To date, FDA has approved more than a dozen of mAbs for cancer treatment, either with a therapeutic effect by themselves (i.e. Campath®, Herceptin®) or linked to a conventional chemotherapeutic drug (ADC, antibody-drug conjugates). Besides the double effect of the latter, ADC can cause more side effects, depending on which drug they are attached to.

1.2.2 mAbs as immune checkpoint inhibitors (ICIs)

T-cells stimulation with immunomodulatory antibodies that block or activate regulatory receptors is sufficient to cause the eradication of some tumors. Particularly, the immune checkpoint inhibitors are mAbs that block T-cells inhibitory receptors. As an example, the blockade of a receptor involved in immune-checkpoint signaling, that is the programmed cell-death protein 1 (PD-1), resulted in a remarkable antitumor activity and therefore it has been approved by the FDA for melanoma treatment and marketed under the name of Nivolumab. However, ICIs present still some limitations regarding toxicity and efficacy in the context of pediatric malignancy, with a certain risk of dose-dependent treatment-related mortality.[18]

1.2.3 Chimeric Antigen Receptor (CAR) T-cells therapy

CAR T-cell therapies are sometimes referred as a cell therapy or an adoptive cell transfer therapy. The goal of this approach is to generate a robust immune-mediated antitumor response through the *ex vivo* manipulation of T cells. First, T cells are recovered from patient's blood and are *ex vivo* genetically altered through gene transfer of a chimeric antigen receptor (CAR) that target an extracellular antigen specific for a certain tumor. Secondly, CAR T-cells are reinfused in the patient, where they can recognize and eradicate cancer cells. Initial clinical trials using CAR T-cells focused on targeting CD19, which is ubiquitously expressed on a broad range of differentiated B cells, to treat diseases such as B-cell acute lymphoblastic leukemia (B-ALL) or non-Hodgkin lymphomas. Despite three CAR T-cell therapies currently approved by FDA, targeting solid tumors with this approach is still a challenge.

1.2.4 Cancer vaccines

Vaccines are among the most important discoveries in human history, having saved billions of lives in the past two centuries. Starting from Edward Jenner's vaccine against smallpox (1798), a plethora of infectious diseases became preventable through vaccination. More recently, immunologists started exploring the possibility of using vaccines against other disorders that involve the immune system, like cancer and certain autoimmune diseases.[19]

Behind the development of tumor vaccine, there is the concept that tumor cells express on their surface macromolecules that are not normally present in healthy cells, the tumour antigens. Cancer vaccines boost the immune system to recognize these antigens and destroy cancer cells that express these molecules on their surface. Particularly, cancer vaccines are designed to promote tumor specific immune responses, mainly through cytotoxic $CD8^+$ T cells specific for MHC class I-restricted tumor antigens, but also through $CD4^+$ T cells specific for MHC class II-restricted tumor antigens.[20]

It is worth to note that, since tumor neoantigens arise during transformation from healthy to malignant cells, the immune system should recognize them as non-self and trigger an immune response by itself. Unfortunately, an effective endogenous immunity against cancer was rarely observed and several mechanisms have been proposed to explain that, such as generation of antigen-loss tumor variants, loss of MHC expression, downregulation of antigen processing machinery and expression of local inhibitory molecules.[20] Thus, in order to be

effective, cancer vaccine should either permit the presentation of the neoantigen in a context of immune stimulation or break down the tolerance of tumors, that are typically poor stimulator of immune responses. Components of infectious agents, immune cells growth factors and tissue damage signals are often employed as adjuvants to guarantee antigen presentation in a context of immune system activation.

Several platforms for cancer vaccination are being tested, including tumor cells or tumor lysate, dendritic cells, viral vectors, peptides and proteins, and nucleic acids (Figure 4).

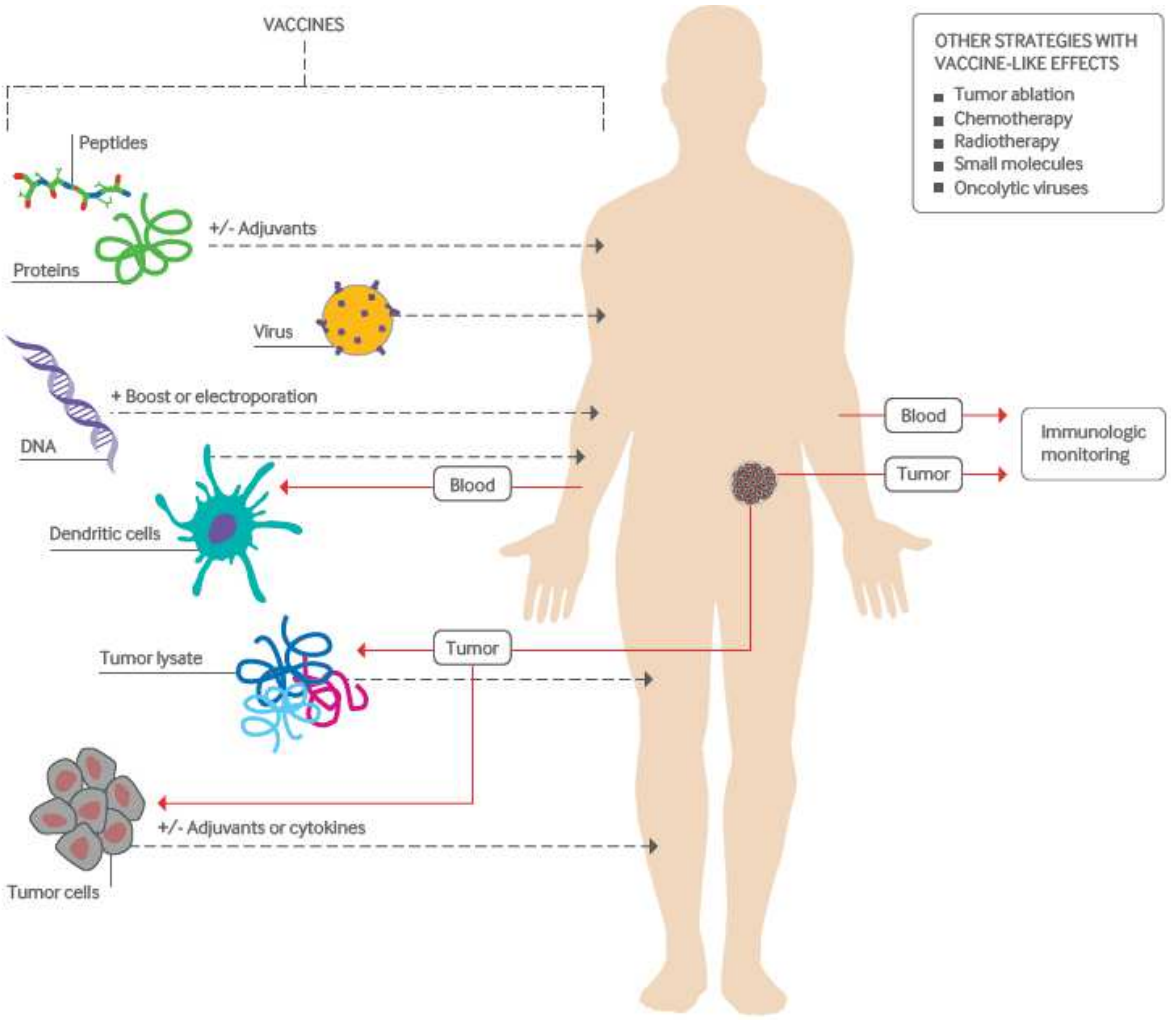

Figure 4. *Different strategies of cancer vaccination. Tumor cells or lysate, nucleic acids, peptides or proteins can be used for cancer vaccination with or without the co-administration of adjuvants.*[21]

Early cancer vaccines used irradiated and inactivated whole tumor cells or tumor cells lysate as carriers of the entire collection of tumor antigens, letting the patient's immune system sort out the relevant ones. The complexity in collection and formulation of autologous whole-tumor cells vaccines have limited the expansion of this approach in the clinic, giving

rise to the development of molecularly defined vaccines based on direct administration of tumor associated antigens (TAAs) by themselves.

Another cell-based vaccination approach involves the use of *ex vivo*-prepared tumor antigen-loaded dendritic cells. DCs can be loaded with autologous or allogeneic tumors, tumor lysates, tumor RNA or DNA and then re-injected in the patient. In this scenario, Sipuleucel-T (Provenge®) was the first therapeutic cancer vaccine to be approved by the FDA for metastatic prostate cancer for its capacity to prolong overall survival in patients with hormone-resistant tumor by an average of 4.1 months during phase III clinical trials. This cellular product consists of autologous APCs loaded with a fusion protein of the prostate differentiation antigen prostatic acid phosphatase (PAP) linked to granulocyte-macrophage Colony Stimulating Factor (GM-CSF).[22]

Thanks to the advent of next-generation sequencing and of novel algorithms for predicting the binding of peptides to MHC proteins, cancer vaccination moved on to the use of patients-personalized tumor associated antigens (TAAs).[23] Particularly, vaccines based on one or more peptides can be injected alone or with adjuvants or with a cytokine (such as GM-CSF to activate APCs).

Furthermore, a different approach based on the delivery of pDNA or mRNA encoding TAAs could also be exploited, thus finding an overlapping between cancer vaccines and gene therapy. Genetic vaccines consist only of plasmid DNA or messenger RNA, which should be internalized by antigen presenting cells and translated into the encoded antigenic protein, thus resulting in an immune response. Nucleic acid-based vaccines appear to have certain advantages over conventional protein vaccines, e.g. the ability to induce a wider range of types of immune response. Indeed, whereas antigen presented in soluble form generally induces only antibody responses, the administration of DNA encoding TAAs provides for antigen presentation by both MHC class I and class II molecules, thus involving cell-mediated and humoral immune response, respectively. Furthermore, the *in vivo* production of the corresponding antigen or protein ensures that protein resembles the normal eukaryotic structure more closely, with related post-translational modifications.[2]

In a study from Sahin *et al.*,[24] 13 patients with stage III or IV melanoma were treated via lymph nodes injection of a personalized RNA-based 'poly-neoepitope' vaccines encoding for 10 selected neoantigens per patient; each patient developed an immune response against at least three mutations represented in poly-neoepitope vaccine.

A deeper insight on gene therapy and on its applicability to cancer vaccination will be investigated in the next chapter. Nevertheless, further studies are needed to optimize the nature of vaccine components and assess the relative advantage of peptide versus DNA- or RNA-based approaches, and to evaluate the right therapy dosing and timing.

1.3 Gene therapy

Gene therapy can be defined as the treatment of acquired and inherited human disorders by the transfer of genetic material as therapeutic substance into specific cells of the patient.

The final goal of gene therapy is to obtain a therapeutic effect, by either correcting genetic defects, over-expressing therapeutically useful proteins, or inhibiting the production of proteins that are involved in diseases progression. Initially, this approach was exploited for the treatment of inherited disorders by replacing an abnormal gene responsible of the disease with the one encoding for the correct protein. A large number of clinical trials focused on cystic fibrosis,[25] hemophilia,[26] Duchenne muscular dystrophy[27] and severe combined immunodeficiencies.[28] Subsequently, researchers moved their attention also to gene therapy applied to cardiovascular diseases, infectious diseases (acquired immune deficiency syndrome, AIDS) and a plethora of other acquired diseases, including cancer (Figure 5). Indeed, DNA damages induced by the carcinogenesis process can be exploited as a target for anticancer gene therapy.

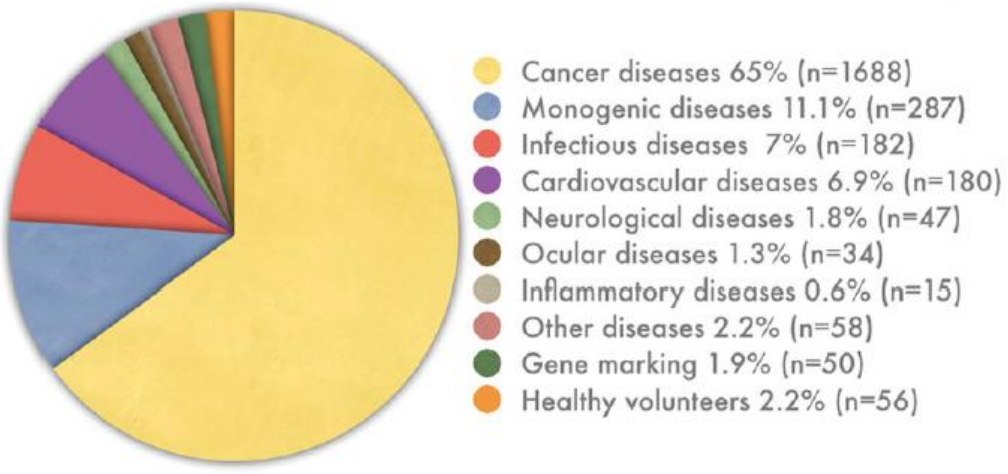

Figure 5. *Indications addressed by gene therapy in clinical trials.*[29]

A number of nucleic acid-based drugs have been developed so far, involving a wide spectrum of therapeutic compounds that act at different steps in the gene transcription-translation machinery, thus requiring specific delivery strategies to target the cellular compartment necessary for their activity.[30] Some examples of biomolecules used in gene therapy are reported in Figure 6 and include plasmid DNA (pDNA), messenger RNA (mRNA), small interfering RNA (siRNA), short hairpin RNA (shRNA) and microRNA (miRNA), and antisense oligodeoxynucleotides (ODN).

Based on their mechanism of action, nucleic acid therapeutics can be categorized as gene substitutes, inhibitors, or vaccines.[30]

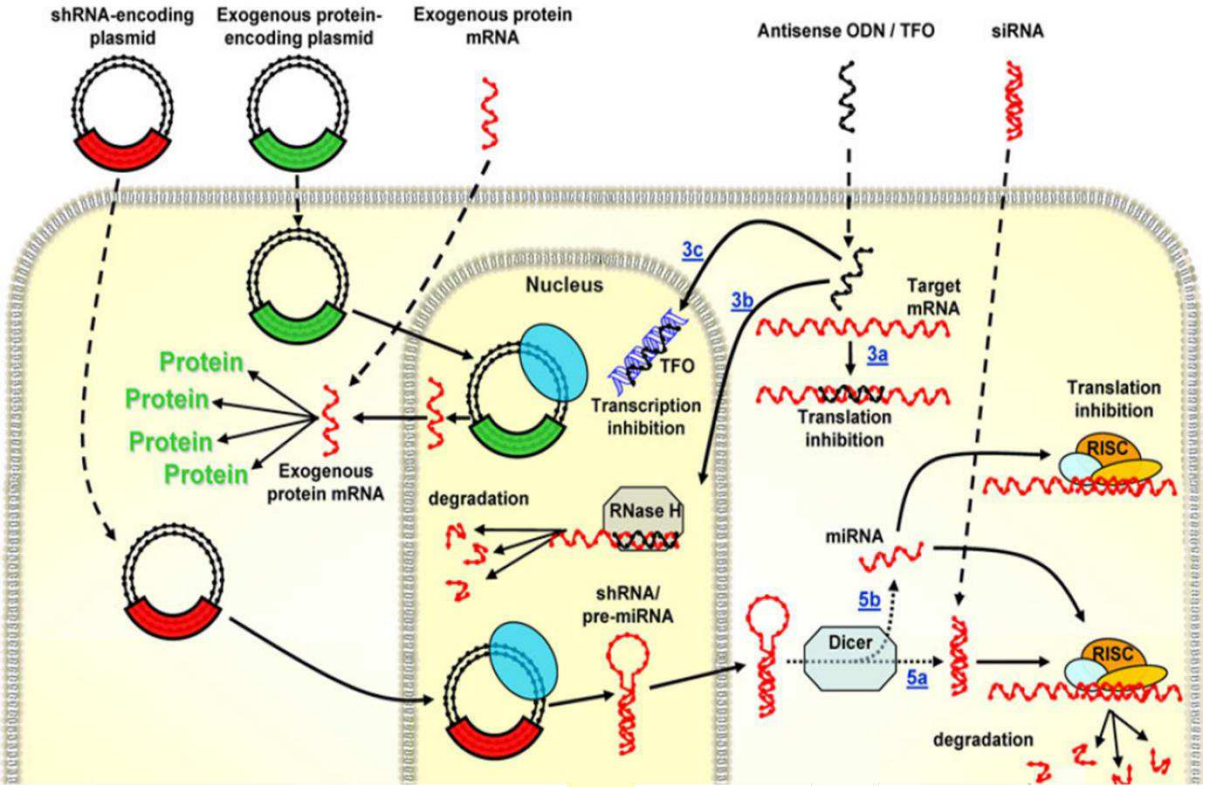

Figure 6. *Schematic representation of nucleic acid-based drugs, of the cellular compartment they need to reach to exploit their effect and of their mechanism of action.*[30]

siRNA, shRNA, miRNA and ODN belong to the category of the gene inhibitors since they work as sequence-specific inhibitors either at the transcriptional (DNA) or at the post-transcriptional (RNA) level. Indeed, antisense nucleotides are short sequence of nucleic acid designed to be complementary to specific DNA or mRNA sequences and to hybridize through Watson-Crick base-pair forces, with (miRNA and siRNA) or without (ODN) the catalysis of cellular enzymes. The activity results in the blockade at some step of the transfer of genetic

information from DNA to protein. Particularly, unmethylated cytosine-phosphate-guanosine (CpG) oligodeoxynucleotides (ODNs) are short single-stranded synthetic DNA molecules that contain a cytosine triphosphate deoxynucleotide (C) connected through a phosphodiester link (p) to a guanine triphosphate deoxynucleotide (G). CpG motifs are considered pathogen-associated molecular patterns (PAMPs) and in their unmethylated form they act as immunostimulant. Indeed, unmethylated CpG ODNs are recognized by Toll-like receptor 9 (TLR9) found in antigen-presenting cells and B cells and more specifically in endolysosomes of immune system cells.[1] Since TLR9 recognition by ODNs was found to stimulate B cells and plasmacytoid dendritic cells (pDCs) and activate both innate and adaptative immune responses, CpG ODNs were investigated for their efficacy in treating infectious diseases, cancers, and allergy. Although different modification of the backbone has been considered to avoid ODNs rapid degradation by DNase, several concerns regarding undesired side effect of modified CpG have moved the research focus on the use of nanocarriers to deliver this class of therapeutics. Indeed, a drug delivery system can simultaneously protect CpG ODN from DNase and improve its cellular uptake, eventually in a specific and targeted manner.[1]

As other interference nucleic acids are not the focus of this thesis project, they will not be described in further detail here.

Regarding pDNA and mRNA, they can be categorized as gene substituents, when they aim to produce lacking, low-expressed or therapeutic proteins, or as gene vaccine, when they encode for antigenic proteins and are aimed at triggering an immunological response. In this work, the use of pDNA as gene vaccine was investigated, but the same concept of pDNA/mRNA transcription in protein can be adapted also to their use as gene substituent. In general, according to the specific application and to the route and strategy of administration, the gene of interest can be inserted into a pDNA or a mRNA vehicle, also designed as the minimal nucleic acid vectors (MNAV) that can be used as therapeutic agent.[31] pDNA can be easily produced in a research or GMP-production scale by simple fermentation of transformed bacteria and by subsequent purification. Furthermore, its double stranded nature guarantees for pDNA high stability also in suboptimal storage condition and for a limited degradability by cellular enzymes. Nevertheless, the need of reaching the nuclear compartment to engage the host transcription machinery represents a hurdle of pDNA applicability in gene therapy. As widely discussed in the next chapter, several formulation strategies were developed to

allow nucleic acids internalization by cells, but the intracellular nuclear targeting is still a capacity that must be further explored.

Unlike pDNA, mRNA activity involves only the cytoplasmic compartment, where it can be directly translated into the encoded protein with a faster onset of action. Despite this advantage, mRNA supports protein synthesis only in a transient way for a short period of time, thus requiring frequent administration. Furthermore, its single strand structure and the fully hydroxylated nature of its ribose portion make mRNA more susceptible to fast degradation. Finally, mRNA production and purification require few more steps in comparison to plasmids synthesis, and pharmaceutical grade mRNA is produced only by two companies, Asuragen and CureVac.

1.4 Gene delivery systems: past, present and future

Since nucleic acids are negatively charged biomacromolecules, their ability to enter into cells is very low. Thus, a question could arise: how can genetic material be delivered into cells and, more specifically, into the proper cellular compartment? Several strategies were adopted by researchers to efficiently deliver nucleic acids into cells and to elicit their therapeutic effects.

In general, two basic mechanisms of transfection can be distinguished: the membrane-disruption mediated mechanism, based on physical method, and the carrier-mediated mechanism (Figure 7).[32]

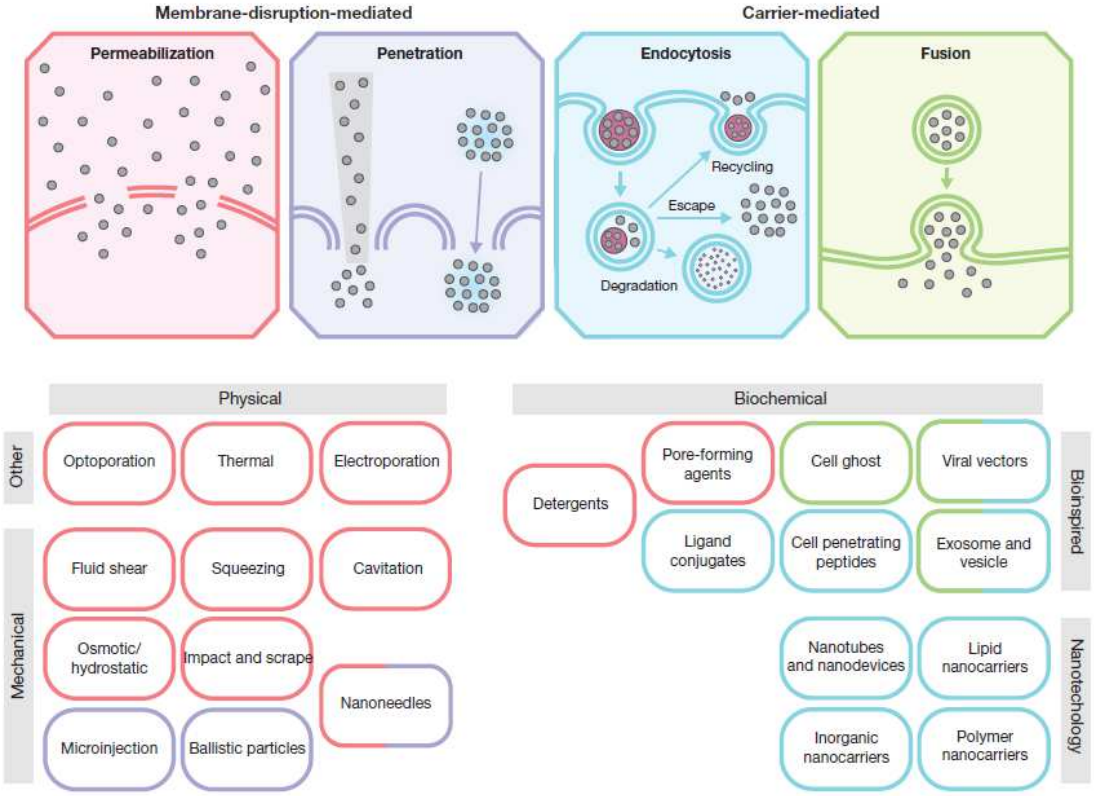

Figure 7. *Map of the different intracellular delivery approaches for nucleic acid-based therapeutics.*[32]

1.4.1 Nucleic acid delivery by physical methods

Physical methods for nucleic acids delivery exploit physical forces, either mechanical or of other nature, to induce the passage through the plasmatic membrane of DNA/RNA, resulting in high gene transfection. For this purpose, many different techniques were used, such as microinjection, electroporation, sonoporation, and ballistic DNA particles.

Briefly, microinjection consists on the direct injection of genetic material into the cell membrane and/or the nuclear envelope one cell at a time through the use of glass microneedles. Despite the high efficiency and specificity, this method is difficult and laborious and its application is limited to *in vitro* and *ex vivo* cell transfection.[33]

Another common tool for gene delivery is the electroporation, that consists into the formation of nanopores in cell membranes induced by the application of an high voltage external electric field for a short period of time, thus inducing skin perturbation and permeabilization, and allowing the genetic material to enter the cytosol. Despite the development of electroporation devices by Genetronics Inc. and others, the high cell mortality associated with the application of the electrical field is a significant drawback that limits its clinical use.[33]

Similarly, sonoporation exploits the acoustic cavitation phenomena induced by application of ultrasound waves with proper frequencies to improve gene transfection by inducing mechanical perturbation of the cell membrane and generating small transient holes in the cell membrane. As for electroporation, the major drawback is the damage of the target cells induced by the technique.[34]

An alternative method is the biolistic delivery, in which naked DNA is precipitated on metal nanoparticles (e.g. gold, silver or tungsten NPs) of 1 μm size. Particle bombardment equipment, such as the helium-driven gene guns, is used to accelerate to high velocity the DNA coated microparticles and allow cell membranes penetration. However, as for others physical techniques, this procedure is applied mainly to adherent cell cultures.

Indeed, gene transfer through physical transfer methods is limited to local targets, such as skin, muscle, or mucosal tissue, while other tissues require invasive surgeries procedures. Furthermore, the generation of holes and their dimension influence both the treatment outcome and the cell viability, thus inducing the researchers to seek for alternative non-physical-mediated gene delivery techniques.

1.4.2 Viral vectors

Recombinant non-pathogenic attenuated viruses are the most effective vectors for gene therapy and they are currently used in more than 67% of clinical gene therapy trials.[29] Adenoviruses, retroviruses, adeno-associated viruses and herpes simplex viruses are the most used vectors in this field and their highly evolved and efficient transfection mechanism is exploited to transfer genetic material into cells. Particularly, viral vectors are generated by replacing a section of the viral genome with a gene encoding for the therapeutic molecule. In 2004 FDA approved the first gene therapy product, a recombinant human p53 adenoviral vector (Gendicine®) for the treatment of head and neck squamous cell carcinoma. Furthermore, the lack of pathogenicity and the easy manipulation of recombinant adeno-associated viruses (AAVs) has brought to the approval of Glybera® in 2012 for the treatment of lipoprotein lipase (LPL) deficiency in patient with multiple attacks of pancreatitis. Finally, oncolytic virotherapy exploits viruses that are able of specifically target to and replicate in tumor cells, resulting either in cell lysis and tumor eradication or in an antitumor immune response. In this context, Imlygic™ was the first oncolytic virus to be marketed for the treatment of melanoma.

Despite the FDA approval of viral vectors and the numerous clinical trials ongoing, the safety concern is the main limit of virus-based gene therapy, since the possibility that the viruses revert to a wild-type virion is always open. In addition, viruses can elicit a strong immune response, as happened in the 1999 when adenoviruses caused 18-years old patient death the day after the administration.[35] Hence, a lot of efforts were done to develop safer non-viral gene delivery systems.

1.4.3 Drug delivery systems: polyplexes and lipoplexes

Safety concerns have prompted the development of synthetic gene delivery vectors not based on viral systems, that can be categorized mainly in lipid-based and polymer-based delivery systems. In both cases, the presence of cationic-charged groups is a common feature required to allow the charge to charge interaction with anionic phosphate groups of the nucleic acids, thus resulting in the formation of complexes. More specifically, complexes obtained with cationic lipids and cationic polymers are referred as lipoplexes and polyplexes, respectively. Since protonable amine groups usually confer the cationic nature to these materials, researchers refer to the N/P ratio as the molar ratio between polymer/lipid positively-charged nitrogen (N) groups and the nucleic acid negatively-charged phosphate (P) groups.

Some general features are required for an efficient gene delivery. Carriers should be stable in the extracellular milieu and must protect loaded nucleic acids from extracellular and intracellular fast degradation. Furthermore, DDSs cellular internalization and the subsequent endosomal escape for cargo access to the cytosol are essential features for the carrier to provide an effective gene therapy. Finally, the systems must be able to release the cargo and, for pDNA delivery, to permit its nuclear entry.

1.4.3.1 Lipid-based systems

Concerning the lipid-based gene delivery systems, several studies have shown their high transfection efficiency both *in vitro* and *in vivo* compared to naked DNA. They are bio-inspired carriers, according to the high biocompatibility and bio-similarity of lipid bilayers with biological membrane. Cationic lipids are usually added to the canonical liposomal formulations. Historically DOTMA ((N-(1-(2,3- dioleyloxy) propyl)-N, N, N-trimethylammonium chloride)) was the first synthetic cationic lipid used for luciferase mRNA

complexation and delivery in 1989, followed by DOTAP ((1,2-dioleoyl-3-trimethylammonium-propane), which is cheaper to synthesize and possesses superior delivery efficiency.[36]

It is worth to note that positively charged lipoplexes while showing good transfection *in vitro*, do not provide satisfying *in vivo* efficacy since cationic liposomes can be quickly eliminated by the mononuclear phagocyte system and showed rapid clearance and inflammatory responses. These drawbacks were overcome by the further decoration of lipoplex surface with poly(ethylene) glycol (PEG) which increases the blood circulation time and reduces the cationic lipid-induced toxicity and liposomes aggregation. On the other hand, PEG chains density and length must be well tailored to avoid a decrease in liposomes cellular uptake. Furthermore, the molar ratio between cationic lipids and anionic nucleic acids should be carefully balanced, since several studies demonstrated that higher charge ratios (that is higher positive charge density) promote higher transfection efficiency, but also reduce the proportion of cell viability.[37]

Regarding lipoplexes endosomal escape, different mechanisms were hypothesized.[30] Szoka and coworkers hypothesized that the flip-flop movements of the negatively charged endosomal phospholipids from the cytoplasmic- to the inner-facing lipid layer destabilize the endosomal membrane and lead to the diffusion and interaction of anionic lipids with cationic lipids of complexes, resulting in membrane fusion and genetic material release in the cytosol.[38] On the other hand, several studies showed that while cationic lipids are necessary for nucleic acids complexation, they play a minimal role in the cell membrane interaction, thus in the endosomal escape process. Zuhorn *et al.* showed that addition of neutral lipid "helper" such as DOPE (1,2-dioleoyl-sn-glycero-3-phosphoethanolamine) improves also the endosomal escape by facilitating liposome transition from a bilayer structure to the highly fusogenic hexagonal arrangement under acidic endosomal pH, thus promoting the fusion or the destabilization of endosomal membrane.[39] Finally, Cornelis *et al.* proposed a detergent-like destabilization mechanism of the endosomal membrane as responsible for the endosomal escape of undissociated lipoplexes.[40]

The success of lipid-based systems in cell transfection is confirmed by the wide use of Lipofectamine® (Invitrogen) as standard transfection reagent, since its launch in 1993. It is composed by cationic lipids, that complex genetic material, and by neutral fusogenic co-helper lipids. However, Lipofectamine® is suitable only for *in vitro* transfection.

Moderna Therapeutics, a clinical stage biotechnology company that is pioneering mRNA therapeutics and vaccines, have developed its proprietary lipid nanoparticles (LNP) formulations for the delivery of mRNA molecules to specific tissues, employing biodegradable ionizable lipids, such as MC3 and its analogues.[41]

Regarding the use of lipoplexes for vaccination, another interesting approach was reported by Hattori *et al.*.[42] They designed and tested *in vivo* a mannosylated cationic liposome (Man-C4-Chol) for the active targeting on DCs by mannose receptor-mediated endocytosis, showing a stronger T cell response when pDNA encoding ovalbumin was delivered through Man-C4-Chol compared to unmodified liposomes.

1.4.3.2 Polymer-based systems

Cationic polymers have emerged as the perfect non-covalent interaction partners for a variety of genetic payloads, providing similar molecular weight but opposite ionic charge. The use of self-assembling polymeric nanocarriers for gene delivery is, however, quite recent, but it has already shown large potential. Polymers can bind, condense, protect, and release nucleic acids into cells, but can also undergo undesired interactions with biological components after administration, resulting in loss of activity and toxicity.

The increasing knowledges on how to tailor cationic polymers for efficient gene delivery and the considerable progresses in synthetic techniques have resulted in the design and synthesis of polymers with different architecture and composition and multiple functions.

Since its use in clinical trials in 1973, diethylaminoethyl (DEAE)-dextran was found to be very useful for the delivery of various infectious viral genomes. However, its relatively low delivery capacity, its toxicity and its non-biodegradability discouraged its subsequent use.[43] In 1975 Farber and colleagues[44] compared the transfection efficiency of DEAE-dextran, spermine, polyornithine, polylysine, and polyarginine, concluding that polyornithine performed best. Despite it is not the best polymeric vector by itself, polylysine (PLL) gains the attention for gene delivery application. Indeed, PLL transfection efficiency was increased through several modifications. For example, George and Catharine Wu firstly reported the higher *in vitro* and *in vivo* performances of PLL conjugated with asialoorosomucoid for asialoglycoprotein receptor-mediated DNA delivery to hepatocytes.[45] Furthermore, since the low efficacy of PLL could be ascribed to the lack of a mechanism of endosomal escape,

several studies considered the addition of an endosomolytic agent either as free molecule, such as chloroquine[46], or by adding imidazole-based moieties to the polymer chain.

In this scenario, polyethylene imine (PEI) became the gold standard for gene delivery for more than a decade. Indeed, PEI and in general polyamines are partially protonated at physiological pH, thus enabling nucleic acids complexation, but their protonation degree further increases in the endosomal vesicles, acting as "proton sponge". The amine groups with pKa<7.4 absorb incoming hydrogen ions, thus inducing an influx of chloride ions which leads to an osmotic pressure increase, that could destabilize the endosome membrane. Only the 15-20% of PEI amines are protonated at pH 7.4, ensuring for high proton sponge ability once exposed to acid environment of the endosomes. Polymers of different molecular weights and different architectures (branched, BPEI, or linear, LPEI) can be generated. It was found that LPEI/DNA complexes perform better than BPEI/DNA, in virtue of a weaker complexation and lower stability that allow a higher and faster gene release and expression.[47] However, PEI is not an ideal gene delivery agent by itself as it is significantly toxic in a molecular weight-dependent manner. PEI with a molecular weight above 2000 Da shows a relevant cytotoxicity, the low molecular weight derivative shows a good biocompatibility but it is ineffective in terms of transfection. Many promising approaches to overcome PEI safety concerns were investigated, such as its N-acylation[48] or PEGylation[49]. Despite the several drawbacks, polyethyleneimine was also used in few clinical trials. As an example, in the phase II trial NCT00595088 the efficacy and safety of DTA-H19/PEI polyplexes (pDNA encoding for the diphtheria toxin A chain under the regulation of the H19 promoter) were evaluated for the treatment of patients with intermediate risk superficial bladder cancer who have failed prior intravesical therapies. The same polymer was complexed also with SST2 and DCK::UMK genes encoding for somatostatin receptor subtype 2 and for critical enzymes for Gemcitabine intracellular metabolism, respectively (gene-therapy product CYL-02). The phase I clinical trial NCT02806687 demonstrated that the gene-therapy product CYL-02 is expressed in pancreatic ductal adenocarcinoma tumors, is distributed within the bloodstream in some extent, and can inhibit primary-tumor progression and dissemination when combined with standard Gemcitabine treatment.

More complex dendrimeric structures were also evaluated for gene delivery, including poly(amidoamine) (PAMAM). The large number of secondary and tertiary amines on PAMAM surface are responsible of the proton sponge effect, thus of the high transfection

efficiency. However, as the dendrimer generation increases, dendrimers become more branched and efficient in transfection, but also less biocompatible.[50]

Looking forward to safer gene delivery systems, scientists get inspired by nature and the use of natural polymers was taken into account. As an example, cyclodextrins, natural cyclic oligosaccharides composed of 6, 7 or 8 glucose units (α-, β- or γ-cyclodextrin), were explored for transgene delivery. Particularly, cationic cyclodextrins were prepared by modification with PEI, PAMAM or other cationic polymers and showed a decreased toxicity with respect to the use of the same polymers by itself.[51] Moreover, chitosan and its quaternized derivatives have been successfully applied for pDNA and siRNA delivery, eventually after modification with targeting ligands or with endosomal escape-promoting groups.[52]

Finally, the design of biodegradable and well-tolerated polymers was a fundamental breakthrough in the field. Since it was demonstrated that the toxicity of cationic polymers increases with the molecular weight, ester bonds, disulfides, ketals, imines and some amide bond were exploited for bioreversible cross-linkage of low MW polymers.[53,54]

As for lipid-based DDSs, mannose-targeted polymers/DNA complexes were studied by Zhou and collaborators for HBV (hepatitis B virus) vaccination.[55] Mannose-bearing chitosan microspheres entrapping HBV DNA/PEI complexes were found to improve the delivery of DNA into antigen-presenting cells and to enhance serum antibody and cytotoxic T lymphocyte responses after intramuscular injection in comparison to non-targeted microspheres and to naked DNA.

1.5 Polyplexes basic features for efficient gene delivery

Gene-delivery vectors must overcome a series of barriers, both in the extracellular and in the intracellular milieu, to deliver genes to the cell nucleus. Similarly to what Nature did with viruses, that are endowed with appropriate and tailored functions to cross biological barriers, synthetic vectors-based gene delivery systems have to be logically instructed with a rational design of their components (namely polymers) to overcome the different barriers. In the following paragraphs the main bottlenecks for an efficient non-viral gene delivery and the design criteria for non-viral vector are extensively discussed.

1.5.1 Protection of genetic material

Cationic polymers condense DNA into small nanoparticles through entropically-driven electrostatic interactions with the sugar-phosphate backbone of the nucleic acid. The formation of these dense assemblies protects genetic material by sterically blocking the access of nucleolytic enzymes, thus ensuring DNA stability for hours. Several studies reported an effect of the polymer structure on DNA binding, with an increased DNA binding for polymers bearing the cationic moieties nearer to the polymer backbone and to a minimum separation along the polymer backbone. However, a too tight nucleic acid condensation could prevent DNA transcription by hampering its release after internalization into cells. Thus, polymer cationic charge must be balanced.[51]

Here, the cationic charge of agmatine was exploited to allow a tight complexation of pDNA and polymers with different cationic block length were designed to tune the complexation strength and the release capacity of the investigated systems.

1.5.2 Polyplexes stability

The stability of polyplexes depends on the polymer structure and the N/P charge ratio. During self-assembling with nucleotides, neutral polyplexes quickly form large aggregates, while positively charged polyplexes typically form colloidal suspensions. Although chemical and physical properties of polyplexes can be controlled during processing and formulation, the main concern regards polyplexes conformational changes when exposed to *in vivo* environment. Indeed, after polyplexes administration serum albumin and other negatively charged proteins can be adsorbed on particles surface, leading to aggregation and subsequent clearance of the systems.[30] Particle colloidal stability is one of the most important requirements for non-viral gene delivery systems. Particularly, the use of polycationic polymers modified with hydrophilic components, such as PEG or N-(2-hydroxypropyl)methacrylamide (HPMA), glycosidic moieties and proteins, that will likely be exposed on the surface of polyplexes, can stabilize polyplexes through steric effect forming an outer corona, thus leading to decreased particle-particle and particle-protein interactions. The molecular weight, the density, the structure and the conjugation method of the hydrophilic components to the polycationic block must be well tailored to reduce the impairment of polyplexes cellular uptake.[51]

In the present project, a mannosylated block was conjugated to a polycationic block both to endow the system with DCs targeting ability, as extensively explained in paragraph 1.6.1, and to provide a hydrophilic corona to the polyplexes to guarantee system stability. Indeed, mannose pendant groups present five hydroxyl groups, providing a high hydrophilic corona once the polyplexes are formed.

1.5.3 Nucleic acid internalization

One of the major barrier polyplexes encounters after administration is the cellular membrane. Although size, shape and surface charge deeply affect polyplexes internalization, it is difficult to predict the specific contribution of each parameter to the uptake rate, route and efficiency. An inverse correlation between polymeric particles size and uptake at a fixed surface charge was found by He and coworkers,[56] while for equally sized nanoparticles, internalization rates increase with surface charge because of the stronger affinity for the negatively charged cell membrane. It is worth to note that the majority of the studies on the effect of these parameters are based on discrete (metallic and/or polymeric) nanoparticles instead of polyplexes.

Regarding the uptake mechanism, positively charged polyplexes bind the cell surface by non-specific charge-charge interactions with cell membrane anionic components and then are internalized mainly by clathrin-mediated, caveolae-mediated, clathrin/caveolae-independent endocytosis or by macropinocytosis.[57]

Polymers with their flexible chemistry can be very exploited for the genetic material delivery to a very specific cells subset. Indeed, different targeting moieties can be attached to the polymer end or as pendant groups either to increase cell uptake or to confer cell specificity for cell surface receptors. Both small molecules, such as glycosidic groups or folic acid, and biomacromolecules, e.g. asialoorosomucoid, epidermal growth factor or transferrin proteins were used for active targeting of gene carriers.[58,59] Notably, in order to ensure the specificity of active delivery of nucleotides-loaded carriers, the contribution of non-specific electrostatic binding to cell surface should be minimized; thus the polymer/DNA ratio should be maintained near electroneutrality. Indeed, efficient active cell targeting requires an optimal tailoring of polyplexes physico-chemical features, ligand-polyplex spacer, ligand-receptor binding strength and optimal ligand valency.

As explained in details in paragraph 1.6.1, in this work mannose was exploited as targeting agent to specifically target antigen presenting cells (i.e. dendritic cells) in view of developing a cancer vaccine. Particularly, polymers with different length of mannosylated block were synthesized to investigate the optimal density and valency of targeting moieties to guarantee an efficient cell selectivity and uptake.

1.5.4 Endosomal escape

Although more than 95% of cells typically internalize gene vectors *in vitro*, the transgene is expressed by less than 50% of them.[51] Regardless of the endocytic pathway of internalization, endosomal escape is an essential step for efficient transfection. Indeed, endosomes can fuse with intracellular acidic vesicles, namely lysosomes, where genetic material can be enzymatically hydrolyzed. To overcome this bottleneck, the use of polymers bearing primary, secondary, and tertiary amines with pKa values between physiological and lysosomal pH is the major adopted strategy. Indeed, these polymers undergo alteration of the protonation degree during endocytic trafficking, thus providing the so called "proton sponge effect": amino groups become protonated in the endo-lysosomal acidic compartment with subsequent vesicles osmotic swelling, rupture of the endosomal membrane, and release of the polyplexes into the cytosol.[60] Alternatively, fusogenic viral or synthetic peptides were also exploited to endow polyplexes with endosomal escape properties. Indeed, the acidic pH induce a structural conformation switch in these peptides, that assume an α-helix conformation that interact with and disrupt endo-lysosomal membrane, allowing the release of the cargo in the cytosol.[61] Finally, in this work a different strategy was exploited for endosomal escape that is based on hydrophobic interactions between the polymer and endosomal membrane, which relies on the inclusion of a butyl-based block on the cationic co-polymers. Indeed, as it was hypothesized for lipoplexes, a hydrophobic block could destabilize the endosomal membrane by inducing flip-flop movements of the negatively charged endosomal phospholipids in the inner layer or a detergent-like destabilization mechanism of the endosomal membrane.

1.5.5 Nuclear entry

Complexes that escape from the endocytic compartments end up in the cytoplasm and, for pDNA-based gene therapies, need to reach the nucleus. Since during cell mitosis the integrity of the nuclear envelope is transiently lost, transfection efficiency is higher when cells are

transfected in this cell cycle step. Nevertheless, also post-mitotic cells like neurons and cardiomyocytes could be transfected. Since many proteins are naturally targeted to the nucleus by short cationic peptide sequences, called nuclear localization signals (NLS), which are recognized by specific nuclear import proteins, namely importins, it was hypothesized that positively charged polyplexes could mimic NLS at some extent, thus permitting nuclear entry even if with limited efficacy.[62] Furthermore, carbohydrate-binding receptors reside also intracellularly and constitute an opportunity to exploit glycosidic moieties not only for the active cell-specific delivery but also for the cytonuclear transport.[63] Nuclear lectins were first detected by Sève *et al.* using neoglycoproteins,[64] strongly suggesting that sugar residues could act as nuclear targeting signal. Particularly, bovine serum albumin (BSA), a non-nuclear protein that usually does not pass through nuclear pores, when substituted with specific carbohydrates can be transported into the nucleus by specific transporters. The study showed that BSA bearing 25 ± 4 α-D-glucosyl (Glc-BSA), β-di-N-acetylchitobiosyl (GlcNAc β-4Glc-NAc-BSA), α -D-mannosyl (Man-BSA) or α-L-fucosyl (Fuc-BSA) residues efficiently entered the nucleus of HeLa cells.[65]

Given these findings, mannose has been selected to develop the polymeric platforms designed in this study as we hypothesized it would have played a triple role: targeting specific cells, stabilizing the complexes by a hydrophilic corona, and also facilitating the nuclear trafficking of our gene delivery systems, which can be helpful for DNA-based vaccines.

It is also worth mentioning, in view of optimizing the nuclear entry, that Kim *et al.* reported a better transfection efficiency of arginine-grafted polyplexes in comparison to the plain version, which was ascribed to a good nuclear localization ability of arginine groups.[66] Furthermore, an effect of the alkyl spacer length on the subcellular localization of non peptidic- guanidine-capped dendrimers was found by Huang *et al.* with dendrimer with an ethyl- or a hexyl- spacer disposing in the nucleus and in the cytosol, respectively.[67] Therefore, our choice of agmatine, since it bears a butyl-spacer and guanidine as cationic pendant group, could also provide additional key features to the polycationic polymer for gene delivery purposes.

1.6 Passive and active targeting

Smart nanocarriers for a controlled and precise release of anticancer therapeutics at the desired site of action were designed exploiting either the tumor leaky vasculature and the particular features of tumor environment or the overexpression of receptors or mutated proteins on the cell membrane. In particular, we can refer to the passive and to the active targeting strategy, respectively.

In this work, we developed nanocarriers for the specific and active targeting of DCs, thus developing systems for subcutaneous injection and that do not need to accumulate in tumor to be effective. As passive delivery strategy is not the focus of this thesis project, it will not be described in further detail here.

In the active targeting approach, specific molecules which interact at the molecular level with an overexpressed receptor on cell membrane are conjugated to the nanocarrier surface, increasing the selective interaction at the target site and the specificity of the therapy. The ligand-receptor binding affinity and specificity, the density of the targeting agent, the stability, the immunogenicity and the chemistry of conjugation are some parameters useful for the choice of the most suitable targeting agent. Many different targeting agents have been investigated in the drug delivery field, ranging from macromolecules such as peptides, proteins, antibodies and nucleic acids to small molecules such as folic acid or sugars.

Here, mannose was used as targeting moiety for the selective and active targeting of the mannose receptor (MR), also called cluster of differentiation CD206, expressed on the surface of antigen presenting cells.

1.6.1 Mannose as targeting molecule

The mannose receptor (MR) is a 180 kDa transmembrane glycoprotein, member of the C-type lectin family of receptors, that present five domains, represented in Figure 8: the N-terminal cysteine-rich (CR) domain, the fibronectin type II (FN II) domain, eight tandem units of C-type lectin-like domains (CTLDs), a transmembrane domain and a cytoplasmic carboxy-terminal domain.[68,69] Each domain appears to have a peculiar function and a different specificity in recognition. Mannose and fucose recognition is restricted to the CTLDs and more specifically only the 4^{th} unit is capable of carbohydrate bind activity, while glycoproteins bearing sulfated sugars are recognized by the CR domain. The extracellular carbohydrate binding domain is Ca^{2+} and pH- dependent and after carbohydrate binding the

short cytoplasmic domain directs the trafficking of these receptors from the plasma membrane to the endosomal apparatus. The progressive acidification of endocytic vesicles promotes the dissociation of Ca^{2+} and the subsequent recycling of receptors on the cell surface. Indeed, MR is an endocytic receptor that continually cycles between the endosomal compartment and the cell membrane.

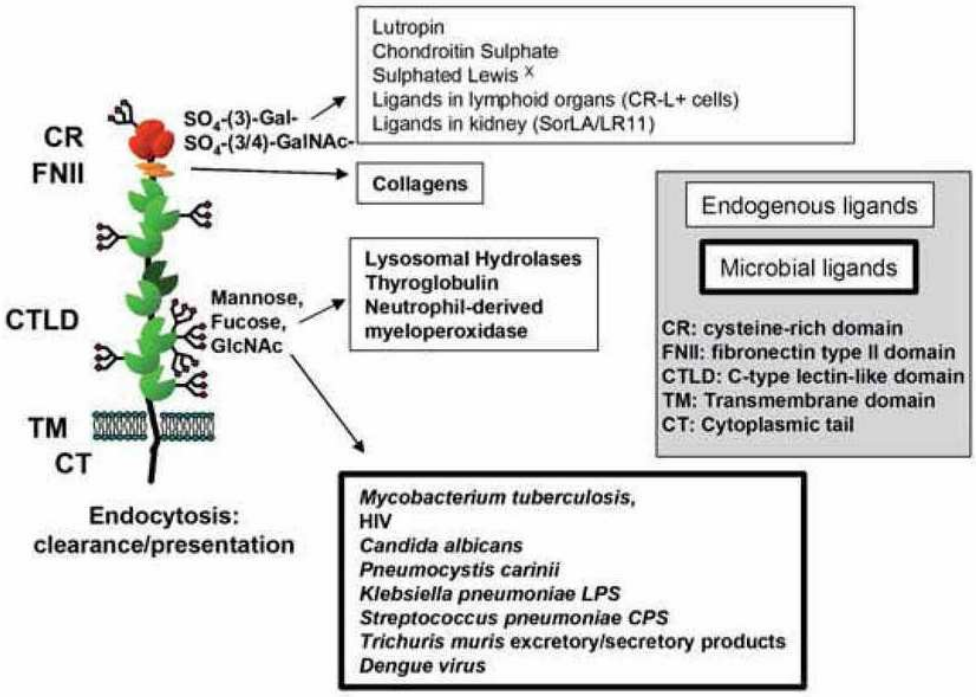

Figure 8. *Schematic representation of the domain structure of MR and endogenous and microbial binding molecules.*[70]

The mannose receptor family includes four members that mediate different functions: Endo 180 (CD280), DEC-205 (DC205), phospholipase A2 receptor (PLA2R) and mannose receptor (MR, CD206). Particularly, the MR is the receptor able to mediate both endocytosis and phagocytosis, facilitating the clearance of pathogenic particulates or endogenous molecules, promoting antigen presentation, stimulating the immune response and preserving the immune homeostasis. Indeed, macrophage MR physiologically recognizes bacteria, fungi, virus, parasites and a variety of other microorganisms and interacts with them, since many pathogens are coated with mannose-based structures.

Mannose receptor is expressed by most tissue macrophages and dendritic cells, particularly monocyte-derived and dermal DCs, as well as by subset of endothelial cells and by specialized cells such as mesangial cells, trachea smooth muscle and retinal pigment epithelium. Surface modification of carriers by mannosylation is a strategy adopted for a

faster and more efficient delivery of most imaging, diagnostic or therapeutic agents that target MR on macrophages or dendritic cells. In this scenario, in 2013 FDA approved the technetium (^{99}Tc)-labelled Tilmanocept (Lymphoseek®) from Navidea Pharmaceuticals. Lymphoseek® is a radioactive diagnostic agent employed for precision imaging and intraoperative detection of sentinel lymph nodes draining a primary tumour in adult patients with breast cancer, melanoma, or localized squamous cell carcinoma of the oral cavity. It is a diagnostic receptor-targeted radiopharmaceutical that accumulates in lymphatic tissue either by passive accumulation thanks to its small diameter (7 nm) or by specifically binding to mannose receptors on the surface of lymph-node resident dendritic cells and macrophages. Indeed, Lymphoseek® consists of multiple units of diethylenetriaminepentaacetic acid (DTPA, as ^{99}Tc chelating moiety) and mannose (as substrate for the MR), each attached to a 10 kDa dextran backbone.

Several strategies have been developed for MR-targeted vaccines, either exploiting natural MR ligands or specific mAb.[4] In our project mannosylated polymers were also designed to induce a faster and more efficient targeting of dendritic cells, thus boosting the internalization of our model or therapeutic macromolecules (oligonucleotides and pDNA) and eventually their processing by APCs.

1.7 Reversible Addition Fragmentation chain Transfer (RAFT) polymerization

Biopolymers, such as proteins and nucleic acids, derive their highly specialized functions from the perfectly tuned monomer sequence, regulated at the molecular scale. Despite Nature's precision in regulating monomers sequence remains unmatched in non-natural macromolecules, over the past 60 years block copolymer synthesis has made considerable progress with the introduction of living anionic polymerization and with the advances of "living" radical polymerization (LRP) techniques, such as atom transfer radical polymerization (ATRP), nitroxide-mediated radical polymerization (NMP) and reversible addition−fragmentation chain transfer (RAFT) polymerization.[71] In this work, multiblock co-polymers were synthesized using RAFT polymerization, a living free-radical polymerization technique invented by Commonwealth Scientific and Industrial Research Organization (CSIRO) and described for the first time in 1998 by Chiefari *et al.*.[72] RAFT polymerization

can be used with a wide range of monomers and reaction conditions and it provides controlled and predictable molecular weight polymers with very narrow polydispersities (low M_w/M_n, Đ) and fully controlled number of monomers for each single block. Furthermore, RAFT technique permits to produce polymers whose extension chain can be easily re-activated to obtain the synthesis of block copolymers, stars, hyper-branched materials or other complex molecular architectures. In an ideal living polymerization, all chains are initiated at the beginning of the reaction, grow at a similar rate and survive the polymerization, without irreversible chain transfer or termination.

What makes the RAFT a living polymerization is the presence of a Chain Transfer Agent (CTA), i.e. RAFT agent, that guarantees the equilibrium between the addition and the fragmentation reactions and the fast exchange between the dormant and the active species. RAFT agents, which general structure is reported in Figure 9, are thiocarbonylthio species with a reactive C=S double bond and two substituents defined as Z and R, that strongly affect CTA activity. RAFT agents can be divided in four classes, depending on the nature of the Z group: dithioesters (1), trithiocarbonates (2, used in this project), dithiocarbonates or xanthates (3), and dithiocarbamates (4).

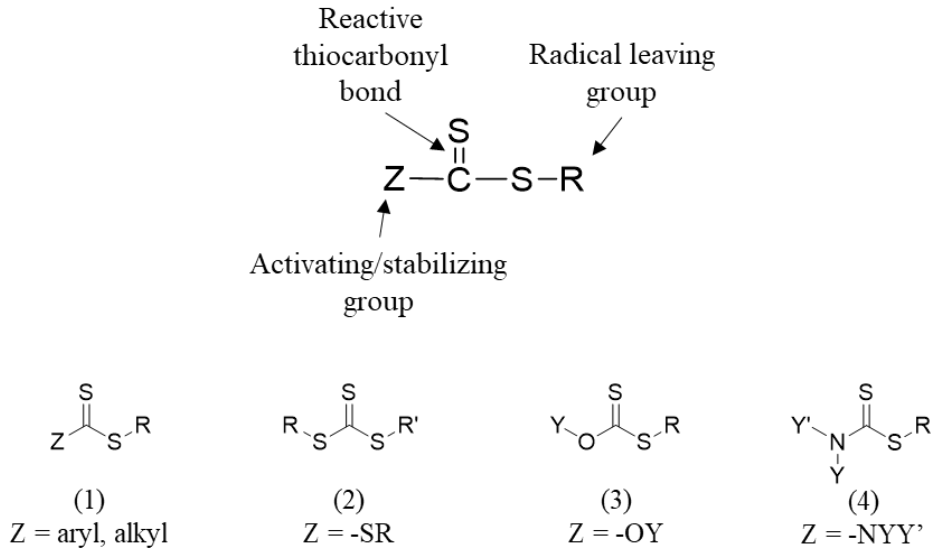

Figure 9. *General structure and different classes of common RAFT agents.*

Selection of the RAFT agent according to the monomers and reaction conditions is crucial for the success of the polymerization. The Z group has the role of controlling the reactivity of the chain-transfer agent, determining either the general reactivity of the C=S bond towards the radical addition or the half-life of the intermediate radical resulting from the addition of the

radical species to the C=S bond for heterolytic cleavage. Mainly, the transfer constant decreases in the series trithiocarbonates > xanthathes > dithiocarbamates. The R group is the free radical leaving group, and the radical generated by homolytic cleavage must be able to initiate the polymerization reaction, in the case of RAFT agent, or simply to add the monomer in the case of macro-chain transfer agent (macro-CTA).

Since radicals are not formed nor destroyed during the chain-transfer reaction, an external source of free radicals (initiator) is required for the RAFT polymerization, even if a low concentration is sufficient to trigger the reaction, thus promoting propagation over termination. The most frequent compounds exploited as initiators are peroxy- and azo-compounds, such as AIBN (azobis-isobutyronitrile) or 4,4'-azobis(4-cyanovaleric acid) (V-501) or 2,2'-azobis[2-(2-imidazolin-2-yl)propane]dihydrochloride (VA-044), that are able to thermally decompose and give two radical species and a molecule of N_2.

As reported in Scheme 1, in the initiation step the decomposition of the initiator (I) and its reaction with the monomer (M) leads to formation of propagating radical chains ($P_n^{\bullet}$). In the early stages, the addition of $P_n^{\bullet}$ to the C=S bond of the RAFT agent and the subsequent fragmentation of the formed radical intermediate gives rise to a polymeric RAFT agent, or macro-CTA ($P_nS(Z)C=S$), and to a new radical ($R^{\bullet}$). Reaction of this radical $R^{\bullet}$ with monomers forms a new propagating radical $P_m^{\bullet}$. The control over polymerization is achieved thanks to the rapid equilibrium between the active propagating radicals ($P_n^{\bullet}$ and $P_m^{\bullet}$) and the dormant polymeric RAFT compound ($P_{n/m}S(Z)C=S$). In this way the radical-radical termination is reduced and there is the same probability to grow for all the chains. At the end of the polymerization, the great majority of the chains contain the thiocarbonylthio moiety as end group, so end-functionalized polymers can be obtained by including functional groups into the R- or Z- groups of the RAFT agent.

The control of polymerization with the RAFT technique is the result of balance between addition, half-life of the radical intermediate, fragmentation, propagation, and the kinetic constants associated with them.[73] Since radical species control the number of "dead" chains, in order to allow a low polydispersity index and minimize the irreversible termination reactions, it is desirable to maintain the amount of radical species, that are related to the initiator concentration, low related to the dormant species. It is worth to note that the mainly bimolecular chain termination reactions are kinetically second-order as in conventional free radicals polymerization, with respect to the concentration of radical species, while the chain

propagation reaction shows a dependency of first order. The addition of the RAFT agent can influence the polymerization kinetic through a period of time with slow or absent polymerization or through a slower reaction than the one of the same reaction without the presence of the transfer agent. The initiation step can be an inhibition step by using RAFT agents that stabilize the radical adduct, e. g. Z = phenyl or other aromatic compounds, or that present an inefficiently reactive or a weak R leaving group.

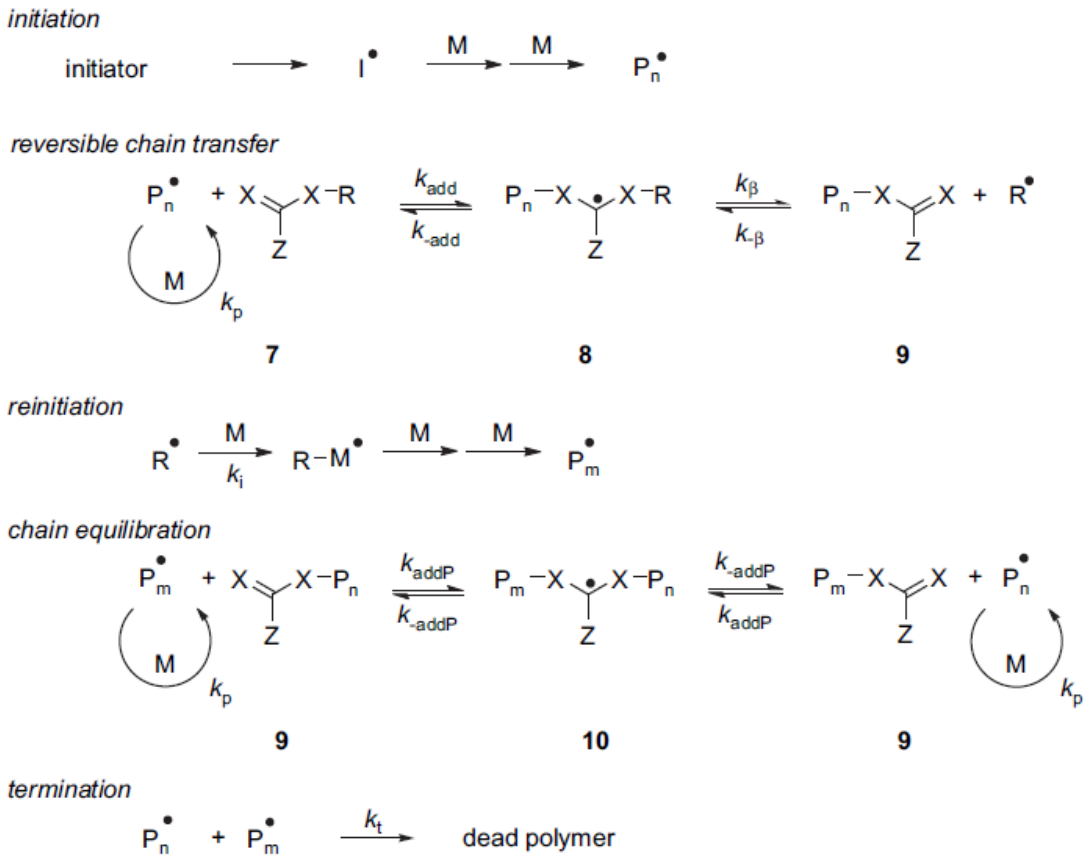

Scheme 1. *Mechanism of RAFT polymerization.*[3]

In here, we used an optimized fast, versatile, efficient and scalable method to prepare multiblock copolymers, known as fast RAFT polymerization and described for the first time by Gody and collaborators.[71,74] This approach permits a one-pot, multistep sequential polymerization in a reduced reaction time (e.g., from 24 to 2 h per block) and without a concomitant loss of livingness. Indeed, since in the RAFT process the number of dead chains is only governed by the number of radicals generated throughout the polymerization and not by their concentration, the rate at which these radicals are generated does not influence the livingness but only the rate at which those radicals terminate. Accordingly, an increase in the

rate of radical generation by using an initiator possessing a high decomposition rate coefficient (k_d) should speed up the polymerization without increasing the number of dead chains.[71] In this project we exploited the low decomposition temperature (44°C in water) of VA-044 to guarantee a high polymers livingness and a fast synthesis (2 h per block) of multiblock copolymer. Furthermore, full monomer conversion, without requiring any purification step between each block, was possible with this approach.

1.8 Aim of the project

Delivery of pDNA encoding Tumour Associated Antigen (TAA) to Antigen Presenting Cells, and in particular Dendritic Cells (DCs), is an emerging and promising approach to trigger immune response against cancer in oncologic patients.

The aim of the present work is the generation of two libraries of biocompatible cationic di-block and tri-block glycopolymers for nucleic acid delivery to Antigen Presenting Cells. The polymers are composed by ***1.*** a hydrophilic mannosylated block, ***2.*** a positively charged agmatine-based block and, eventually, ***3.*** a hydrophobic butyl-based block. In particular, the agmatine block is responsible for the condensation of nucleic acids by charge-charge interaction forming stable glycopolyplexes (GPPs), thus reducing nucleotides negative charge that usually hinders cell membrane crossing. Guanidine groups are expected to enable DDSs nuclear localization, improving transfection efficiency and performance of the formed polyplexes. The mannosylated block is expected to play a double role: it acts as the targeting agent to actively and selectively direct the GPPs to DCs expressing the Mannose Receptor (MR), that is known to bind mannose with high affinity, and secondly, it endows GPPs of a hydrophilic outer corona that confer colloidal stability to the systems. Finally, a 2nd generation of polymers has been designed by including a third block of butyl acrylate aimed at promoting GPPs endosomal escape.

The synergic effect of each portion is expected to improve the delivery of nucleotides (e.g. ODNs, siRNA, mRNA or pDNA), by preventing their enzymatical degradation and enhancing their selective uptake by antigen presenting cells through MR. Moreover, the presence of a hydrophobic block should prompt the nucleic acid release from endosomes and, where required, their nuclear localization. After preliminary studies with a model scrambled ssDNA sequence, pDNA was selected as gene therapy molecule in virtue of its easy and rapid *in vitro* GMP-certified production and its high stability. Indeed, as described in Figure 10, the final goal of the project is to set up a delivery system for pDNA encoding tumor-associated antigen (TAA) capable of an efficient and selective targeting of dendritic cells either *in vitro* and *in vivo*, thus triggering the direct immune response and a long-term memory against cancer, after pDNA transcription and translation and antigen presentation through the MHC complexes. Indeed, the systems are designed either for prophylactic or for therapeutic anticancer vaccination, enabling their subcutaneous administration for cancer prevention or eradication.

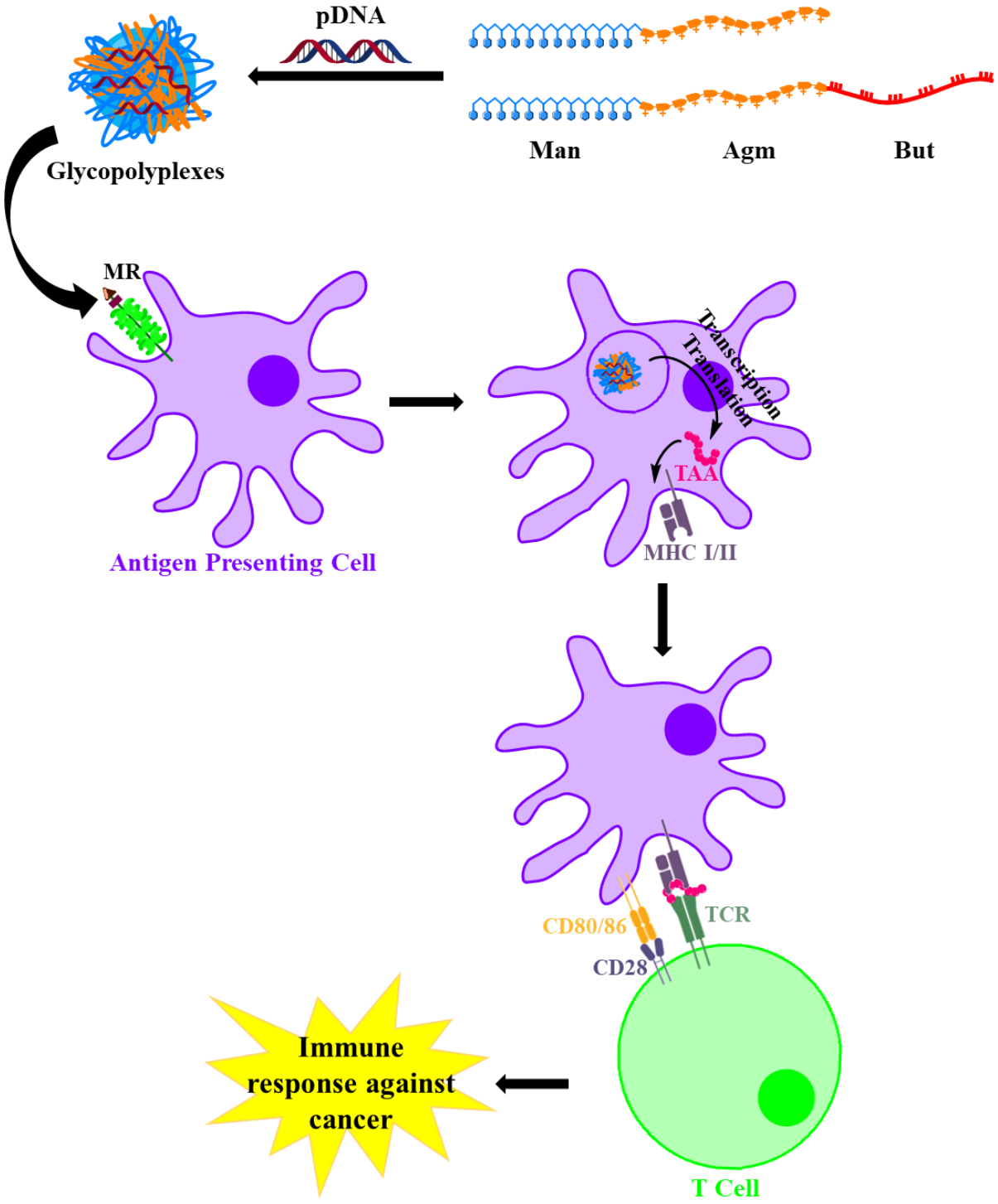

Figure 10. *Schematic representation of the glycopolyplexes formation and their mechanism of action within the immune system. After internalization by APCs, pDNA coding for TAA is transcribed and translated in the corresponding antigen. Antigen presentation by Major Histocompatibility Complex to T cells triggers the immune response and the memory against cancer.*

MATERIALS AND METHODS

2.1 Reagents

- Acryloyl chloride, Agmatine sulfate, Carbon disulfide, Ethanethiol, 4,4'-azobis(cyanopentanoic acid), N-Hydroxyethyl acrylamide, n-Butyl acrylate (But), 2,2'-azobis[2-(2-imidazolin-2-yl)propane]dihydrochloride (VA044), 1,4-Dioxane, Dimethylsulfoxide deuterated (DMSO-d_6), Boron trifluoride diethyl etherate (BF_3Et_2O), Deuterium oxide (D_2O), Tetrahydrofuran (THF), Acetone, Acetonitrile (MeCN), Methanol (MeOH), Chloroform ($CHCl_3$), Ammonium acetate, Acrylamide/bis acrylamide 30/1 solution, Low-medium EEO Agarose, Ammonium persulfate (APS), Boric Acid, Glycerol, Xylene Cyanol FF, Tris(hydroxymethyl)amminomethane chloride (Tris HCl), Ethylenediaminetetraaceticacid (EDTA), (4-(2-hydroxyethyl)-1-piperazineethanesulfonic acid) (HEPES), Dimethylsulfoxide (DMSO), Thiazolyl blue tetrazolium bromide (MTT), silicagel (60 Å, particle size 35-70 μ), Triton X-100, were obtained from Sigma Aldrich (St.Louis, MO, USA) and Fisher Scientific (Hampton, New Hampshire, USA).
- α-D-Mannose pentaacetate was purchased from Apollo Scientific (Stockport, UK).
- Analytical thin-layer chromatography (TLC) was carried out on aluminum sheets coated with silica gel obtained from MACHEREY-NAGEL GmbH & Co. KG (Düren, Germany).
- 19 nucleotides scramble single-strand DNA (ss-DNA) (5'-GAGATGTAAGGCCAGGCCG-3'), cyanin-3 labeled ss-DNA (Cy3-ssDNA) and cyanin-5 labeled ss-DNA (Cy5-ssDNA) were supplied by BIOMERS.NET GmbH (Ulm, Germany).
- pEGFP-N_3 from Addgene (Watertown, MA, USA) was kindly donated by Dr Marco Pirazzini (Department of Biomedical Sciences, University of Padova).
- CMV-promoted plasmid coding for ovalbumin (pOVA) was obtained by GeneScript (Leiden, Netherlands).
- pDNA were amplified by *E. coli* bacterial cell transformation using One Shot TOP10 Chemically competent E. coli (Invitrogene, Carlsabad, USA) and purified with a

NucleoBondXtra Midi kit (Macherey-Nagel GmbH, Düren, Germany). pDNA concentration and purity were measured on a NanoDrop One (ThermoFisher, UK) prior to complexation.

- GelRed nucleic acid staining solution 10000 X in water was purchased from Biotium (Fremont, CA, USA).
- Primary labeled antibodies for flow cytometry studies were supplied by BioLegend (San Diego, California, USA), eBiosciences (Waltham, MA, USA) or Proimmune (Magdalen Centre, Oxford, UK).
- Fetal bovine serum (FBS), Dulbecco's modified Eagle medium (DMEM), Ham's F12 medium (F12), Opti-MEM reduced serum medium, Roswell Park Memorial Institute (RPMI 1640) medium, α-Minimum Essential Medium (α-MEM), Non-essential aminoacids 100x solution, β-mercaptoethanol, L-Glutamine, Penicillin/Streptomycin solution, Geneticin (G418) disulfate salt, Trypsine solution, phosphate buffered saline (PBS) with and without calcium and magnesium, paraformaldehyde (PFA), DAPI and all the other reagents for cell culture were purchased from Sigma-Aldrich (St.Louis, MO, USA), Fisher Scientific (Hampton, New Hampshire, USA) or Gibco ThermoFisher Scientific (Waltham, MA, USA) companies.
- CHO (Wild Type Chinese Hamster Ovarian cell line), CHO-MR^+ (Mannose Receptor expressing CHO cell line) and DC2.4 (Dendritic Cell) cells were kindly donated by Prof. Luisa Martinez-Pomares (Faculty of Medicine & Health Sciences, University of Nottingham).
- Murine DC line JAWS II were purchased from ATCC (Manassas, VA, USA).
- The mouse melanoma cell line B16-OVA expressing chicken OVA was kindly provided by Prof. Richard Vile (Mayo Clinic, Rochester, MN, USA).
- The mouse Melanoma cell line B16-F1was kindly provided by Prof. Véronique Préat, (Université Catholique de Louvain, Louvain Drug Research Institute, Brussels, Belgium).
- The water used in this work was "ultrapure" water (MilliQ-grade, 0.06 μSiemens cm^{-1}, resistivity 18.2 MΩ cm) purified with a Millipore MilliQ purification system (MA,USA).
- Organic solvents, salts and buffers were purchased from Sigma Aldrich (St. Louis, MO, USA) and Fisher Scientific (Hampton, New Hampshire, USA).

2.2 Scientific equipment

- Bruker DPX400 Ultrashield 400 MHz (Billerica, MA, USA) and Spectrospin AMX 300 MHz (Fallanden, Switzerland) were used for monomers and polymers characterization. The data were processed with MestReNova 6.0.2 software.
- Solvents were evaporated with Buchi Rotavapor R-100 with Buchi Vacuum pump V-100 Buchi Heatingbath B-100 and Buchi interface I-100 (Cornaredo, Italy).
- Samples were centrifuged with Z300 Hemle Labortechnik (Wehingen, Switzerland) and on a Sigma 1-14 Laborzentrifugen from Sigma Aldrich (Saint Louis, MO, USA).
- Buffers were filtered with Millipore systems using 0.22 μm cellulose acetate filter (Bendford, MA, USA) and sonicated by Power Sonic 410 di Hwashin Technology (Seoul, Korea).
- pH determination was performed using Seven Easy S20-K Mettler Toledo pHmeter, supplied with the electrode Mettler Toledo InLab 413 (Schwerenbach, Switzerland).
- Hetassic HETO Lab Equipment (Birkerod, Denmark) freeze dryer was used for lyophilization.
- The Mass spectroscopy analysis were carried out with the Applied Biosystem Mariner ESI-TOF mass spectrometer (Monza, Italy).
- IR spectra were recorded on a FT-IR BXII Perkin Elmer (Norwoworkl, CT, USA).
- Polymers molecular weight and polydispersity were assessed by gel permeation chromatography (GPC) using the Viscotek TDA 302 system (Malvern, UK) equipped with a Refractometer (RI), a Low-Angle Light Scattering (LALS), a Right-Angle Light Scattering (RALS) and a Differential Viscosimeter (Visc). The data were elaborated by the Omnisec software 5.1.
- Dialysis membranes with a MW cut-off of 3.5 kDa were purchased by Spectrum Laboratories, Inc. (Rancho Dominguez, CA, USA).
- Gel electrophoresis was performed either with an Amersham Biosciences miniVE Electrophoresis and Electrotransfer Unit system, GE Healthcare (Milan, Italy) for acrylamide gel or with a Fisherbrand™ Sub-Gel Midi Horizontal Gel Electrophoresis Unit (Fisher Scientific, Hampton, USA) for agarose gel. Gel images were obtained with UV transilluminator ChemiDoc™ XRS + imaging system with Image Lab™ image acquisition and analysis software (Bio-Rad Laboratories, Headquarters, CA).

- The size characterization and the Zeta potential analyses were obtained by Dynamic Light Scattering and Doppler electrophoresis using Zetasaizer Nano ZS (Malvern Instrument Ltd., UK).
- Transmission electron microscopy (TEM) was performed using a Tecnai G2 (FEI, Oregon, USA). Samples were placed on a copper grid, the excess was removed with filter paper and then stained with uranyl acetate (1% w/v in deionized water). Images were elaborated by ImageJ Software 1.51.
- Multiwell plates detections were analyzed with the ELISA plate reader BIO-TEKTM INSTRUMENTS INC. EL 3II5X (Winooski, USA).
- The cell culture work was carried out under sterile conditions, using a biological safety cabinet International Pbi (Milan, Italy); cells were grown using CO_2 incubator International Pbi (Milan, Italy).
- Cytometric analyses were performed using a F500 Beckman Coulter flow cytometer (Becton, Dickinson and Company, Buccinasco, Milan) for uptake studies, with BD FACSCanto™ II from BD (Franklin Lakes, NJ, USA) for transfection studies and BD LSRFortessa™ from BD for immunological analysis. Results were processed with Flowing Software 2.5.1 (by Perttu Terho) and FlowJo Software v10.

2.3 Gel Permeation Chromatography (GPC)

Polymer molecular weights and polydispersity index (Đ) were assessed by GPC analysis with Malvern Viscotek TDA302 system thermostated at 40 °C equipped with TOSOH G4000 (10 μm, 7.8×300 mm) and G3000 (7 μm, 7.8×300 mm) PWXL columns in series eluted with 0.4 M ammonium acetate buffer pH 4.5. Data acquisition was performed by Omnisec 5.1 software using pullulan standard for calibration.

2.4 Removal of polymerization inhibitor from butyl acrylate

The phenolic inhibitor hydroquinone monomethyl ether (MEHQ) was removed from n-Butyl acrylate (10 mL) prior to use, by washing three times butyl acrylate with 10 mL of a 5% w/v NaOH solution in deionized water and drying the overlying phase containing the

monomer over anhydrous Mg_2SO_4.[75] The purified monomer was stored at -20° C to avoid spontaneous polymerization.

2.5 Synthesis of 4-cyano-4-(ethylsulfanylthiocarbonylsulfanyl)pentanoic acid

The synthesis of the RAFT agent 4-cyano-4-(ethylsulfanylthiocarbonylsulfanyl)pentanoic acid was performed in a two-step reaction according to the procedure described by Truong *et al.*.[76]

Synthesis of bis(ethylsulfanylthiocarbonyl)disulphide. In a 2 neck round bottom flask, 9.6 mL of a 0.5 mg/mL NaOH aqueous solution (0.12 mol) was added dropwise over 5 minutes under nitrogen atmosphere to a stirred solution of ethanethiol (7.4 mL, 0.10 mol) in a mixture of water/acetone 20:5 (25 mL) cooled on ice. Carbon disulfide (CS_2) (8.37 g, 0.11 mol) was added to the reaction with cooling and constant stirring over a 1 hour period and the reaction was stirred until total consumption of CS_2, that was checked by extended range ^{13}C-NMR. Potassium ferrocyanide (36.21 g, 0.11 mol) was immediately added and stirred for 30 min at 0 °C, until the solution turned dark yellow and a precipitate was observed. The reaction mixture was extracted with DCM and the organic layer was then washed twice with aqueous saturated $NaHCO_3$ (2x 30 mL), twice with distilled water (2x 30 mL) and dried with $MgSO_4$. After filtration the solvent was removed under reduced pressure to yield bis(ethylsulfanylthiocarbonyl)disulphide as a crude orange oil residue (9.5 g, 0.035 mols, 70% yield). The crude product was characterized by ^{1}H-NMR and ^{13}C-NMR and was used for the next step reaction without further purification.

^{1}H-NMR (400 MHz, $CDCl_3$, δ, ppm): δ 1.36 ppm (t, 3H, C*H*$_3$, 7.5 Hz), δ 3.31 ppm (q, 2H, C*H*$_2$, 7.5 Hz).

^{13}C{^{1}H}-NMR (400 MHz, $CDCl_3$, δ, ppm): δ 12.5 ppm (1C, *C*H$_3$), δ 32.7 ppm (1C, *C*H$_2$), δ 221.4 ppm (1C, -S*C*(S)S-).

Synthesis of 4-cyano-4-(ethylsulfanylthiocarbonylsulfanyl)pentanoic acid. 5 g of crude bis(ethylsulfanylthiocarbonyl)disulphide (0.021 mol) were dissolved in ethanol and 4,4'-azobis(cyanopentanoic acid) (8.30 g, 0.029 mol) was added. The reaction mixture was

degassed by nitrogen bubbling for 10 min, heated up at 60 °C and left under stirring at this temperature overnight. The reaction was then cooled down to room temperature and the solvent was evaporated under reduced pressure. The final product was purified by column chromatography on SiO_2 and was eluted using a gradient of DCM/EtOAc from 10:0 to 9:1. Two column purifications were necessary to remove traces of starting material. The solvent was removed under reduced pressure to yield the RAFT agent 4-cyano-4-(ethylsulfanylthiocarbonylsulfanyl)pentanoic acid (1.8 g, 8 mmol, 38% yield) as a yellow powder. The product was characterized by ^{1}H-NMR, ^{13}C-NMR and ESI-TOF mass spectrometry.

^{1}H-NMR (400 MHz, $CDCl_3$, δ, ppm): δ 1.36 ppm (t, 3H, C*H*$_3$CH$_2$, 7.4 Hz), δ 1.89 ppm (s, 3H, C*H*$_3$C), δ 2.48 ppm (m, 2H, C*H*$_2$CH$_2$COOH), δ 2.68 ppm (m, 2H, CH$_2$C*H*$_2$COOH), δ 3.33 ppm (q, 2H, C*H*$_2$, 7.4 Hz).

^{13}C{^{1}H}-NMR (400 MHz, $CDCl_3$, δ, ppm): δ 12.85 ppm (1C, *C*H$_3$CH$_2$), δ 25.02 ppm (1C, *C*H$_3$C), δ 29.48 ppm (1C, CH$_2$*C*H$_2$COOH), δ 31.55 ppm (1C, *C*H$_2$CH$_2$COOH), δ 33.69 ppm (1C, CH$_3$*C*H$_2$), δ 46.37 ppm (1C, CH$_3$*C*CN), δ 119.03 ppm (1C, *C*N), δ 176.18 ppm (1C, CH$_2$*C*OOH), δ 216.77 ppm (1C, S*C*(S)S).

ESI-TOF expected m/z $[M\text{-}Na]^+$ 286.0001, found 285.9994 (100.0%).

2.6 Synthesis of D-mannopyranosyloxyethyl acrylamide (Man)

D-mannopyranosyloxyethyl acrylamide (Man) was synthesized according to Obata *et al.*,[77] with slight modifications.

Synthesis of intermediate 2,3,4,6-O-tetraacetyl-D-mannopyranosyloxyethyl acrylamide. α-D-Mannose pentaacetate (10 g, 25.63 mmol) was dissolved in anhydrous acetonitrile (MeCN) (100 mL) and N-hydroxyethyl acrylamide (3.54 g, 30.76 mmol, 3.19 mL) was added under stirring. The reaction mixture was cooled down to 0 °C in an ice bath and then boron trifluoride diethyl etherate (BF_3Et_2O) (21.82 g, 153.78 mmol, 20 mL) was added dropwise over 1 hour. The reaction was left under stirring at room temperature (RT) for 48 hours. At scheduled times, the progress of the reaction was monitored by ^{13}C-NMR analysis in deuterated dimethylsulfoxide (DMSO-d_6) of samples withdrawn from the reaction solution,

by checking the shift of the anomeric carbon from 88 ppm in the starting material, to 97 ppm in the product.

At completion of the reaction, the solution was diluted with isopropanol and then the organic solvent was removed under reduced pressure. The yellowish viscous mixture was re-dissolved in dichloromethane (CH_2Cl_2), washed with saturated sodium bicarbonate ($NaHCO_3$) (3x100 mL) and then with deionized water (DI water) (2x100 mL). The organic layer was dried over magnesium sulfate ($MgSO_4$) and evaporated under reduced pressure. The crude product was purified by flash chromatography (Silica gel 60 Å, particle size 35-70 μm, gradient elution from 100% diethyl ether (Et_2O) to 100% ethyl acetate (EtOAc)). Fractions were analyzed by thin layer chromatography (TLC) (Et_2O/EtOAc 9:1 as eluent) and the appropriate were concentrated to give the 2,3,4,6-O-tetraacetyl-D-mannopyranosyloxyethyl acrylamide (3.40 g, 7.64 mmol, 29.79% mol/mol). The intermediate was characterized by ^{1}H-NMR, ^{13}C-NMR, ESI-TOF mass spectrometry and FT-IR spectroscopy.

^{1}H-NMR (400 MHz, DMSO-d_6, δ, ppm): δ 1.93 ppm (s, 3H, C*H*$_3$), δ 2.02 ppm (s, 3H, C*H*$_3$), δ 2.03 ppm (s, 3H, C*H*$_3$), δ 2.11 ppm (s, 3H, C*H*$_3$), δ 3.37 ppm (dt, J = 7.0, 3.5 Hz, 2H, OCH$_2$C*H*$_2$NH), δ 3.52-3.60 ppm (m, 2H, OC*H*$_2$CH$_2$NH), δ 3.97 ppm (m, 2H, CHC*H*$_2$COCH$_3$), δ 4.12 ppm (m, 1H, C*H*CH$_2$COCH$_3$), δ 4.89 ppm (d, J = 1.3 Hz, 1H, C*H anomeric*), δ 5.10 ppm (t, J = 9.9 Hz, 1H, C*H*), δ 5.15 ppm (dd, J = 3.5, 1.6 Hz, 1H, C*H*), δ 5.18 ppm (dd, J = 9.9, 3.5 Hz, 1H, C*H*), δ 5.60 ppm (dd, J = 10.1, 2.2 Hz, 1H, CH=C*H*H), δ 6.09 ppm (dd, J = 17.1, 2.2 Hz, 1H, CH=CH*H*), δ 6.25 ppm (dd, J = 17.1, 10.1 Hz, 1H, C*H*=CH$_2$), δ 8.30 ppm (t, J = 5.4 Hz, 1H, N*H*).

^{13}C{^{1}H}-NMR (400 MHz, DMSO-d_6, δ, ppm): δ 20.37 ppm (1C, *C*H$_3$), δ 20.41 ppm (1C, *C*H$_3$), δ 20.42 ppm (1C, *C*H$_3$), δ 20.55 ppm (1C, *C*H$_3$), δ 38.84 ppm (1C, *C*H$_2$NH), δ 60.22 ppm (1C, CH*C*H$_2$), δ 62.32 ppm (1C, *C*H$_2$CH$_2$NH), δ 65.92 ppm (1C, *C*HOC=O), δ 66.74 ppm (1C, *C*HOC=O), δ 68.34 ppm (1C, *C*HOC=O), δ 69.17 ppm (1C, *C*HCH$_2$OC=O), δ 97.16 ppm (1C, *C anomeric*), δ 125.65 ppm (1C, CH=*C*H$_2$), δ 132.05 ppm (1C, *C*H=CH$_2$), δ 165.31 ppm (1C, NH*C*=O), δ 169.95 ppm (1C, *C*=OCH$_3$), δ 170.05 ppm (1C, *C*=OCH$_3$), δ 170.08 ppm (1C, *C*=OCH$_3$), δ 170.51 ppm (1C, *C*=OCH$_3$).

ESI-TOF expected m/z [M-H]$^{+}$ 446.428, found 446.1674.

FT-IR ν = 3385, 2943, 1751, 1663, 1544, 1374, 1230, 1138, 1087, 981, 689, 601 cm^{-1}.

Deprotection of 2,3,4,6-O-D-mannopyranosyloxyethyl acrylamide to yield D-mannopyranosyloxyethyl acrylamide. 2,3,4,6-O-tetraacetyl-D-mannopyranosyloxyethyl acrylamide (3.40 g, 7.64 mmol) was dissolved in 38 mL of a potassium hydroxide (KOH) (42.87 g, 0.764 mmol) methanolic solution. The mixture was left under stirring at RT for 48 hours and then passed through a short pad of silica (Silica gel 60 Å, particle size 35-70 μm, eluent CH_3OH). The organic solvent was removed under reduced pressure to yield D-mannopyranosyloxyethyl acrylamide as white powder (2.055 g, 7.41 mmol, 97.11% mol/mol). The product was characterized by ^{1}H-NMR, ^{13}C-NMR, ESI-TOF mass spectrometry and FT-IR spectroscopy.

^{1}H-NMR (400 MHz, DMSO-d_6, δ, ppm): δ 3.30 ppm (m, 2H, C*H*$_2$NH), δ 3.37 ppm (m, 2H, C*H*$_2$OH), δ 3.42 ppm (m, 1H, C*H*OH), δ 3.45 ppm (m, 2H, C*H*$_2$CH$_2$NH), δ 3.59 ppm (m, 1H, C*H*OH), δ 3.62 ppm (m, 1H, C*H*OH), δ 3.64 ppm (m, 1H, C*H*OH), δ 4.47 ppm (t, J = 5.7 Hz, 1H, O*H*), δ 4.58 ppm (bs, 1H, O*H*), δ 4.62 ppm (d, J = 1.4 Hz, 1H, C*H anomeric*), δ 4.69 ppm (d, J = 3.9 Hz, 1H, O*H*), δ 4.73 ppm (d, J = 4.1 Hz, 1H, O*H*), δ 5.58 ppm (dd, J = 10.1, 2.3 Hz, 1H, CH=C*H*H), δ 6.08 ppm (dd, J = 17.1, 2.3 Hz, 1H, CH=CH*H*), δ 6.25 ppm (dd, J = 17.1, 10.1 Hz, 1H, C*H*=CH$_2$), δ 8.14 ppm (t, J = 5.4 Hz, 1H, N*H*).

^{13}C{^{1}H}-NMR (400 MHz, DMSO-d_6, δ , ppm): δ 39.58 ppm (1C, *C*H$_2$NH), δ 61.71 ppm (1C, *C*H$_2$OH), δ 65.83 ppm (1C, *C*H$_2$CH$_2$NH), δ 67.45 ppm (1C, *C*HOH), δ 70.71 ppm (1C, *C*HOH), δ 71.37 ppm (1C, *C*HOH), δ 74.49 ppm (1C, *C*HCH$_2$OH), δ 100.46 ppm (1C, *C anomeric*), δ 125.56 ppm (1C, CH=*C*H$_2$), δ 132.17 ppm (1C, *C*H=CH$_2$), δ 165.17 ppm (1C, NH*C*=O).

ESI-TOF expected m/z $[M\text{-}Na]^+$ 300.2597, found 300.1083.

FT-IR ν = 3302, 2925, 2854, 2364, 1638, 1420, 1542, 1364, 1247, 1053, 877, 654, 612 cm^{-1}.

2.7 Synthesis of Agmatine Acrylamide (Agm)

Agmatine Acrylamide (Agm) was synthesized according to the procedure described by Algotsson M. et al.,[78] with slight modifications. Agmatine Sulfate (2 g, 8.76 mmol) was dissolved in a 30 mM solution of K_2CO_3 (16 mL, 0.48 mmol) under stirring and the reaction mixture was cooled down at 0 °C in an ice bath. Acryloyl chloride (7.12 mL, 87.6 mmol) was added in 350 μL aliquots. The pH of the solution was monitored and maintained in a range of

8-9 by addition of the required amount of 2 M NaOH solution. The reaction was monitored by TLC using 100% methanol (MeOH) as eluent until the disappearance of the violet spot visualized by ninhydrin staining (0.2% w/v ethanolic solution). Subsequently, the mixture was acidified to pH 2 with 1 M HCl. The excess of acryloyl chloride hydrolysis product acrylic acid was removed by extraction with 10x15 mL of chloroform ($CHCl_3$) and the purification was monitored by TLC using 100% methanol (MeOH) until complete disappearance of the acrylic acid spot in the organic phase. The aqueous phase was collected, neutralized with 1 M NaOH and traces of solvent were removed under vacuum. The aqueous phase containing product was freeze-dried, re-dissolved in MeOH and passed through a short pad of silica to remove salts (Silica gel 60Å, particles size 35-70 μm). The solvent was removed under reduced pressure and the pure product was re-dissolved in DI water and recovered by lyophilization. Acryloyl agmatine was obtained as a white powder (1.2 g, 6.5 mmol, 74.2% mol/mol yield) and was characterized by ESI TOF mass spectrometry, FT-IR, ^{1}H-NMR and ^{13}C-NMR.

^{1}H-NMR (400 mHz, D_2O, δ, ppm) δ 1.62 ppm (m, 4H, $NHCH_2C\mathit{H_2}C\mathit{H_2}CH_2$); δ 3.22-3.31 ppm (m, 4H, $NHC\mathit{H_2}CH_2CH_2C\mathit{H_2}NH$); δ 5.77 ppm (dd, *J*=9.8, 1.8 Hz, 1H $CH\mathit{H}$=CH); δ 6.18 ppm (dd, *J*=17.1, 1.8 Hz, 1H, $C\mathit{H}$H=CH); δ 6.29 ppm (dd, *J*=17.1, 9.8 Hz, 1H, CH_2=$C\mathit{H}$).

^{13}C{^{1}H}-NMR (400 mHz, D_2O, δ, ppm) δ 25.41 ppm (1C, $NHCH_2\mathit{C}H_2CH_2CH_2NH$); δ 25.77 ppm (1C, $NHCH_2CH_2\mathit{C}H_2CH_2NH$); δ 39.07 ppm (1C, $NH\mathit{C}H_2$); δ 40.78 ppm (1C, $\mathit{C}H_2NH$); δ 127.39 ppm (1C, $\mathit{C}H_2$=CH); δ 130.25 ppm (1C, CH_2=CH); δ 156.83 ppm (1C, $NH_2\mathit{C}NH$); δ 168.32 ppm (1C, NHC=O).

ESI-TOF expected m/z $[M\text{-}H^+]^{1+}$ 185.13, found 185.140.

FT-IR ν = 3314, 2875, 1648, 1605, 1264, 1087, 610, 553 cm^{-1}.

2.8 Typical polymerization conditions: synthesis of Man_x-*b*-Agm_y and Man_x-*b*-Agm_y-*b*-But_z block co-polymers

According to procedure reported by Guillaume *et al.*,[71] three different diblock (Man_x-*b*-Agm_y) and two different triblock (Man_x-*b*-Agm_y-*b*-But_z), co-polymers were synthesized by Fast RAFT polymerization using different CTA:monomers feed ratios and sequentially polymerizing Man, Agm and, only for the tri-blocks, butyl acrylate.

Synthesis of Man_x-b-Agm_y diblock co-polymers. The general polymerization procedure is described for Man_{58}-*b*-Agm_{45}. Briefly, D-Mannopyranosyloxyethyl acrylamide (80 mg, 0.289 mmol) was dissolved in filtered MilliQ water (74 µL) and placed in a tube equipped with a magnetic follower. 19.2 µL of a 62 mg/mL RAFT agent stock solution in dioxane (1.19 mg, 0.00451 mmol) was added. The tube was then placed in an ice bath and 2.92 µL (0.029 mg, 0.0000902 mmol) of a freshly prepared VA-044 initiator stock solution in filtered MilliQ water (10 mg/mL) was added to the reaction mixture under stirring. The tube was sealed with a rubber septum and deoxygenated by gentle Argon bubbling for 10 minutes. The polymerization was started by placing the tube in an oil bath pre-heated at 60 °C. The reaction was monitored by ^{1}H-NMR in DMSO-d_6 analyzing samples withdrawn from the polymerization mixture at 2 hours to verify that the monomer conversion was >90%. The generated macro-CTA Man_{58} was characterized by ^{1}H-NMR and GPC to evaluate the M_n and Đ.

^{1}H-NMR (400 mHz, DMSO-d_6, δ, ppm): δ 0.75-2.13 ppm (m, 3H, C*H*C*H*$_2$ polymer backbone); δ 4.47-4.69 ppm (m, 4H, C-O*H* sugar); δ 4.62 ppm (d, 1H, O-C*H* anomeric); δ 8.13 ppm (s, 1H, N*H*).

Conversion = 91%; $M_{n,th}$ = 16.3 kDa; DP_{th} = 58; $M_{n\ (GPC,\ aqueous)}$ = 18.6 kDa; Đ $_{(GPC,\ aqueous)}$ = 1.04.

After mannose monomer conversion was >90%, agmatine acrylamide (53.2 mg, 0.289 mmol) was dissolved in 93 µL of MilliQ water in a separate tube and then transferred to the reaction vessel (theoretical molar ratio Man/Agm 64:64). The reaction vessel was placed in an ice bath and 2.92 µL (0.029 mg, 0.0000902 mmol) of a freshly prepared VA-044 initiator stock solution in MilliQ filtered water (10 mg/mL) was added to the reaction mixture under stirring. Then the reaction mixture was degassed by argon bubbling for 10 minutes. The polymerization was started by placing the tube in an oil bath pre-heated at 60 °C. After 2 hours the conversion was monitored by ^{1}H-NMR in DMSO-d_6 on sample withdrawn from the reaction vessel and the polymerization was considered complete when agmatine acrylamide conversion was >70-80%, otherwise a second addition of the VA-044 initiator was made until that conversion percentage was reached. The polymer was then dialyzed against DI water for 48 hours using a 3.5 kDa MWCO dialysis membrane to remove the unreacted monomers. The

product was freeze-dried and the polymer was recovered as a yellowish powder and analyzed by ^{1}H-NMR and GPC.

^{1}H-NMR (400 mHz, DMSO-d_6, δ, ppm): δ 0.66-2.33 ppm (bm, 10H, C*H*C*H*$_2$ polymer backbone, N-CH$_2$-C*H*$_2$-C*H*$_2$-CH$_2$ agmatine); δ 4.46-4.96 ppm (m, 4H, C-O*H* sugar); δ 4.67 ppm (s, 1H, O-C*H* anomeric); δ 6.7-8.07 ppm (bm, 5H, N*H* mannose, N*H* agmatine, N*H* guanidyl group).

Conversion = 90%; $M_{n,th}$ = 24.6 kDa; DP_{th} = 103; $M_{n\ (GPC,\ aqueous)}$ = 66.9 kDa; Đ $_{(GPC,\ aqueous)}$ = 1.29.

Polymers Man$_{15}$-*b*-Agm$_{12}$ and Man$_{29}$-*b*-Agm$_{25}$ were synthesized under identical conditions but the [Man]:[Agm]:[CTA]:[VA-044] molar ratios of [16]:[16]:[1]:[0.02] and [32]:[32]:[1]:[0.02] were used, respectively.

Synthesis of Man$_x$-b-Agm$_y$-b-But$_z$ triblock co-polymers. The Fast RAFT polymerization of tri-block copolymers was performed by sequentially polymerizing Man and Agm as described in the previous paragraph but without isolating the obtained diblock co-polymers that served instead as macro-CTAs for the chain extension with Butyl Acrylate (But). The general polymerization procedure is described for Man$_{62}$-*b*-Agm$_{52}$-*b*-But$_{32}$. Butyl acrylate (20.7 µL, 18.5 mg, 0.144 mmol) was added to Man$_{62}$-*b*-Agm$_{52}$ macro-CTA considering a Man/Agm/But feed ratio of 64:64:32. The tube was placed in an ice bath and 8.9 µL (0.029 mg, 0.0000902 mmol) of a freshly prepared VA-044 initiator stock solution in water (10 mg/mL) was added to the reaction mixture under stirring. The solution was degassed by argon bubbling for 10 minutes. The polymerization was initiated by placing the tube in an oil bath pre-heated at 60 °C. The reaction was monitored at 2 hours by ^{1}H-NMR analysis in DMSO-d_6 of a sample withdrawn from the polymerization mixture. Sequential additions of VA-044 aliquots as described above followed by 2 hours polymerization at 60 °C were performed until butyl acrylate conversion reached at least 90%. Polymer was dialyzed against DI water for 48 hours using a 3.5 kDa MWCO dialysis membrane to remove the unreacted monomers. The product aqueous solution was freeze-dried and the polymer was recovered as a yellowish powder and characterized by ^{1}H-NMR and GPC.

^{1}H-NMR (400 mHz, DMSO-d_6, δ, ppm): δ 1.30 ppm (t, 3H, C*H*$_3$ butyl); δ 1.36-2.5 ppm (bm, 27H, C*H*C*H*$_2$ polymer backbone, N-CH$_2$-C*H*$_2$-C*H*$_2$-CH$_2$ agmatine, O-CH$_2$-C*H*$_2$-C*H*$_2$-CH$_3$ butyl); δ 4.39 ppm (m, 2H, O-C*H*$_2$-CH$_2$-CH$_2$-CH$_3$ butyl); δ 4.94-5.50 ppm (m, 8H, C-O*H*

sugar); δ 5.10 ppm (s, 2H, O-C*H* anomeric); δ 7.15-8.8 ppm (bm, 10H, N*H* mannose, N*H* agmatine, N*H* guanidyl group).

Conversion = 100% $M_{n,th}$ = 31.1 kDa; DP_{th} = 146, $M_{n\ (GPC,\ aqueous)}$ = 38.4 kDa; $Đ_{\ (GPC,\ aqueous)}$ = 1.07.

Triblock co-polymer Man_{29}-*b*-Agm_{29}-*b*-But_9 was synthesized under identical conditions but a [But]:[macro-CTA]:[VA-044] molar ratio of [9]:[1]:[0.04] was used.

2.9 Complexation studies with nucleic acids

Complexation studies with model ssDNA. Preliminary glycopolyplexes (GPPs) formulation studies were carried out by mixing a 100 µM solution of model 19-base ssDNA sequence (0.52 µL, 300 ng, 52 pmol) with increasing amount of 5 or 0.5 mg/mL polymers solution to achieve different nitrogen to phosphate (N/P) molar ratios (0, 0.5, 1, 3, 5, 7, 10, 15, 20). The mixtures were incubated for 1h at room temperature and then diluted to 10 µL with MilliQ water and added of 2 µL of a 30% v/v glycerol/water solution (loading buffer). The samples were analyzed by vertical gel electrophoresis using a 12% v/v polyacrylamide gel. The gel was run at 100 V for 1 hour using Tris-Borate-EDTA (TBE, 0.1 M Tris base, 0.1 M boric acid, 0.002 M EDTA) as running buffer. The bands corresponding to ssDNA were visualized under ultraviolet light after staining by immerging the gel for 30 minutes in 50 mL of MilliQ water containing 10 µL of 10000X GelRed® nucleic acid gel staining. The gels were imaged using a Perkin Elmer UV-Transilluminator Geliance 600 Imaging System.

Complexation studies with plasmid DNA encoding enhanced green fluorescent protein (pEGFP) or ovalbumin (pOVA). pDNA complexation studies were performed assembling glycopolyplexes (GPPs) by simple mixing pEGFP-N3 (Addgene) solution (0.69 µL, 100 ng, 0.03422 pmol) or pOVA (Genescript) solution (1 µL, 100 ng, 0.02463 pmol) with increasing amount of polymer to achieve different nitrogen to phosphate (N/P) molar ratios (0, 1, 2.5, 5, 10, 15, 20). The mixtures were incubated for 1 hour at room temperature, diluted to 10 µL with MilliQ water and then added of 2 µL of loading buffer. The samples were analyzed by 1% agarose gel electrophoresis at 100 V for 45 minutes, using Tris-Ammonium-EDTA (TAE, 40 mM Tris base, 40 mM acetic acid, 1 mM EDTA) as running buffer. The bands

corresponding to ssDNA were visualized under ultraviolet light after staining by immerging the gel for 30 minutes in 70 mL of MilliQ water containing 14 µL of 10000X GelRed® nucleic acid gel staining. The gels were imaged using a Perkin Elmer UV-Transilluminator Geliance 600 Imaging System.

2.10 Particle size and Zeta potential analyses

The mean particle diameter of the GPPs and polydispersity index (PDI) were determined by Dynamic Light Scattering (DLS) using Malvern Instrument Ltd. Zetasizer Nano ZS (Malvern, UK) at a constant scattering angle of 173° and 25 °C. GPPs solutions were prepared in PBS at the fixed ssDNA and pDNA concentrations of 24 µg/mL and 5 µg/mL, respectively, using for each formulation the minimum N/P ratio that guarantees for complete nucleotides complexation.

Specifically, 2.08 µL of a 100 µM ssDNA solution (1.2 µg, 0.208 nmol) was mixed with polymer solution in MilliQ water containing 37.6 µg, 18.2 µg and 9.14 µg of Man_{15}-*b*-Agm_{12}, Man_{29}-*b*-Agm_{25} and Man_{58}-*b*-Agm_{45}, respectively, to achieve the final N/P ratios of 20, 10 and 5, respectively, and at an N/P ratio of 3 for Man_{29}-*b*-Agm_{29}-*b*-But_{9} (5.4 µg) and Man_{62}-*b*-Agm_{52}-*b*-But_{32} (6.6 µg) . The samples were incubated at room temperature for 1 hour, diluted to the final volume of 50 µL with PBS, pH 7.4, and analyzed.

For pDNA-complexes, pEGFP (250 ng, 0.08555 pmol, 1.72 µL) was mixed with polymers solution at 0.5 mg/mL concentration in MilliQ water of Man_{15}-*b*-Agm_{12} (4.48 µL, 2.24 µg) and Man_{29}-*b*-Agm_{25} (4.18 µL, 2.09 µg) at N/P ratio of 5 and of Man_{58}-b-Agm_{45} (2.23 µL, 1.12 µg), Man_{29}-*b*-Agm_{29}-*b*-But_{9} (1.87 µL, 0.94 µg) and Man_{62}-*b*-Agm_{52}-*b*-But_{32} (2.34 µL, 1.17 µg) at N/P ratio of 2.5. The samples were incubated at room temperature for 1 hour and then diluted to the final volume of 50 µL with PBS, pH 7.4, and analyzed.

The Zeta potential (ZP) of either polymers alone or ssDNA-based polyplexes were investigated by laser doppler electrophoresis at a final polymer concentration of 0.1 mg/mL in 5 mM HEPES buffer at the N/P ratios reported above.

2.11 Transmission Electron Microscopy

Glycopolyplexes solutions were prepared in MilliQ water as described in the paragraph 2.9 "Complexation studies with nucleic acids", using either ssDNA or pDNA at a final polymer concentration of 0.25 mg/mL. Polymer/ssDNA polyplexes were prepared at the same N/P ratios used for the DLS analysis and TEM images for all the synthesized polymers were acquired. In the case of pDNA, only Man_{58}-b-Agm_{45}/pDNA, Man_{29}-*b*-Agm_{29}-*b*-But_{9}/pDNA and Man_{62}-*b*-Agm_{52}-*b*-But_{32}/pDNA complexes were analyzed by TEM at 2.5 and 5 N/P ratios.

Samples were deposited on a small holey carbon-coated support grid (400 mesh) and the solvent was allowed to dry at room temperature. Samples were analyzed in negative staining mode by Transmission Electron Microscopy (TEM, Tecnai G2 microscope (FEI)), using 1% w/v aqueous uranyl acetate as contrast agent. The average diameter of GPPs and the percentage of spherical, rod- or toroid-shaped complexes were evaluated by ImageJ software v.1.51 by measuring 50 individual polyplexes.

2.12 Heparin displacement assay

Polymers ability to tightly complex and retain DNA was evaluated by displacement studies monitoring ssDNA or pEGFP release in presence of a poly anionic competitive macromolecule, heparin. Polymer/ssDNA and polymer/pEGFP polyplexes were prepared at the selected N/P ratios using 300 ng and 100 ng of DNA, respectively. GPPs were incubated for 15 minutes with increasing concentration of heparin (0.15-10 IU/mL) and loaded into a 12% polyacrylamide or 1% agarose gel for ssDNA and pDNA-based complexes, respectively. The conditions used for gel preparation, running and visualization were as reported in the paragraph 2.9 "Complexation studies with nucleic acids".

2.13 GPPs stability in physiological media

Glycopolyplexes samples were prepared by mixing 4.16 µL of 100 µM ssDNA (2.4 µg) with Man_{15}-*b*-Agm_{12} (77 µg, N/P 20), Man_{29}-*b*-Agm_{25} (36.4 µg, N/P 10), Man_{58}-b-Agm_{45} (18.3 µg, N/P 5), Man_{29}-*b*-Agm_{29}-*b*-But_{9} (10.8 µg, N/P 3) or Man_{62}-*b*-Agm_{52}-*b*-But_{32} (13.2

μg, N/P 3) polymers solution. After preparation, the samples were equilibrated at room temperature for 1 hour and then *a.* dilute to 100 μL with PBS and then analyzed at regular intervals over a two weeks period, storing the solutions at 4 °C or *b.* diluted to 100 μL with PBS added of 10% Fetal Bovine Serum and incubated at 37 °C, analyzing the samples at regular intervals for 48 hours.

2.14 *Ex vivo* hemolysis assay

5 mL of rat blood was centrifuged at 500 g for 5 minutes at 4 °C. As reported in the protocol from Evans *et al.*,[79] red blood cells (RBCs) were washed three times with saline solution (0.9% w/v in water) and twice with PBS at pH 6. The pellet containing RBCs was diluted in PBS, pH 6, at a final concentration of 2% v/v. 180 μL of RBCs suspension was mixed with 20 μL of polymers solutions at the concentrations 500-50 μg/mL (final polymer concentrations tested: 50 and 5 μg/mL) and incubated for 1 hour at 37 °C.
After incubation, the samples were centrifuged at 500 g for 5 minutes and 100 μL of the supernatant was transferred in a 96-well plate and the absorbance of the released hemoglobin was detected at 490 nm with an ELISA plate reader (BIO-TEKTM INSTRUMENTS INC. EL 3II5X). The percentage of hemolysis was normalized with respect to that induced by a 1% Triton X-100 considered as positive control (100% of hemolysis) after background subtraction (absorbance due to the phosphate buffer set as negative control).

2.15 Cell culture

CHO (Chinese hamster ovary cells, wild type) and CHO-MR^+ (Mannose receptor expressing CHO cells) were grown at 37 °C, in 5% CO_2 atmosphere, using Ham's F12/Dulbecco Modified Eagle Medium (DMEM) (50:50) supplemented with 10% FBS, 2 mM L-glutamine, 100 U/mL penicillin, 100 μg/mL streptomycin. CHO-MR^+ cells were grown in the presence of 0.6 mg/mL of geneticin to maintain clone selection.
DC2.4 cells (Dendritic Cells) were grown at 37 °C, in 5% CO_2 atmosphere, using Roswell Park Memorial Institute (RPMI 1640) medium supplemented with 10% FBS, 2 mM L-

glutamine, 100 U/mL penicillin, 100 μg/mL streptomycin, 1% Non-Essential Aminoacid and 50 μM β-mercaptoethanol.

JAWS II murine dendritic cells were grown in α-MEM supplemented with 20% FBS, 4 mM L-glutamine, 100 U/mL penicillin and 100 μg/mL streptomycin at 37 °C, in 5% CO_2 atmosphere. GM-CSF was freshly added at 5 ng/mL concentration.

B16-OVA mouse melanoma cells were grown at 37 °C, in 5% CO_2 atmosphere, using low glucose RPMI supplemented with 10% FBS, 2 mM L-glutamine, 100 U/mL penicillin and 100 μg/mL streptomycin. Geneticin at a concentration of 5 mg/mL was added to maintain clone selection.

B16-F1 mouse melanoma cells were grown at 37 °C, in 5% CO_2 atmosphere, using Minimum Essential Medium (MEM) supplemented with 10% FBS, 1% NEAA, 100 U/mL penicillin and 100 μg/mL streptomycin.

2.16 Cell biocompatibility studies

CHO and CHO-MR^+ cells were seeded in a 96 well plate ($1x10^4$ cell/well) in DMEM/F12 complete medium and after overnight culture the medium was replaced with 100 μL of polymer/ssDNA glycopolyplexes suspensions prepared as described in the paragraph 2.9 "Complexation studies with nucleic acids" in DMEM/F12 using an oligo concentration ranging from 125 to 1000 nM and the following N/P ratios: 20, 10, 5, 3 and 3, for Man_{15}-*b*-Agm_{12}/ssDNA, Man_{29}-*b*-Agm_{25}/ssDNA, Man_{58}-*b*-Agm_{45}/ssDNA, Man_{29}-*b*-Agm_{29}-*b*-But_9/ssDNA and Man_{62}-*b*-Agm_{52}-*b*-But_{32}/ssDNA, respectively. After 24 hours incubation, cells were washed with 2x100 μL PBS and the cell survival was assessed through 3-(4,5-dimethylthiazol-2-yl)-2,5-diphenyl tetrazolinium bromide (MTT) assay.[80] 180 μL of serum-free medium was added to each well followed by 20 μL of MTT solution (5 mg/mL in PBS). After 3 hours of incubation at 37 °C, the medium was removed and replaced with 200 μL of dimethyl sulfoxide (DMSO). Plates were left 15 minutes under gentle shaking to allow formazan crystal dissolution and then analyzed via spectrophotometric measurement at 570 nm. The cell viability was calculated using cell incubated with medium only as positive control (100% viability).

2.17 Polymer/ssDNA glycopolyplexes association to cells expressing MR

In order to evaluate polymer/ssDNA internalization by cells, the complexes were prepared with labeled Cyanine 3-ssDNA (Cy3-ssDNA). CHO and CHO-MR^+ cells were seeded at a density of $2x10^5$ cells/well in complete DMEM/F12 and DC2.4 cells were seeded at a density of $5x10^4$ cell/well in complete RPMI-1640 medium in a 24-well plate. After overnight culture, cells were washed twice with 500 µL of PBS and treated with 400 µL of polymer/Cy3-ssDNA complex solutions prepared in serum-free DMEM/F12 or RPMI medium as described in the paragraph 2.9 "Complexation studies with nucleic acids", using a 125 nM Cy3-ssDNA concentration and the same N/P ratios reported in the paragraph 2.16 "Cell biocompatibility studies". The GPPs suspensions were prepared in medium without FBS. Following either 30 minutes or 1 hour of incubation, the treatments were removed and cells were washed twice with 500 µL of PBS. 100 µL of a 0.06% w/v trypsin solution in PBS was added to each well to harvest the cells and then added of 200 µL of PBS with Ca^{2+} and Mg^{2+}. Cells were transferred into flow cytometry tubes, fixed with 100 µL of a 4% v/v paraformaldehyde (PFA) solution in PBS and analyzed with a FC500 Beckmann Coulter flow cytometry with CXP acquisition. The mean fluorescence intensity was detected on FL2 (argon laser 488 excitation, 575-540 nm detection). Data collection was carried out with at least $1x10^4$ events per sample. Data were analyzed with Flowing software v.2.5.1 (Turku Centre for Biotechnology, Finland).

2.18 Evaluation of GPPs endosomal escape properties by Förster Resonance Energy Transfer

CHO-MR^+ cells were seeded at a density of $2.5x10^4$ cells/well on a 24-wells plate containing glass dishes and were grown overnight. Cells were then incubated at 37 °C with 400 µL of Man_{58}-*b*-Agm_{45}/ssDNA GPPs at a N/P ratio of 5 and prepared as described in the paragraph 2.9 "Complexation studies with nucleic acids" in serum-free DMEM/F12 using both Cy3- and Cy5-ssDNA, at a concentration of 125 nM. After 2 hours incubation, cells were washed twice with 400 µL of PBS and then further incubated with DMEM/F12 added of 10% of FBS for other 2, 6 or 24 hours. Subsequently, cells were washed three times with 400 µL of PBS and samples were fixed by incubation for 15 minutes at room temperature with

300 µL of a 4% PFA solution in PBS. Afterwards, the PFA solution was discarded and cells were rinsed with 3x 400 µL of PBS, following by nuclei staining with 300 µL of a 4.5 µg/mL solution of DAPI for 10 minutes. Finally, glass dishes were gently rinsed three times with 300 µL of PBS and once with MilliQ water before being mounted on microscope slides using Mowiol® aqueous mounting media.

Cells were imaged with a Zeiss™ confocal laser-scanning microscope (LSM 800, Zeiss, Jena, Germany) using an immersion lens with 63x magnification, with wavelengths at 410-540 nm (blue, DAPI) for nuclei detection, 540-612 nm for Cy3-ssDNA detection (red) and 645-700 nm for Cy5-ssDNA detection (green). These settings were applied for images acquisition before and after a high-power laser was applied for Cy5 probe bleaching. The images were then processed with ZEN 2 (blue edition) from Zeiss™ Software. The increase in Cy3 emission after Cy5 bleaching due to a decrease of Förster Resonance Energy Transfer (FRET) was calculated as energy transfer efficiency (Eff $_{FRET}$) for the endosomal escape evaluation according to the following equation:

$$Eff_{FRET} = (D_{post}-D_{pre})/D_{post} \quad (1)$$

with D_{pre} and D_{post} referring to the donor fluorescence intensities before and after acceptor photobleaching.

2.19 Cell transfection studies with model plasmid DNA: pEGFP

2.19.1 Transfection efficiency quantitative evaluation by flow cytometry with polymer/pEGFP polyplexes

CHO and CHO-MR$^+$ cells (1.5x10^4 cells/well) or DC2.4 cells (2.5x10^4 cells/well) were seeded in a 48-wells plate and were grown overnight. GPPs were formulated, as described in the paragraph 2.9 “Complexation studies with nucleic acids” in Optimem® medium, at a 2.5 µg/mL pEGFP concentration, and at the N/P ratio of 5 for Man$_{15}$-*b*-Agm$_{12}$/pEGFP and Man$_{29}$-*b*-Agm$_{25}$/pEGFP GPPs and at the N/P ratio of 2.5 for Man$_{58}$-*b*-Agm$_{45}$/pEGFP, Man$_{29}$-*b*-Agm$_{29}$-*b*-But$_9$/pEGFP and Man$_{62}$-*b*-Agm$_{52}$-*b*-But$_{32}$/pEGFP GPPs. Cells were incubated for 6 hours at 37 °C with 200 µL of GPPs and then washed twice with 100 µL of PBS and further incubated for 24 hours post-transfection (24 hpt) in serum-supplemented DMEM/F12 and RPMI for CHO/CHO-MR$^+$ and DC2.4 cell lines, respectively. Finally, cells were washed

again with 100 µL of PBS and detached using a 0.06% w/v trypsin solution in PBS. Trypsin was then diluted with 200 µL of PBS containing Ca^{2+} and Mg^{2+} and cells were transferred into flow cytometry tubes, fixed with 100 µL of a 4% v/v PFA solution in PBS and analyzed with a BD FacsCANTOII flow cytometer. The mean fluorescence intensity and the percentage of positive cells were detected on FITC channel. Untreated cells for each cell line served as negative controls. Data collection was carried out with at least $1x10^4$ events per sample. Data were analyzed with Flowing software v.2.5.1.

2.19.2 Transfection efficiency qualitative evaluation by confocal microscopy

CHO and CHO-MR^+ cells were seeded at a density of $2.5x10^4$ cells/well on a 24-wells plate containing glass dishes and were grown overnight. Cells were incubated for 6 hours at 37 °C with 400 µL of Man_{58}-*b*-Agm_{45}/pEGFP GPPs N/P 2.5 prepared as described in the paragraph 2.9 "Complexation studies with nucleic acids", using 2.5 µg/mL pEGFP concentration, and then washed twice with PBS and further incubated for 24 hours. Subsequently, cells were washed twice with 400 µL of PBS, fixed by incubation for 15 minutes with a 4% PFA solution in PBS at room temperature and rinsed with 3x 400 µL of PBS, following by nuclei staining with 300 µL of a 4.5 µg/mL solution of DAPI for 10 minutes. Finally, glass dishes were gently rinsed three times with 300 µL of PBS and once with MilliQ water before being mounted on microscope slides using Mowiol® aqueous mounting media.

Cells were imaged with a Zeiss™ confocal laser-scanning microscope (LSM 800, Zeiss, Jena, Germany) using an immersion lens with 63x magnification, with wavelengths at 353 nm (blue, DAPI) for nuclei detection and 488 nm (green, EGFP) for EGFP detection. The images were then processed with ZEN 2 (blue edition) from Zeiss™ Software.

2.20 Dendritic cells activation and cross presentation experiment induced by polymer/pOVA glycopolyplexes

Murine dendritic cells JAWS II were seeded at a density of $5x10^5$ cells in a 12-well plate and were grown overnight in αMEM supplemented with 20% FBS and with 5 ng/mL GM-CSF, freshly added. Man_{58}-*b*-Agm_{45}/pOVA, Man_{29}-*b*-Agm_{29}-*b*-But_9/pOVA and Man_{62}-*b*-Agm_{52}-*b*-But_{32}/pOVA were formulated in Optimem® medium at N/P ratio 2.5, using 2.5

μg/mL Ovalbumin-encoding plasmid (pOVA). L-PEI$_{25kDa}$/pOVA complexes at 10 N/P ratio were used as control. Cells were incubated for 6 hours at 37 °C with 400 μL of GPPs and then washed once with 500 μL of PBS and further incubated for 24 hpt in α-MEM supplemented with 20% FBS and 5 ng/mL of GM-CSF. After incubation, cells were washed once with 500 μL of PBS and detached by incubation with 500 μL of 25 mM EDTA solution for 5 minutes at 37 °C. Cell suspensions were centrifuged, transferred in a V-bottom 96-well plate and incubated for 10 minutes at 4 °C with 40 μL of Fc-receptor blocking solution (2 μL of Purified anti-mouse CD16/32 Antibody, Biolegend, in 38 μL of PBS). Subsequently, cells were stained for 30 minutes at 4 °C with FITC anti-mouse CD11c (1:50 dilution, 1 μL/sample), PerCP anti-mouse CD86 (1:40 dilution, 1.25 μL/sample) and PE anti-mouse H-2K^b bound-SIINFEKL (1:50 dilution, 1 μL/sample) antibodies solutions. Finally, cells were centrifuged at 1500 rpm for 5 minutes, and the cell pellet was washed twice with 100 μL of PBS, fixed by incubation at 4 °C for 10 minutes with 100 μL of a 4% PFA solution in PBS, rinsed 2x 100 μL of PBS and resuspended in 180 μL of PBS. An unstained sample was also prepared for each condition as control. Samples were analyzed with a BD Facs Fortessa LSR II flow cytometer. Untreated cells were used as negative control. The percentage of positive cells was detected, acquiring at least 1x10^4 events per sample. Data were analyzed with FlowJo software v.10.

2.21 *In vivo* studies

All animal protocols were reviewed and approved by the experimental animal committee of the University of Helsinki (Helsinki, Finland) and the Provincial Government of Southern Finland.

C57BL/6JOlaHsd immune competent female *naïve* mice were purchased from Envigo (Horst, The Netherlands) and used at 6-10 weeks of age and housed in ventilated cages and clinically controlled rooms. Animals had free access to water and food and the animal body weight was constantly monitored. All the treatments were performed under isoflurane anesthesia. The treatment effect on tumor growth was evaluated by measuring the tumor volume every other day using an electronic caliper and tumor volume was calculated according to the formula (2):

$$\text{volume} = \text{length} \times \text{width}^2/2 \quad (2)$$

Body weights were assessed after tumor volume measurements.

2.21.1 *In vivo* prophylactic approach: prime and boost

C57BL/6 mice were randomly assigned to the treatment groups. Six groups of 10 mice per group were defined: Group 1 (Mock, untreated group), Group 2 (pOVA, subcutaneous injection of pOVA), Group 3 (Man_{58}-*b*-Agm_{45}/pEGFP, subcutaneous injection of Man_{58}-*b*-Agm_{45} /pEGFP complex), Group 4 (Man_{62}-*b*-Agm_{52}-*b*-But_{32}/pEGFP, subcutaneous injection of Man_{62}-*b*-Agm_{52}-*b*-But_{32}/pEGFP complex), Group 5 (Man_{58}-*b*-Agm_{45}/pOVA, subcutaneous injection of Man_{58}-*b*-Agm_{45}/pOVA complex), Group 6 (Man_{62}-*b*-Agm_{52}-*b*-But_{32}/pOVA, subcutaneous injection of Man_{62}-*b*-Agm_{52}-*b*-But_{32}/pOVA complex). All glycopolyplexes were prepared at an N/P ratio of 2.5 in PBS as described in the paragraph 2.9 "Complexation studies with nucleic acids".

Each mouse was subcutaneously injected (100 µL) in the right flank at day -14, -13 (prime) and -7 (boost) before tumor implantation with 12.5 µg of pDNA for the treated groups and with PBS for the control group. B16-OVA melanoma cells ($3x10^5$ cells/mouse) were subcutaneously injected in the right flank of the mice seven days after the last boosting (day 0) and the tumor progression was monitored every other day using an electronic caliper. Animals were sacrificed 21 days after tumor implantation or when the end points were reached, namely when tumor volume reached 1000 mm^3 or at 20% body weight loss.

2.21.2 *In vivo* therapeutic approach

C57BL/6 mice were divided in two groups. One group was subcutaneously injected with $3x10^5$ B16-OVA melanoma cells (B16-OVA tumor-bearing mice) and the other group with $1x10^5$ B16-F1 melanoma cells (B16-F1 tumor-bearing mice) in both flanks.

Six groups of 4 mice per group were defined either for B16-OVA-bearing mice or for B16-F1-bearing mice: Group 1 (Mock, untreated group), Group 2 (pOVA, subcutaneous injection of pOVA), Group 3 (Man_{58}-*b*-Agm_{45}/pEGFP, subcutaneous injection of Man_{58}-*b*-Agm_{45}/pEGFP complex), Group 4 (Man_{62}-*b*-Agm_{52}-*b*-But_{32}/pEGFP, subcutaneous injection of Man_{62}-*b*-Agm_{52}-*b*-But_{32}/pEGFP complex), Group 5 (Man_{58}-*b*-Agm_{45}/pOVA, subcutaneous injection of Man_{58}-*b*-Agm_{45}/pOVA complex), Group 6 (Man_{62}-*b*-Agm_{52}-*b*-But_{32}/pOVA, subcutaneous injection of Man_{62}-*b*-Agm_{52}-*b*-But_{32}/pOVA complex). All glycopolyplexes

were prepared at an N/P ratio of 2.5 in PBS as described in the paragraph 2.9 "Complexation studies with nucleic acids".

Each mouse was peritumorally injected at day 2, 6, 10 and 16 post tumors implantation with 100 µL containing 25 µg of pDNA for the treated groups or with PBS for the control group. The tumor progression was monitored every other day using an electronic caliper. Animals were sacrificed 21 days after tumor implantation and tumors and spleen were collected from each mouse for the immunological analysis.

Immunological analysis on tumor samples. Tumors from C57BL/6 mice with B16-OVA and B16-F1 tumors were smashed, filtered through a 70-µm cell strainer and cultured overnight in RPMI medium supplemented with 20% FBS. Four random tumor samples from each group were selected for the tumor T cell staining, plated in a V-bottom 96-well plate and incubated for 10 minutes at 4 °C with 40 µL of Fc-receptor blocking solution (2 µL of Purified anti-mouse CD16/32 Antibody, Biolegend, in 38 µL of PBS). Subsequently, 10 µL of Pro5 MHC Pentamer R-PE (Proimmune) was added to each well and the plate was incubated for 10 minutes at room temperature. Cells were washed once with 100 µL of PBS and then stained at 4 °C for 30 minutes with 50 µL of antibody staining solution containing PerCP/Cy5.5 anti-mouse CD3ε (1:40 dilution, 1.25 µL/sample), APC anti-mouse CD4 (1:40 dilution, 1.25 µL/sample) and FITC anti-mouse CD8 (1:33 dilution, 1.5 µL/sample) antibodies. Finally, cells were centrifuged at 1500 rpm for 5 minutes, and cell pellet was washed twice in PBS, fixed by incubation for 10 minutes at 4 °C with 100 µL of a 4% PFA solution in PBS, rinsed twice with 100 µL of PBS and resuspended in 180 µL of PBS. An unstained sample was also prepared for each condition and used as control. Samples were analyzed at BD Accuri C6 Plus flow cytometer. The percentage of positive cells was detected, acquiring at least $1x10^5$ events per sample. Data were analyzed with FlowJo software v.10.

Immunological analysis on splenocytes. Spleen from C57BL/6 mice with B16-OVA and B16-F1 tumors were smashed, filtered through a 70-µm cell strainer and cultured overnight in RPMI medium supplemented with 20% FBS. Splenocytes from each group were pooled together and treated for 5 minutes at room temperature with ACK (ammonium chloride 155 mM, potassium bicarbonate 10 mM, EDTA 0.1 mM) lysing buffer to allow the lysis of RBC. The amount of SIINFEKL ($OVA_{257–264}$) -specific activated, interferon-γ secreting splenic T cells were measured by ELISpot assay (CTL, Ohio USA) according to the manufacturer's instructions. Briefly, splenocytes were centrifuged at 1200 rpm for 5 minutes and cell pellet

was resuspended in CTL-test^{TM} medium. $3x10^5$ cells/well were seeded in a precoated murine IFN-γ ELISpot 96-well plate and were stimulated with the following conditions: 1x cell activation cocktail (eBioscience) (positive control), PBS (negative control), 2 μg of SIINFEKL ($OVA_{257–264}$) peptide (for OVA specific response), 2 μg of $GP100_{44-59}$ peptide (for aspecific response).

After 72 hours of stimulation, ELISpot plate was processed following the manufacturer's instruction for IFN-γ detection. The plate was let dry and sent to CTL-Europe GmbH for counting of the spots. Number of spots was normalized respect to spots on cell stimulated only with PBS (negative control).

RESULTS AND DISCUSSION

3.1 Synthesis of 4-cyano-4-(ethylsulfanylthiocarbonylsulfanyl)pentanoic acid

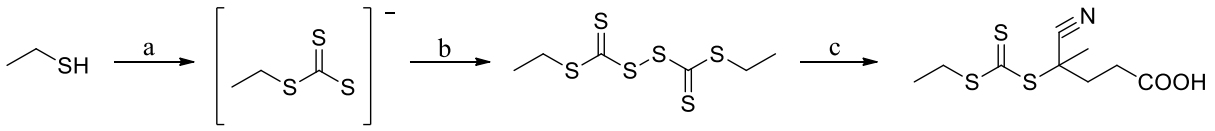

Scheme 2. *Synthesis of 4-cyano-4-(ethylsulfanylthiocarbonylsulfanyl)pentanoic acid. Reagents and conditions: a) CS_2, basic condition, water:acetone 4:1, 0 °C; b) $K_3[Fe(CN)_6]$; c) 4,4'-azobis(cyanopentanoic acid), EtOH, 60 °C, o.n..*

The two step synthesis of 4-cyano-4-(ethylsulfanylthiocarbonylsulfanyl)pentanoic acid was performed as reported by Ghadban and collaborators,[81] with slight modifications. Particularly, the RAFT agent was prepared by reaction of radicals with bis(thioacyl)disulphides, as reported in Scheme 2.

In the first step the nucleophile ethanethiolate ion (SEt^-), formed by ethanethiol in basic conditions, reacts with the electrophilic carbon atom of carbon disulfide CS_2. The resulting sodium carbodithioate salt was subsequently oxidized by adding potassium ferricyanide directly on the reaction solution, with formation of the reaction intermediate bis(ethylsulfanylthiocarbonyl)disulfide as a crude orange oil residue, that was characterized by ^{1}H-NMR (Figure 11) and ^{13}C-NMR (Figure 12).

In the second step of the reaction the crude intermediate was used without further purifications. The radical decomposition of bis(ethylsulfanylthiocarbonyl)disulfide was induced by radicals derived from thermal decomposition of azo-initiators. Here, 4,4'-azobis(cyanopentanoic acid) was reacted at 60 °C, with formation of N_2 and of the corresponding radicals, that reacted with disulfide bond of the intermediate. The final product 4-cyano-4-(ethylsulfanylthiocarbonylsulfanyl)pentanoic acid was purified by silica-gel chromatography to eliminate the unreacted materials and side products. ^{1}H-NMR (Figure 13), ^{13}C-NMR (Figure 14) and ESI-TOF mass spectrometry confirmed the identity of the RAFT agent.

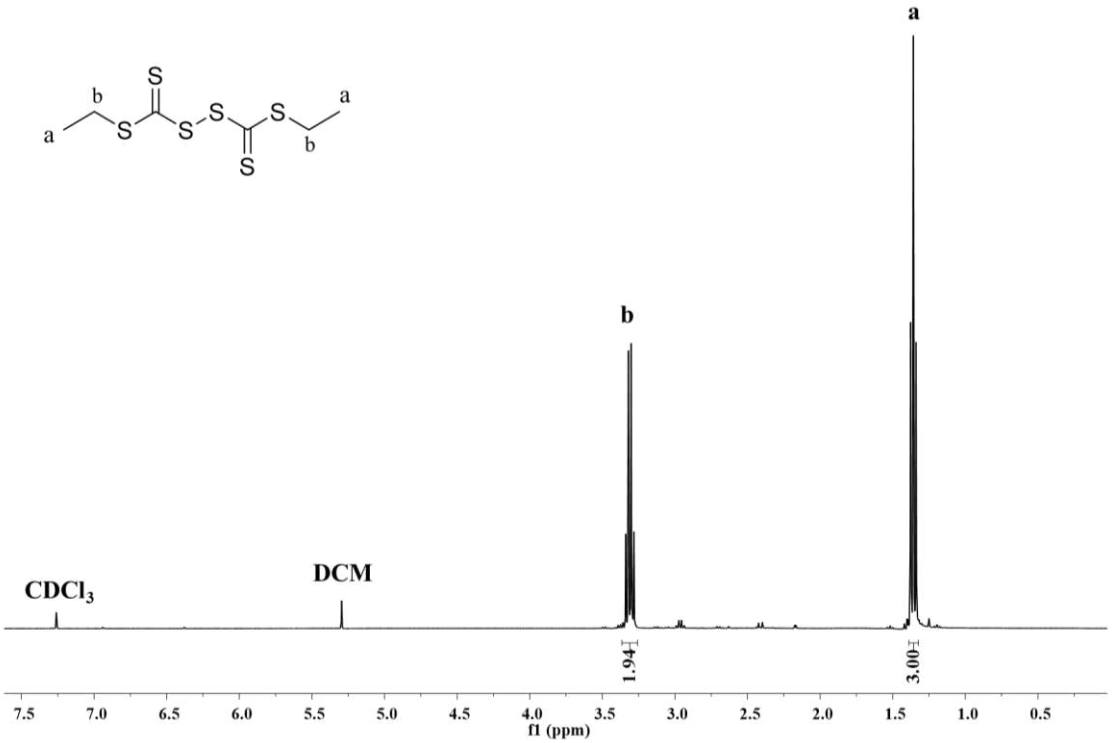

Figure 11. *^{1}H-NMR spectrum in $CDCl_3$ of bis(ethylsulfanylthiocarbonyl)disulfide.*

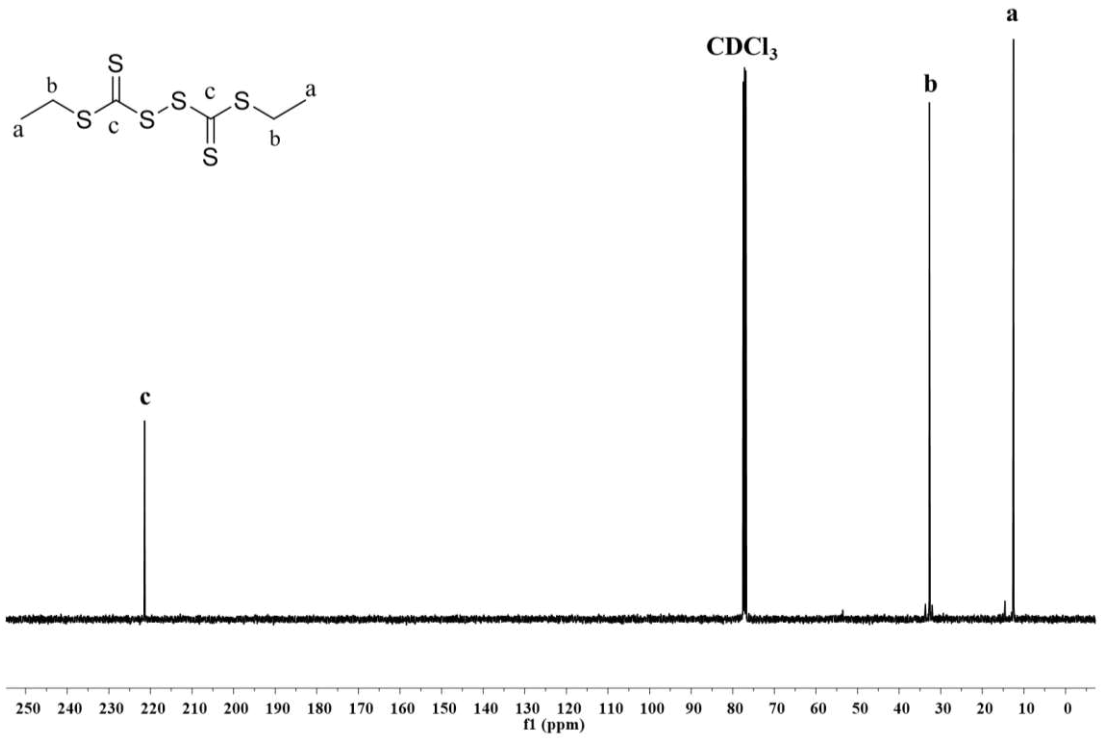

Figure 12. *^{13}C-NMR spectrum in $CDCl_3$ of bis(ethylsulfanylthiocarbonyl)disulfide.*

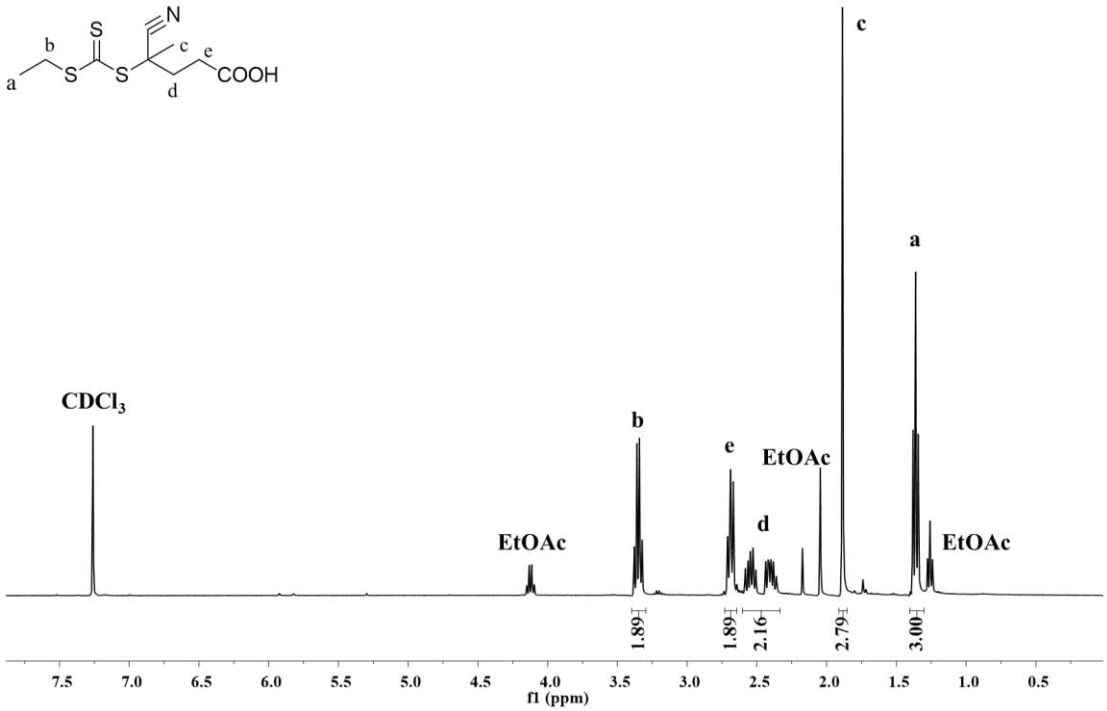

Figure 13. *^{1}H-NMR spectrum in $CDCl_3$ of 4-cyano-4-(ethylsulfanylthiocarbonylsulfanyl)pentanoic acid.*

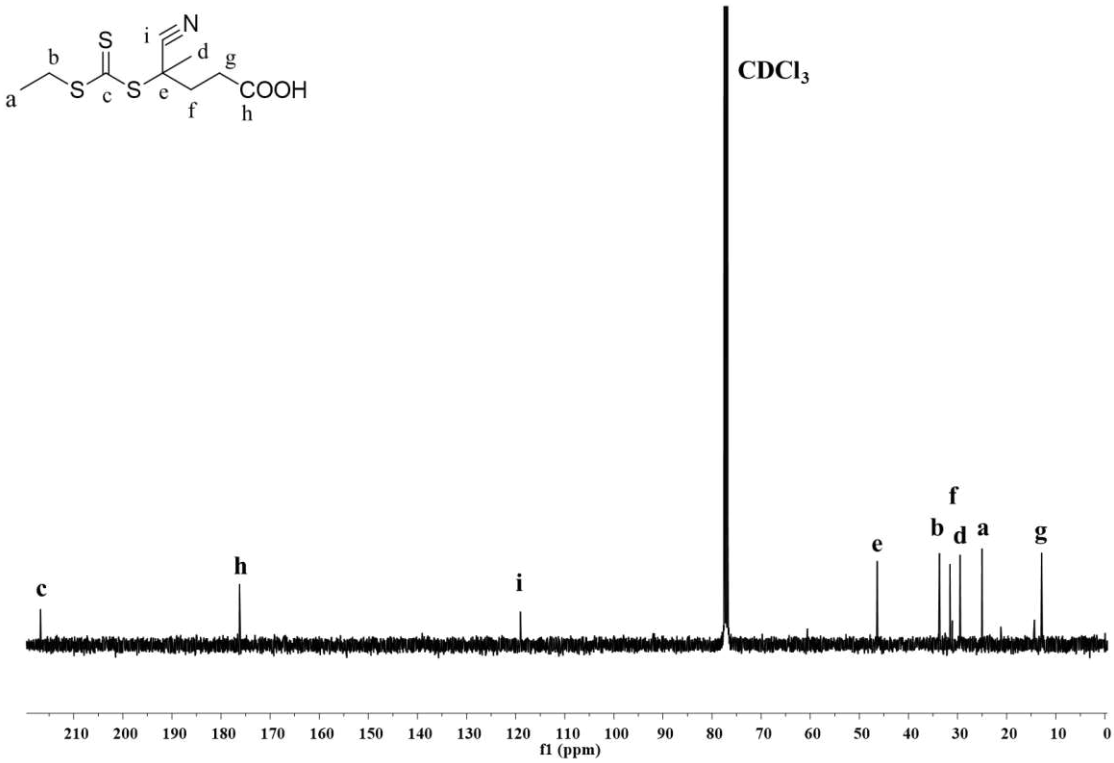

Figure 14. *^{13}C-NMR spectrum in $CDCl_3$ of 4-cyano-4-(ethylsulfanylthiocarbonylsulfanyl)pentanoic acid.*

3.2 Synthesis of D-mannopyranosyloxyethyl acrylamide

The two-step synthesis of D-mannopyranosyloxyethyl acrylamide was performed according to an adapted protocol reported in literature for the O-glycosylation of D-Mannose pentaacetate.[77] In the first step the commercially available D-mannose pentaacetate was condensed with an aliphatic alcohol to produce the intermediate 2,3,4,5-O-tetraacetyl-D-mannopyranosyloxyethyl acrylamide and afterwards the intermediate was deprotected under basic conditions yielding the final product (Scheme 3).

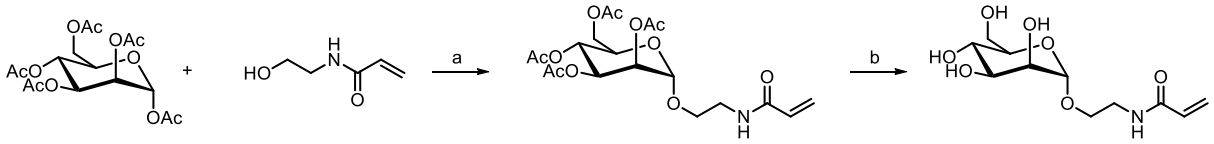

Scheme 3. *Synthesis of D-mannopyranosyloxyethyl acrylamide. Reagents and conditions: a) BF_3Et_2O, anhydrous MeCN, 0 °C, 48h; b) KOH 0.02 M, CH_3OH, RT, 18h.*

In the first step of synthesis, the N-hydroxyethyl acrylamide was added to a solution of D-Mannose pentaacetate in anhydrous acetonitrile. Afterwards, BF_3Et_2O was added dropwise to the solution maintained at 0 °C on an ice bath. BF_3Et_2O was used as Lewis acid catalyst to allow the assisted removal of the acetyl leaving group at the anomeric carbon atom and the O-glycosylation selectively in position 1 of the sugar, that is the reactive carbonyl group of the carbohydrate in its acyclic form. At scheduled times, the progress of the reaction was monitored by ^{13}C-NMR in DMSO-d_6 of samples withdrawn from the reaction vessel, by checking the shift of the anomeric carbon from 88 ppm to 97 ppm. The addition of isopropanol and afterwards the extraction with $NaHCO_3$ and DI water were used to remove the excess of BF_3Et_2O and neutralize the mixture. The intermediate was obtained as a yellow viscous oil after the evaporation of the organic solvent. The crude was purified by silica-gel chromatography to eliminate the unreacted materials and side products. ^{1}H-NMR, ^{13}C-NMR, FT-IR spectroscopy and ESI-TOF mass spectrometry confirmed the identity of the intermediate. In particular, both the shifts of anomeric carbon from 88 to 97 ppm (Figure 16) and that of the hydrogen bound to the same carbon (Figure 15) suggested the success of the reaction. Furthermore, the appearance of a peak at 8.3 ppm in the ^{1}H-NMR indicated the amide bond formation.

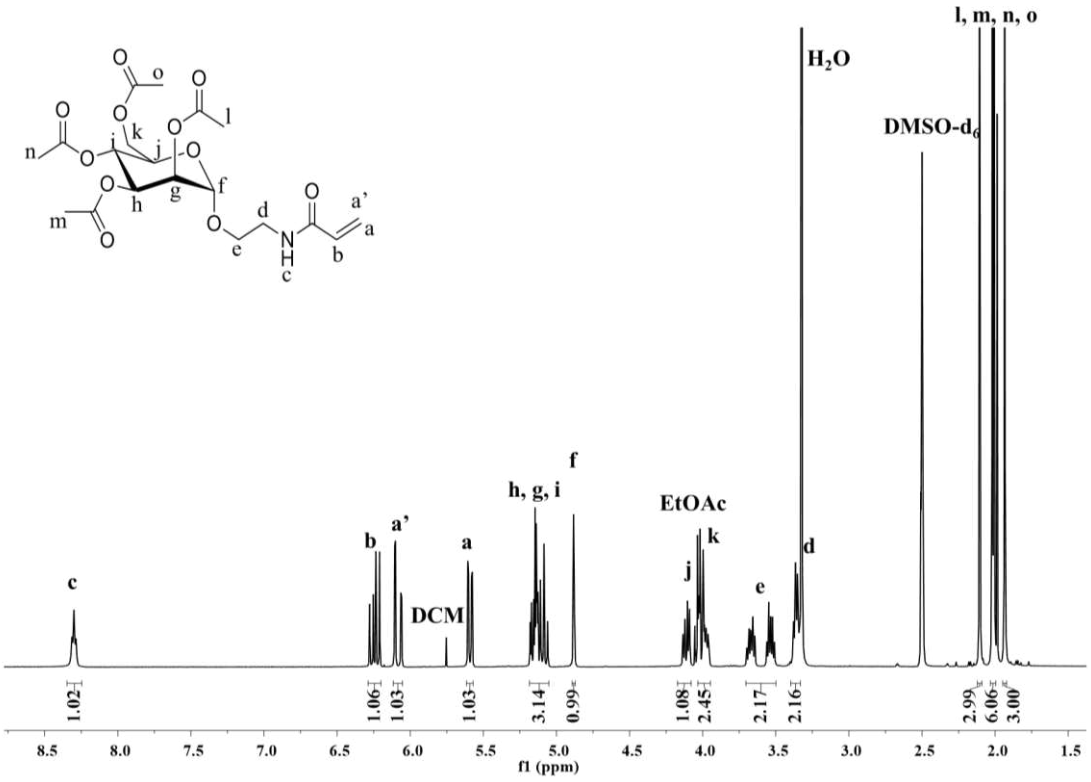

Figure 15. *[1]H-NMR spectrum in DMSO-d_6 of 2,3,4,5-O-tetraacetyl-D-mannopyranosyloxyethyl acrylamide.*

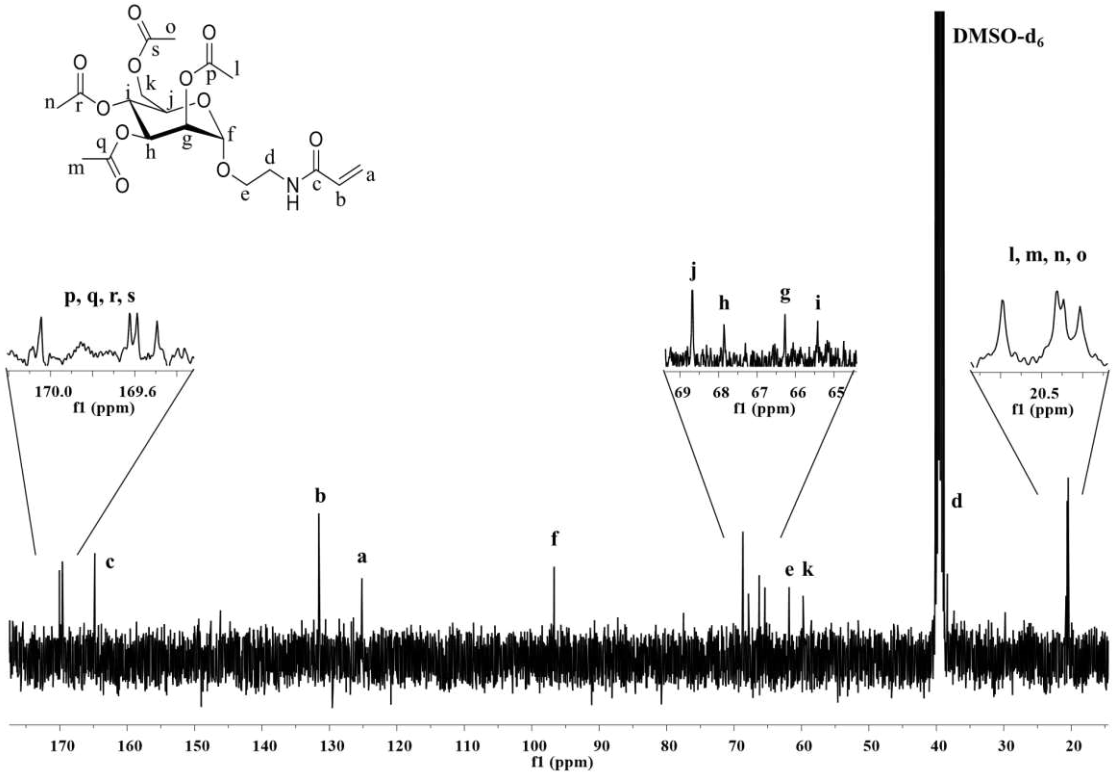

Figure 16. *[13]C-NMR spectrum in DMSO-d_6 of 2,3,4,5-O-tetraacetyl-D-mannopyranosyloxyethyl acrylamide.*

The ESI-TOF mass spectrometry analysis, carried out in positive mode, showed a signal at m/z of 446.1674 $[M-H]^+$, in agreement with the expected mass of 446.428 g mol^{-1}.
Deacetylation of 2,3,4,6-O-tetraacetyl-D-mannopyranosyloxyethyl acrylamide was performed by esters hydrolysis using a methanolic solution of KOH and yielded the D-mannopyranosyloxyethyl acrylamide. The product was then purified passing the solution through a short pad of silica and characterized by ^{1}H-NMR, ^{13}C-NMR, FT-IR spectroscopy and ESI-TOF mass spectrometry.

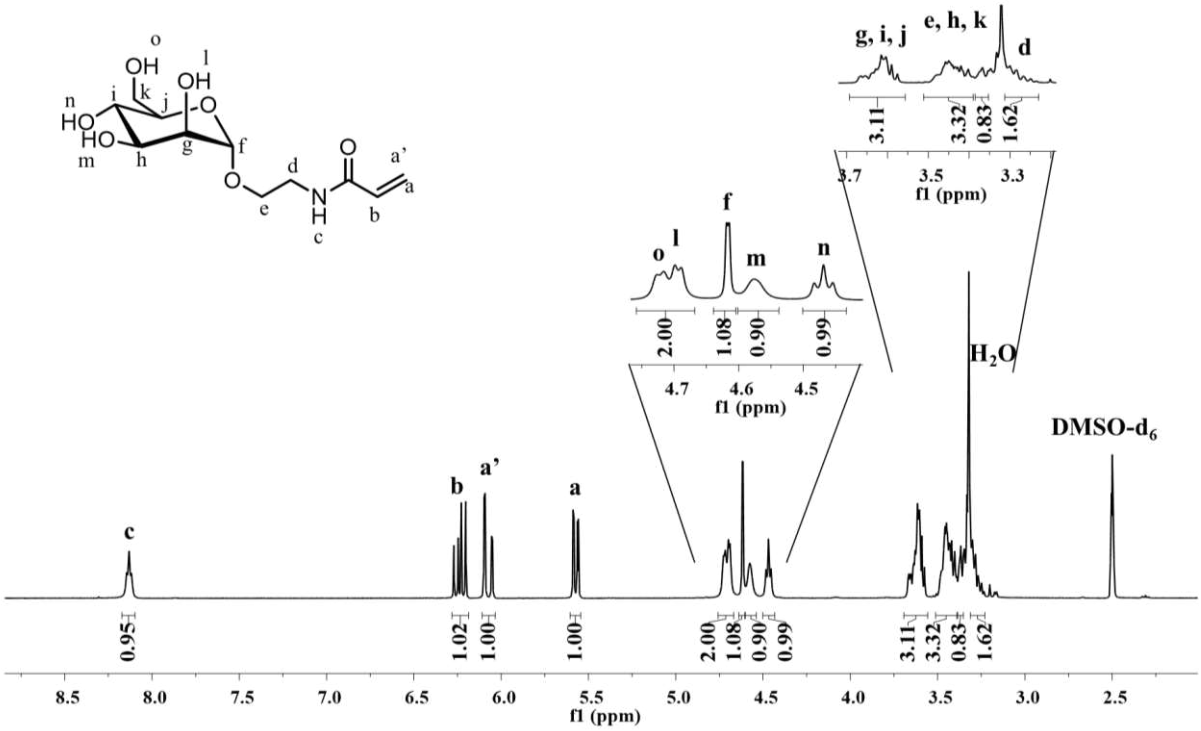

Figure 17. *^{1}H-NMR spectrum in DMSO-d_6 of D-mannopyranosyloxyethyl acrylamide.*

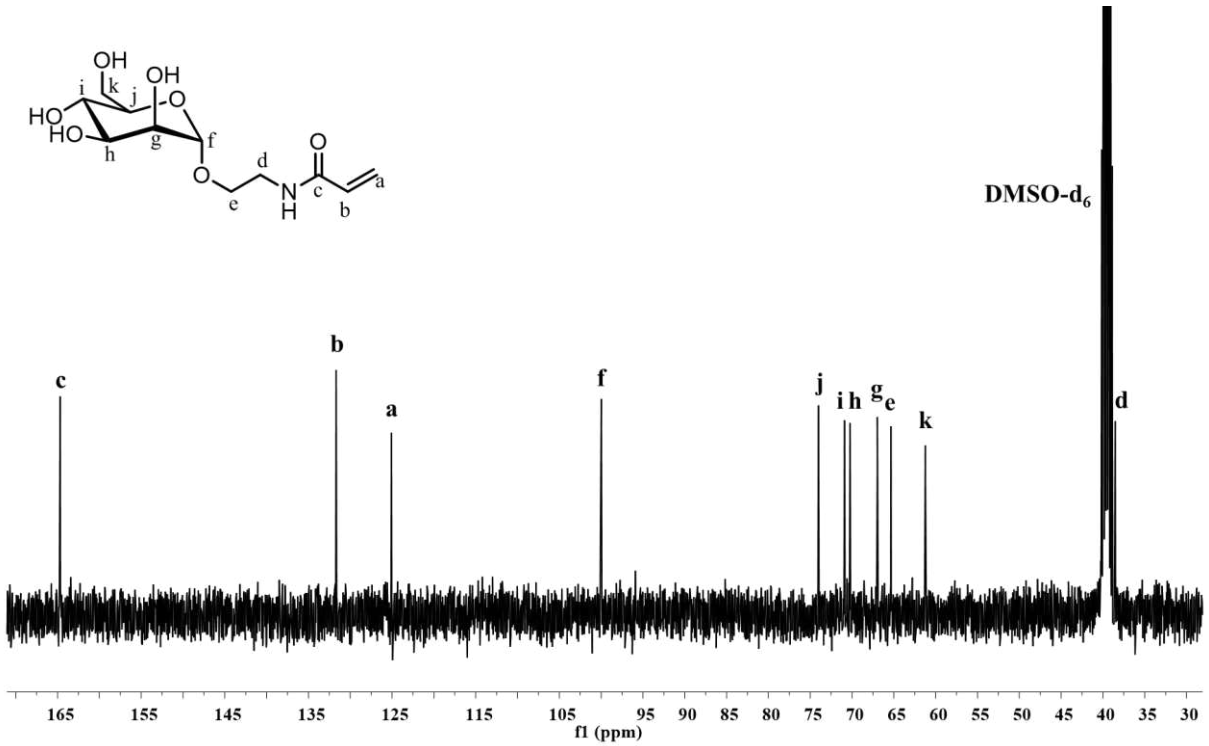

Figure 18. *^{13}C-NMR spectrum in DMSO-d_6 of D-mannopyranosyloxyethyl acrylamide.*

The ESI-TOF mass spectrometry analysis, carried out in positive mode, showed a signal at m/z of 300.1061 $[M+Na]^+$, in agreement with the expected mass of 300.11 g mol^{-1}. Furthermore, the hydrolysis of ester groups was confirmed also by FT-IR spectrum of D-mannopyranosyloxyethyl acrylamide, which showed the presence of the signal related to the stretching of OH group at 3500 cm^{-1}, the disappearance of the C-O-C signal at 1230 cm^{-1} and of the C=O peak at 1750 cm^{-1}.

3.3 Synthesis of Agmatine Acrylamide

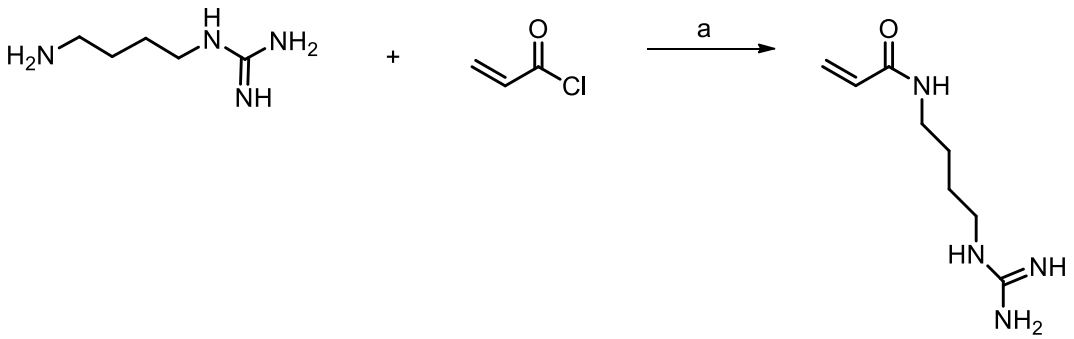

Scheme 4. *Synthesis of agmatine acrylamide. Reagents and conditions: a) K_2CO_3 30 mM, 0 °C, o.n..*

Agmatine acrylamide was synthesized according to a one step process described in Scheme 4 and reported by Algotsson M. et al.[78] During the acylation process, agmatine sulfate was maintained under basic conditions (K_2CO_3) to avoid amine protonation and the loss of nucleophilicity, which dictate the reactivity. Agmatine free amine reacted with acryloyl chloride electrophilic carbonyl group thus replacing the leaving group (Cl^-), which led to the formation of the desired product, agmatine acrylamide (Agm).

The progress of the reaction was monitored by thin layer chromatography (TLC) until complete disappearance of the free amine purple spot, visualized by ninhydrin staining. The reaction was carried out using an excess of acryloyl chloride, which allowed to overcome the problem of its rapid inactivation in the aqueous basic conditions adopted for the reaction and to achieve an excellent yield of conjugation. As a consequence, a purification step by extraction was required to remove the acrylic acid side product.

^{1}H-NMR and ^{13}C-NMR analysis after purification confirmed the identity and the purity of the product (Figure 19 and Figure 20).

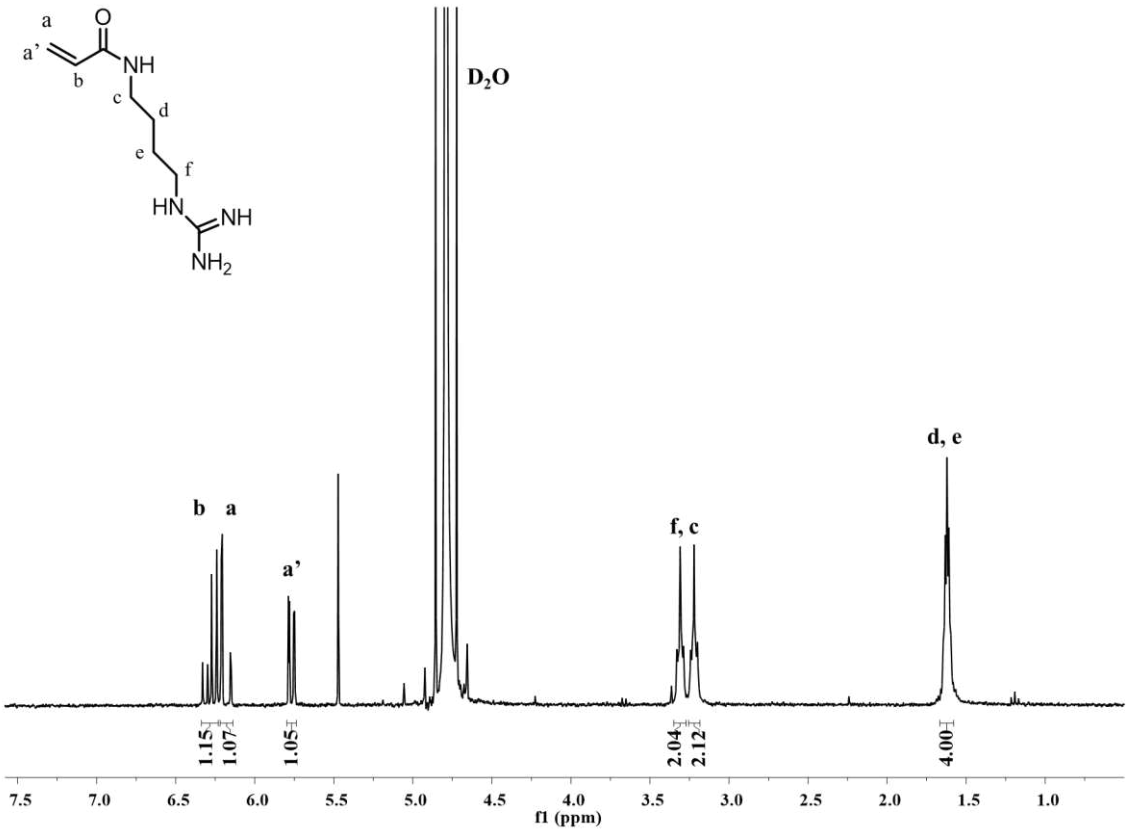

Figure 19. *^{1}H-NMR spectrum in D_2O of pure agmatine acrylamide.*

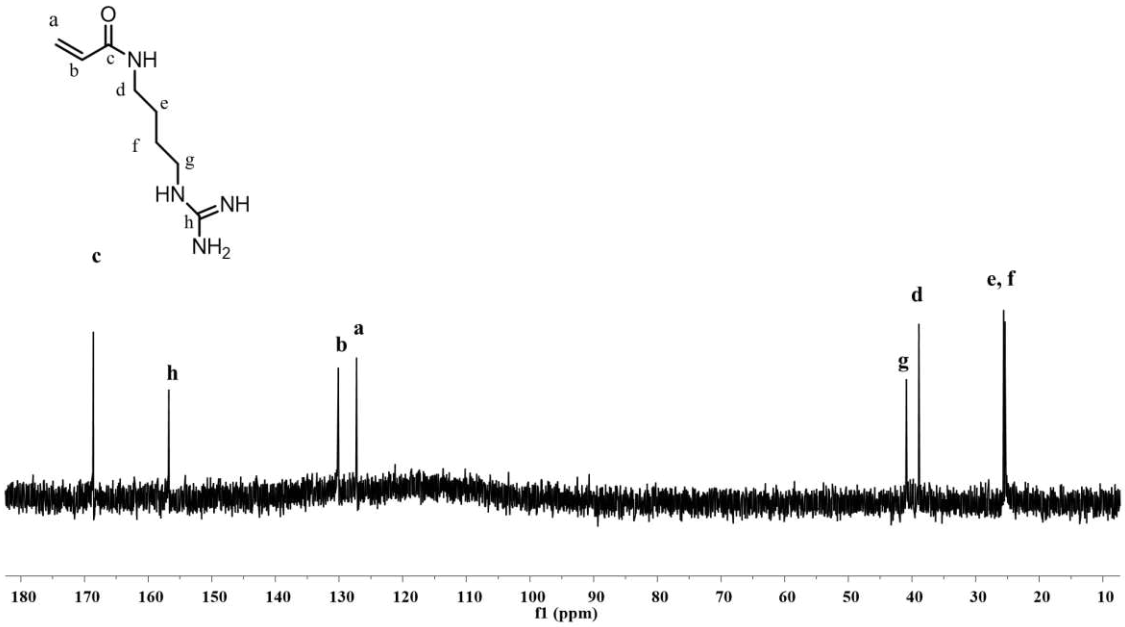

Figure 20. *^{13}C-NMR spectrum in D_2O of pure agmatine acrylamide.*

The pure product was also analyzed by ESI-TOF mass spectroscopy, which showed the ion m/z 185.140 corresponding to the mono charged species. Moreover, the FT-IR analysis further confirmed the presence of the product as the signal at 3367 cm^{-1}, attributed to the newly formed secondary amide bond, was detected.

3.4 Synthesis and characterization of diblock and triblock co-polymers

Block co-polymers are emerging as a powerful tool in the drug delivery field in virtue of their easy production, their versatility and their tunable characteristics. The different specific functions of each monomer allow to design tailored co-polymers for a variety of applications. The intrinsic multifunctionality of polymers can inherently fulfill several requirements for the delivery of nucleic acid, from the active targeting to specific cell types to the endosomolytic function, from the nuclear entry to the protection from nuclease degradation.[82]

In this PhD project, two different generations of cationic block co-polymers were designed and investigated for the non-viral nucleotides or gene delivery. The two small polymer libraries have been instructed for the delivery of genetic materials encoding TAAs to dendritic cells. Particularly, the 1st generation of polymers included a positively charged agmatine-based block for nucleic acid electrostatic complexation and a mannosylated block was used

for the active targeting to the APCs. Furthermore, the addition of a hydrophobic butyl-based block endowed the 2nd generation polymers with endosomolytic properties, improving genetic materials release to the cytoplasm after internalization.

A living radical polymerization technique, called Reversible Addition Fragmentation chain Transfer (RAFT) polymerization (see paragraph 1.7), was chosen for its experimental simplicity compared to other polymerization techniques and because it allows for the precise control on polymers molecular weight. Furthermore, the optimized one-pot rapid method described by Gody *et al.*[71] was adopted, thus enabling full monomer conversion and no purification steps at the end of each block synthesis. RAFT polymerization involves the use of a chain transfer agent (CTA), also called RAFT agent, that here was represented by 4-cyano-4-(ethylsulfanylthiocarbonylsulfanyl)pentanoic acid. The transfer of the S=C(S)S- moiety from the RAFT agent to the radical monomer results in a polymer containing the same functionality and capable to reinitiate a new living polymerization, acting as a macro-CTA. Here, the choice of a trithiocarbonate RAFT agent was driven by its efficacy in polymerization of acrylic monomers and by the demonstrated negligible cytotoxicity of its terminal groups.[83]

The water soluble azo initiator 2,2'-azobis[2-(2-imidazolin-2-yl)propane]dihydrochloride (VA-044) was used as source of initiating radicals and thermally activated at 60 °C to trigger the polymerization. Its low decomposition temperature (half-life of 10 h at 44 °C in water) guarantees for a fast polymerization without affecting the livingness, as the initiator undergoes 95% consumption in 2 hours of reaction.[71] Furthermore, the chosen CTA/initiator molar ratio was 1:0.02 to minimize the number of initiator-derived chains involved in the formation of dead chains, resulting in product with very low PDI and controlled molecular weight.

Finally, also the inert atmosphere obtained by argon bubbling decreased the number of dead chains by excluding the presence of oxygen in the reaction vessel, which is a polymerization retarder and can cause free radical polymerization and chain termination.

Fast RAFT polymerization allows to push the monomer conversion to almost 100%, while still yielding polymers with very low dispersity and predetermined molecular weight. In our investigations, monomer conversion was checked after 2 hours by ^{1}H-NMR analysis and calculated by comparing the integrals of the vinyl protons signals of the monomers at 5.6-6.3 ppm, which decreased during the polymerization, with the signal relative to the anomeric

proton of D-mannopyranosyloxyethyl acrylamide monomer and polymer repeating units, as shown by the equation below:

$$Conversion\ \% = 100\ \times \frac{A - M}{A} \tag{3}$$

where M is the integral of a monomer vinyl proton, and A is the integral of the anomeric mannose proton for both monomer and polymer repeating units (these peaks are overlapped in the ^{1}H-NMR spectrum).

3.4.1 Synthesis of 1st generation polymers: Man_x-*b*-Agm_y

Di-block copolymers were synthesized using identical monomer feed ratio but increasing total monomers units, that is different CTA/monomer feed ratios (corresponding to different final polymer length and molecular weights), to investigate the effect of each monomer on the biopharmaceutical proprieties of the polymer and of the polyplexes.

The general scheme of reaction to obtain the 1st generation polymers is reported in Scheme 5.

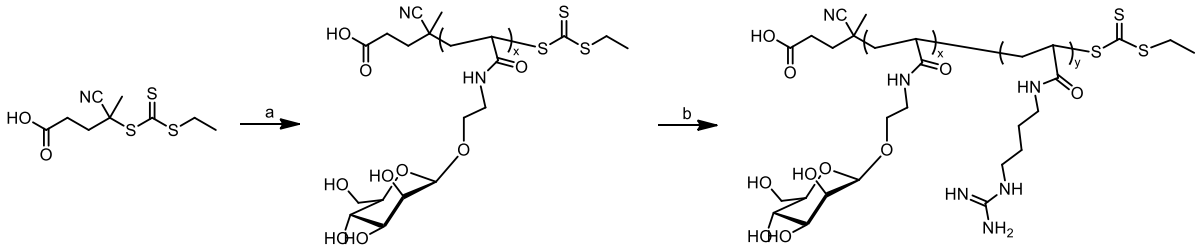

Scheme 5. *Synthesis of Man_x-b-Agm_y 1st generation polymers. Reagents and conditions: a) D-mannopyranosyloxyethyl acrylamide, VA-044, water/dioxane 80:20 v/v, Ar atmosphere, 60 °C, 2h; b) agmatine acrylamide, VA-044, water/dioxane 80:20 v/v, Ar atmosphere, 60 °C, 2h.*

The influence of ligand valency on the targeting of dendritic cells by mannosylated liposomes or polymers was investigated by Espuelas *et al.*[84] and by Raviv and coworkers[85], respectively. Particularly, these authors screened the improved efficacy of their platforms after modification with mono-, di- or tri-valent mannoses. In this thesis project, we evaluated the effect of multivalency in mannose receptor affinity and binding by synthesizing polymers with a high number of mannose units. Starting from the example of the commercially available Lymphoseek®, which presents 12-20 mannose units for each dextran backbone, Man and Agm were used as monomers to generate 3 block-copolymers with different

polymerization degrees (DP, monomer units): Man_{15}-*b*-Agm_{12}, Man_{29}-*b*-Agm_{25} and Man_{58}-*b*-Agm_{45}. The feed ratios used and the main features of the synthesized polymers are summarized in Table 1.

***Table 1**. Man_x-b-Agm_y diblock copolymers feed ratios, conversion percentage (C%), final composition, M_n and Đ.*

Polymers [a]	[CTA]:[Man]:[Agm] Feed ratio	C %[a]	[Man]:[Agm][b] Final ratio	$M_{n,th}$ [c] (kDa)	$M_{n,GPC}$ [d] (kDa)	Đ[c]
Man_{15}-*b*-Agm_{12}	1:16:16	94; 75	1.2:1	6.6	12.4	1.13
Man_{29}-*b*-Agm_{25}	1:32:32	91; 78	1.2:1	12.9	29.8	1.43
Man_{58}-*b*-Agm_{45}	1:64:64	91; 70	1.3:1	24.6	66.9	1.29

[a]Conversion percentage is reported as Man%; Agm% as determined by ^{1}H-NMR

[b]Copolymers composition (DP_{Man} and DP_{Agm}) was estimated by ^{1}H NMR in DMSO-d_6.

[c]Copolymer theoretical molecular weight was calculated according to the following equation: $M_{n,th}=[([M]_0/[CTA]_0) \times MWmon \times Conv] + [MWmacro\text{-}CTA]$, where MW: molecular weight; e $[M]_0$ and $[CTA]_0$: initial molar concentration of the monomer and the chain transfer agent; Conv: conversion.

[d]Determined by GPC using 0.4 M ammonium acetate, pH 4.5 as mobile phase, in a system calibrated with pullulan standard.

The polymerization was performed in a mixture of water/Dioxane (80:20 v/v). Water was selected as solvent because, in addition of being environmentally friendly and allowing the production of water-soluble macromolecules, it is also known to increase the propagation rate (k_p) of vinyl monomers and consequently the polymerization rate (Rp), thus it is the solvent of choice for the fast RAFT procedure.[86] On the other hand, the addition of 20% v/v dioxane was mandatory to ensure complete solubilization of the CTA, which otherwise would have led to the loss of molecular weight control. 4-cyano-4-(ethylsulfanylthiocarbonylsulfanyl)pentanoic acid was chosen because of the higher hydrolytic stability of trithiocarbonates compared to other CTAs.[3]

In the first step, an initial D-mannopyranosyloxyethyl acrylamide monomer concentration of 3 M was used, which provided a workable solution viscosity. Under these conditions, mannose monomer successfully polymerized with a monomer conversion higher than 90% for all the synthesized blocks, resulting in a quantitative yield and in the possibility to circumvent

intermediate purification. The conversion was calculated by comparing the integrals of amide group in the monomer (t, 1H, N*H*, 8.3 ppm) and in the polymer (br, 1H, N*H*, 7.2-8.0 ppm). Moreover, vinylic protons signals at 5.57, 6.07 and 6.24 ppm (Figure 15) almost disappeared, while peaks corresponding to the newly formed polymer backbone were found at 0.66-2.30 ppm (Figure 21). For the first step of polymerization a monomer conversion of 91%, for the [CTA]:[Man] ratios of 1:16 and 1:32, and of 94%, for the [CTA]:[Man] ratio of 1:64, were achieved, resulting in Man_{15}, Man_{29} and Man_{58} macro-CTAs.

The obtained macro-CTA (Man_x) still bears a reactive trithiocarbonate functional group that can interact again with other monomers for the chain elongation in a one-pot sequential polymerization procedure. Accordingly, agmatine acrylamide at 3 M concentration was directly added to the reaction mixture and the polymerization was conducted under the same conditions described for the first step. The second block extension step did not require further addition of dioxane because the macro-CTA was fully water-soluble. Under these conditions, agmatine monomer successfully polymerized with a monomer conversion higher than 70-80% although at least three addition of the radical source were required. The Agm conversion was calculated by monitoring the decrease from time 0 to 2 hours reaction of the agmatine vinylic protons signals (5.50-6.20 ppm) as compared to the anomeric and hydroxyl protons (4.4-4.9 ppm) of Man_x macro-CTAs set as reference integrals. The reaction was stopped at a monomer conversion of 70-80% for all the polymers obtaining Man_{15}-*b*-Agm_{12}, Man_{29}-*b*-Agm_{25} and Man_{58}-*b*-Agm_{45} as diblock polymers.

As an example, the ^{1}H-NMR spectra and the peak attribution of the macro-CTA Man_{58} and of the diblock co-polymer Man_{58}-*b*-Agm_{45} are reported in Figure 21 and Figure 22, respectively.

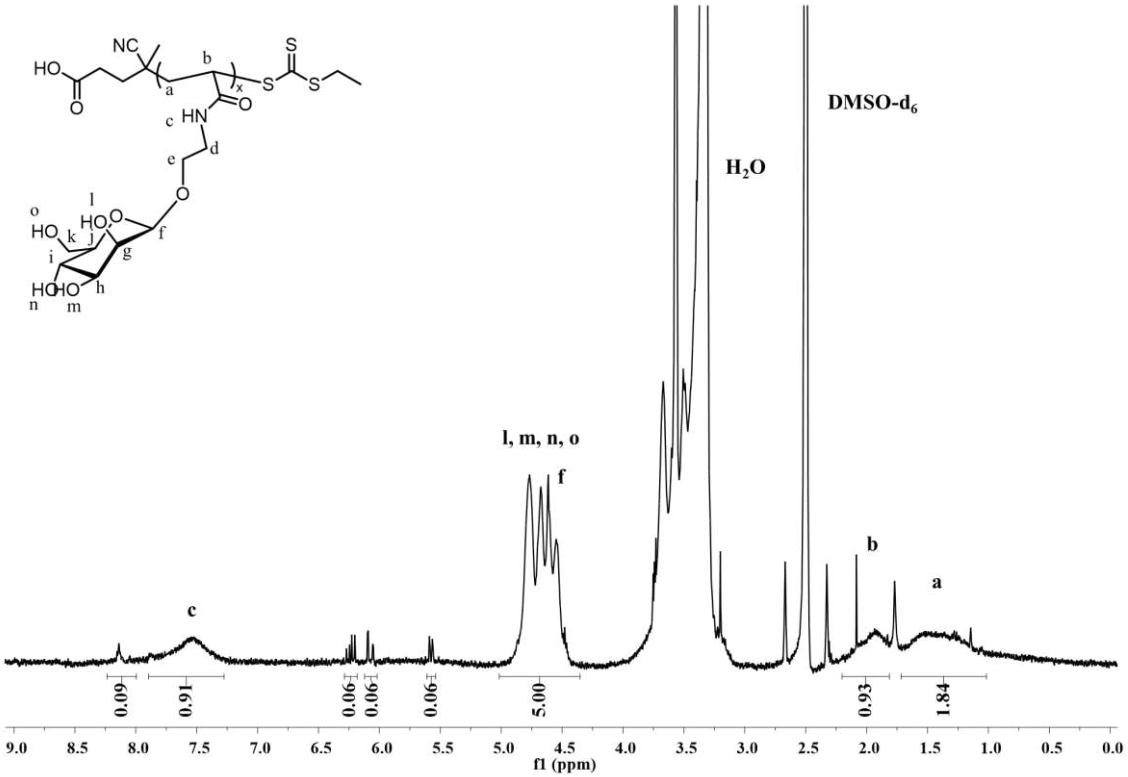

Figure 21. *^{1}H-NMR spectrum in DMSO-d_6 of the macro-CTA Man_{58} at the end of the polymerization.*

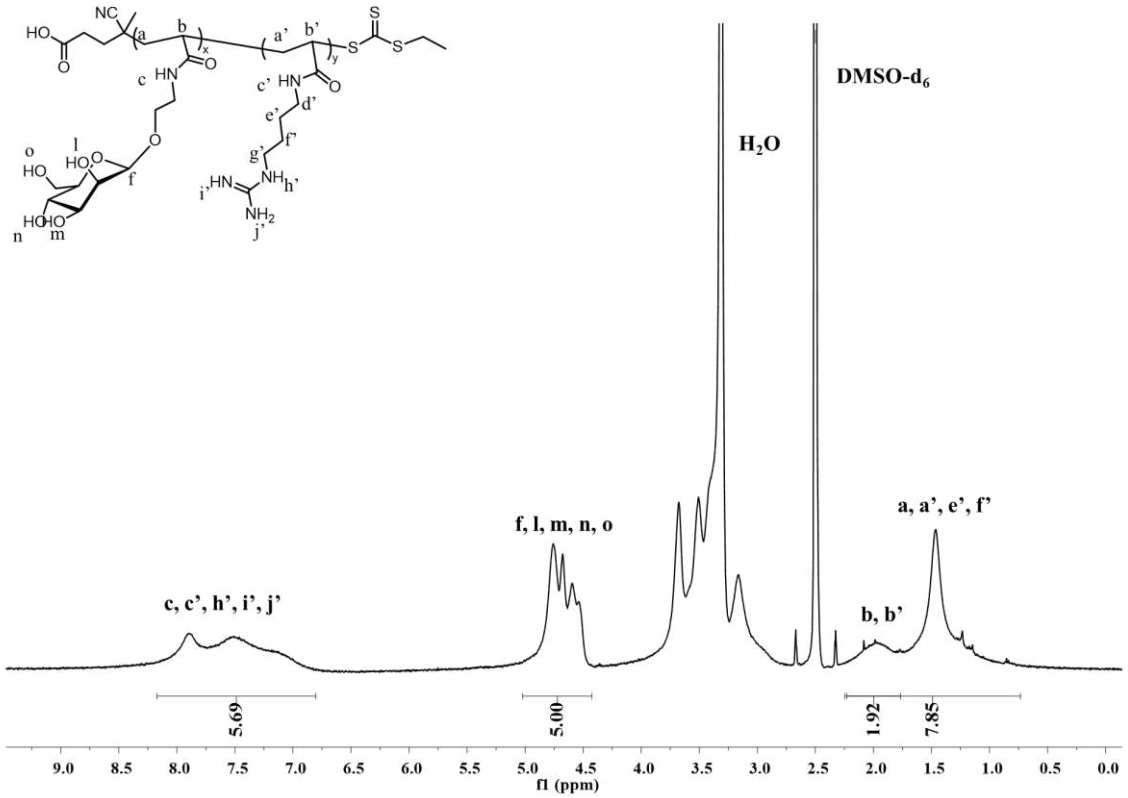

Figure 22. *^{1}H-NMR spectrum in DMSO-d_6 of Man_{58}-b-Agm_{45} after purification by dialysis.*

After purification by dialysis, diblock co-polymers were characterized by gel permeation chromatography (GPC) using a Viscotek TDA302 system. A fairly high ionic strength, low pH eluent (ammonium acetate 0.4 M, pH 4.5) was selected to prevent polymers enthalpic interactions with the stationary phase in the column, due to ion exclusion and ion interaction phenomena. It should be mentioned that the pH of eluent was adjusted to 4.5 using acetic acid, which might act as organic modifier, reducing possible hydrophobic interactions between polymers and the stationary phase.[87] A relatively low polydispersity index in the range of 1.13-1.43 was found for the polymers. The experimental molecular weights were found to be slightly higher than the theoretical probably due to substantial differences in the hydrodynamic volume of the novel synthesized materials as compared to the pullulan standard used for instrument calibration. Indeed, aqueous GPC is problematic for the analysis of polyelectrolytes due to their interactions and the lack of suitable calibration standards.[87]

3.4.2 Synthesis of 2nd generation polymers: Man_x-*b*-Agm_y-*b*-But_z

Two triblock copolymers were synthesized using the poly$(Man)_x$-*b*-$(Agm)_y$ as cationic hydrophilic block and macro-CTA and the commercially available purified butyl acrylate (But) as monomer.

Mannose and agmatine acrylamide were used as monomers for the first and the second block and the synthesis proceeded as reported in Scheme 6. Regarding the third block, a small amount of water was added to the reaction mixture to reduce the viscosity and favor a homogeneous polymerization, and the butyl acrylate was added directly into the reaction vessels. Nevertheless, a higher concentration of initiator (macro-CTA/VA-044 1:0.04 molar ratio) was required to efficiently polymerize this monomer. The macro-CTA/monomer feed ratio was 1:0.5.

Two block-copolymers with different polymerization degrees (DP, monomer units) were obtained, Man_{29}-*b*-Agm_{29}-*b*-But_9 and Man_{62}-*b*-Agm_{52}-*b*-But_{32}, and their properties are reported in Table 2.

Table 2. *Man_x-b-Agm_y-b-But_z triblock copolymers feed ratios, conversion percentage (C%), final composition, M_n and Đ.*

Polymers [a]	[CTA]:[Man]:[Agm]:[But] Feed ratio	C %[a]	[Man]:[Agm]:[But][b] Final ratio	$M_{n,th}$ [c] (kDa)	$M_{n,GPC}$ [d] (kDa)	Đ[c]
Man_{29}-*b*-Agm_{29}-*b*-But_9	1:32:32:9	91; 91; 100	1:1:0.3	14.8	31.1	1.16
Man_{62}-*b*-Agm_{52}-*b*-But_{32}	1:64:64:32	97; 81; 100	1.2:1:0.6	31.1	38.4	1.07

[a]Conversion percentage is reported as Man%; Agm%; But% as determined by ^{1}H-NMR

[b]Copolymers composition (DP_{Man}, DP_{Agm} and DP_{But}) was estimated by ^{1}H NMR in DMSO-d_6.

[c]Copolymer theoretical molecular weight was calculated according to the following equation: $M_{n,th}=[([M]_0/[CTA]_0) \times MWmon \times Conv] + [MWmacro\text{-}CTA]$, where MW: molecular weight; $[M]_0$ and $[CTA]_0$: initial molar concentration of the monomer and the chain transfer agent; Conv: conversion.

[d]Determined by GPC using 0.4 M ammonium acetate, pH 4.5 as mobile phase, in a system calibrated with pullulan standard.

The triblock copolymers were designed to have identical Man and Agm units of the corresponding diblock copolymers Man_{29}-*b*-Agm_{25} and Man_{58}-*b*-Agm_{45}, to evaluate the effects of this hydrophobic block on the physicochemical, colloidal and biological properties of the 2nd generation as compared to the 1st generation polymers. A third smaller 2nd generation polymer was not synthesized, since the corresponding 1st generation Man_{15}-*b*-Agm_{12} was not performing as expected (*vide infra*). Furthermore, it was decided to use a butyl acrylate/mannose acrylate monomer ratio of 0.3:1 or 0.5:1 for Man_{29}-*b*-Agm_{29}-*b*-But_9 and Man_{62}-*b*-Agm_{52}-*b*-But_{32}, respectively, to maintain the high solubility of the polymers in aqueous media and to avoid the generation of self-assembling material, which could affect nucleic acid complexation.

The general scheme for 2nd generation polymer synthesis is reported in Scheme 6.

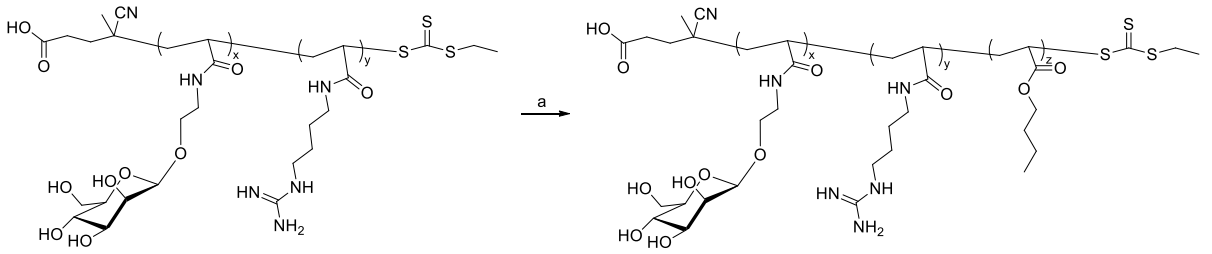

Scheme 6. *Synthesis of Man$_x$-b-Agm$_y$-b-But$_z$ 2nd generation polymers. Reagents and conditions: a) VA-044, water/dioxane 80/20, Ar atmosphere, 60 °C, 2h.*

The first two steps of the triblock co-polymers polymerization were performed in a mixture of water/Dioxane (80:20 v/v), following procedure and details reported in paragraph 3.4.1, which resulted in macro-CTAs Man$_{29}$-*b*-Agm$_{29}$ and Man$_{62}$-*b*-Agm$_{52}$.

All steps were monitored by ^{1}H-NMR to assess the polymerization yield analyzing samples withdrawn from the reaction mixture. As an example, the ^{1}H-NMR spectrum of Man$_{62}$-*b*-Agm$_{52}$-*b*-But$_{32}$ is reported in Figure 23.

The chain elongation with butyl acrylate was confirmed by the disappearance of vinylic protons at 5.9-6.3 ppm and the chemical shift of the methylene protons from 4.38 ppm in the monomer (t, 2H) to 4.08-4.12 (bm, 2H) in the polymer. Integrals from mannose anomeric and hydroxyl protons (4.94-5.50 ppm) were used as reference for monomer conversion evaluation. A single addition of VA-044 initiator was sufficient to achieve 100% monomer conversion in the two polymerizations performed, obtaining Man$_{29}$-*b*-Agm$_{29}$-*b*-But$_9$ and Man$_{62}$-*b*-Agm$_{52}$-*b*-But$_{32}$.

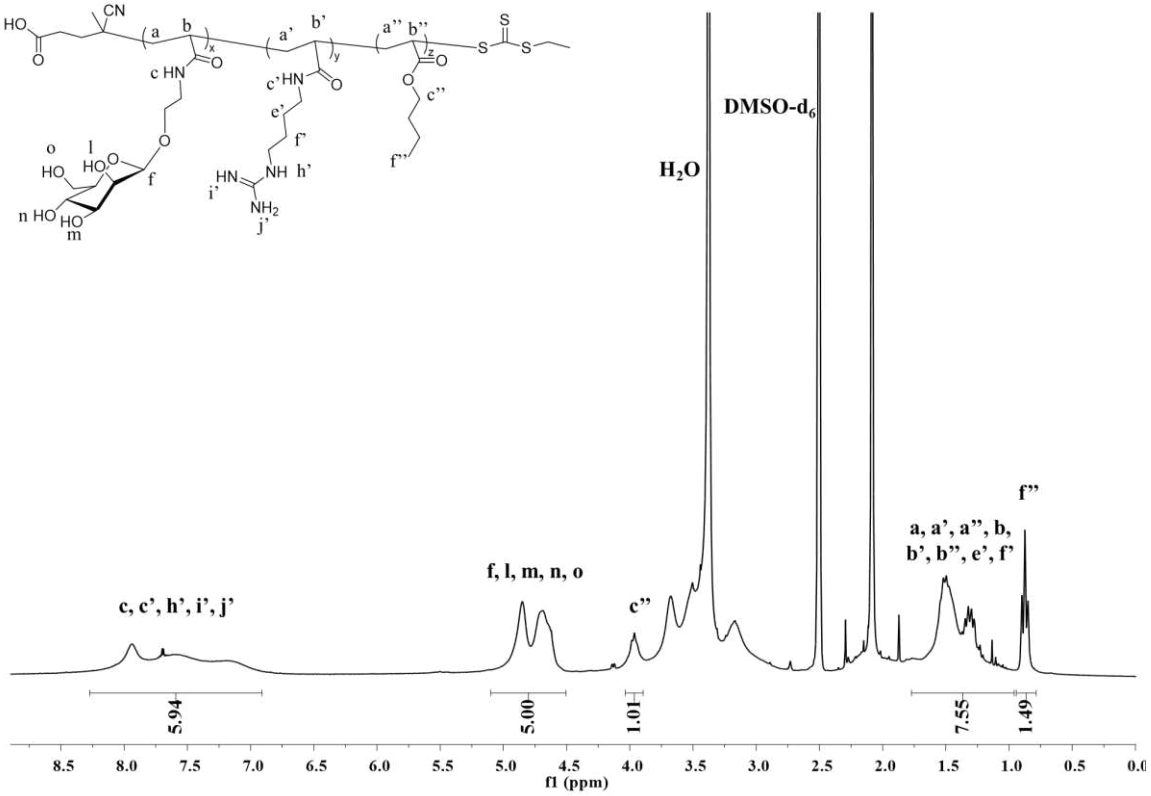

Figure 23. *^{1}H-NMR spectrum in DMSO-d_6 of Man_{62}-b-Agm_{52}-b-But_{32} after purification by dialysis.*

After purification by dialysis the 2nd generation polymers were analyzed by GPC as reported for the 1st generation resulting in a very low polydispersity index (1.16 for Man_{29}-*b*-Agm_{29}-*b*-But_{9} and 1.07 for Man_{62}-*b*-Agm_{52}-*b*-But_{32}), confirming that the polymerization proceeded in a controlled manner.

3.5 Polymers/DNA complexation studies

Cationic polymers have suitable features for physical encapsulation of nucleic acids according to noncovalent electrostatic interactions. Indeed, cationic polymers and nucleic acids are macromolecules with size in the same range but with opposite charge.[82] The novel materials we investigated were designed to include a nucleotide complexing portion, represented by agmatine, bearing a high cationic charge due to protonation of the guanidine group (pKa = 12.48) at physiological pH. Agmatine-based polymers were designed to induce the formation of stable and tightly complexed particles, enabling the charge pairing and shielding the negatively charged sugar-phosphate backbone of DNA, which may favor the

interaction with cells and the cellular uptake by preventing nucleic acids electrostatic repulsion with the negatively charged cell surface. Importantly, in virtue of the encapsulation of the genetic material, the system is also expected to provide nucleic acid protection against fast degradation operated by nucleases.

Electrophoretic mobility shift assays were performed to investigate polymers DNA complexation ability at different nitrogen to phosphate (N/P) ratios, which is calculated as the molar ratio between positively charged nitrogen groups in the polymer backbone due to agmatine, and negatively charged phosphate groups of nucleic acid. Primarily, the assay provided crucial information concerning the N/P ratio required for complete DNA complexation was taking place. Indeed, when complexed with polymers, DNA does not migrate in acrylamide or agarose gel, while the appearance of a band in the gel indicates either a partial complexation or a release of the nucleic by the complex.

In the preliminary screening, polyplexes were assembled using a 19-base ssDNA or plasmid DNA encoding Enhanced Green Fluorescent Protein (pEGFP), as models for CpG ODNs and high molecular weight DNA coding for tumour antigens, respectively, in view of developing the system for nucleic acid-based immunotherapy. It should be underlined that, as reported by Blakney *et al.*[88], there is not *a-one-size-fits-all* polymer for nucleic acid delivery, but rather each nucleic acid species benefits from a tailored delivery system.

Moreover, the integrity and the stability of polyplexes were investigated in presence of increasing concentration of the competitive anionic compound heparin, that is present in the human serum in the plasma at a concentration of 0.15 International Unit (IU)/mL.[89] Considering that the physiological environment is characterized by the presence of polyanions, such as serum proteins, extracellular matrix components, and cell surface glycosaminoglycans, the competition between these biological anions and nucleic acids may cause the displacement and release of DNA from the GPPs, thus hampering GPPs stability and transfection efficiency after administration.

3.5.1 Complexation studies with model ssDNA

ssDNA 19-nucleotides model sequence underwent gel electrophoresis in a 12% w/v acrylamide gel in presence of increasing ratio of block copolymers to evaluate the N/P ratio at which the DNA complexation was complete.

Figure 24, panel a), shows the electrophoretic profiles of the ssDNA/polymer mixtures. The ssDNA complexation efficiency with 1st generation polymers was found to be correlated to the molecular weight and agmatine units. Particularly, Man_{15}-*b*-Agm_{12}, Man_{29}-*b*-Agm_{25} and Man_{58}-*b*-Agm_{45} were able to complex ssDNA at N/P ratios 20, 10 and 5, respectively. It is worth mentioning that, by definition, at the same N/P ratio an equal number of guanidine groups are involved in the DNA complexation, no matter which polymer is used. Accordingly, it could be assumed that the complexation ability of a defined number of agmatine groups is higher when they are all close to each other in the same polymeric block than when they are located in different polymer chains. On the contrary, 2nd generation polymers complexation efficiency was not affected by the increase in agmatine block length, being ssDNA completely complexed at N/P ratio 3 either for Man_{29}-*b*-Agm_{29}-*b*-But_{9} or Man_{62}-*b*-Agm_{52}-*b*-But_{32}. We can therefore postulate that the presence of the third block enhanced ssDNA packing, maybe cooperating with hydrophobic interaction with purines and pyrimidines aromatic rings.

Glycopolyplexes were formulated for all the following studies at the N/P ratios reported above and highlighted in the panel a), in order to guarantee a complete complexation of the ssDNA. In view of an *in vivo* application, polyplexes stability and integrity were evaluated in presence of heparin in a concentration range of 0.15-10 IU/mL (Figure 24, panel b).

These delivery systems are intended for subcutaneous injection and displacement studies with heparin provide crucial information about their stability in presence of anions occurring in the physiological environment. Particularly, Man_{15}-*b*-Agm_{12}/ssDNA, Man_{29}-*b*-Agm_{25}/ssDNA and Man_{58}-*b*-Agm_{45}/ssDNA polyplexes were found to strongly retain ssDNA after 15 minutes incubation with heparin at concentration up to 2, 4 and 6 IU/mL, respectively, which are about 12-, 27- and 40-times higher as compared to the physiological value (i.e. 0.15 IU/mL). This confirmed the strong electrostatic interaction occurring between the guanidine group in the polymer and the sugar-phosphate backbone of ssDNA.

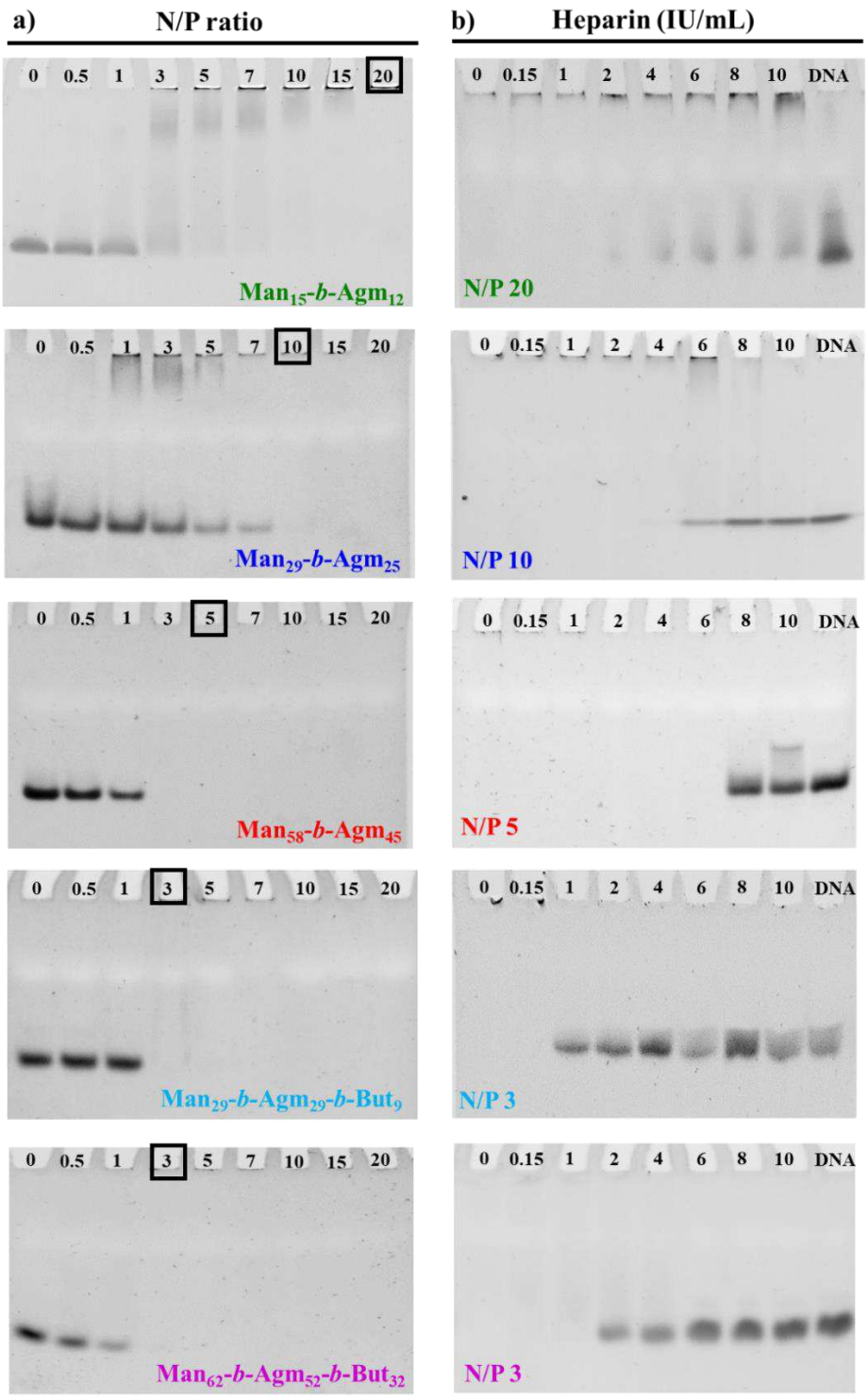

Figure 24. *(a) Gel mobility assay of, from top to bottom, Man_{15}-b-Agm_{12}/ssDNA, Man_{29}-b-Agm_{25}/ssDNA, Man_{58}-b-Agm_{45}/ssDNA, Man_{29}-b-Agm_{29}-b-But_9/ssDNA and Man_{62}-b-Agm_{52}-b-But_{32}/ssDNA. N/P ratios in the range 0-20 were tested for gel mobility assay. The ratios selected for all the following studies are encircled with a black rectangle. (b) GPPs stability evaluation by heparin displacement assay. Polyplexes were prepared at the N/P ratios reported in the left bottom corner and heparin was used in a concentration range of 0-10 IU/mL. Free ssDNA was used as positive control.*

Furthermore, for Man_x-*b*-Agm_y/ssDNA polyplexes the stability was found to linearly increase according to the molecular weight of the polymer used (Man_{58}-*b*-Agm_{45}/ssDNA > Man_{29}-*b*-Agm_{25}/ssDNA > Man_{15}-*b*-Agm_{12}/ssDNA), which was in agreement with the complexation efficiency discussed above. On the other hand, despite the butyl-based block seemed to ameliorate the complexation performances as shown previously, it was also responsible of a decreased stability of the polyplexes in presence of anionic competitors. Indeed, ssDNA is completely released at a heparin concentration of 1 and 2 IU/mL for Man_{29}-*b*-Agm_{29}-*b*-But_9/ssDNA and Man_{62}-*b*-Agm_{52}-*b*-But_{32}/ssDNA, respectively. We speculated that the lower stability of butyl-bearing glycopolyplexes could be ascribed to the different rearrangement of the GPPs generated with the triblock co-polymers in comparison to the diblock counterparts with looser interactions, which also reflects in different colloidal morphology also confirmed by TEM analysis (*vide infra*).

3.5.2 Complexation studies with plasmid DNA encoding enhanced green fluorescent protein (pEGFP) or ovalbumin (pOVA).

In view of glycopolymers application as vectors for pDNA-based immunotherapy, the study of their capacity to successfully complex high molecular weight DNA is crucial. EGFP-encoding plasmid (pEGFP) (100 ng) and ovalbumin-encoding plasmid (pOVA) (100 ng) underwent gel electrophoresis in a 1% w/v agarose gel in presence of increasing ratio of block copolymers to evaluate the N/P ratio at which full complexation of pDNA occurs (Figure 25, panel a).

The complexation efficiency of pDNA was also found to be dependent by polymers MW but at a lower extent with respect to the ssDNA. However, a N/P ratio of 5 was required to completely complex pEGFP with Man_{15}-*b*-Agm_{12} and Man_{29}-*b*-Agm_{25}, while for Man_{58}-*b*-Agm_{45} a N/P ratio of 2.5 was appropriate. Similarly to the behavior observed for the complexation of ssDNA, the pDNA complexation efficiency with the 2nd generation polymers was not affected by their molecular weight, with a full complexation at an N/P ratio of 2.5 for both Man_{29}-*b*-Agm_{29}-*b*-But_9 and Man_{62}-*b*-Agm_{52}-*b*-But_{32}. Glycopolyplexes were therefore formulated for all the following studies at the N/P ratios reported above, that allow complete complexation. Interestingly, the N/P ratios required to achieve full pDNA complexation for both generations of polymers were lower than those found for ssDNA complexation, maybe

because the different conformation and structure of the two genetic materials offer better opportunity for crosslinking, thus facilitating the assembly.

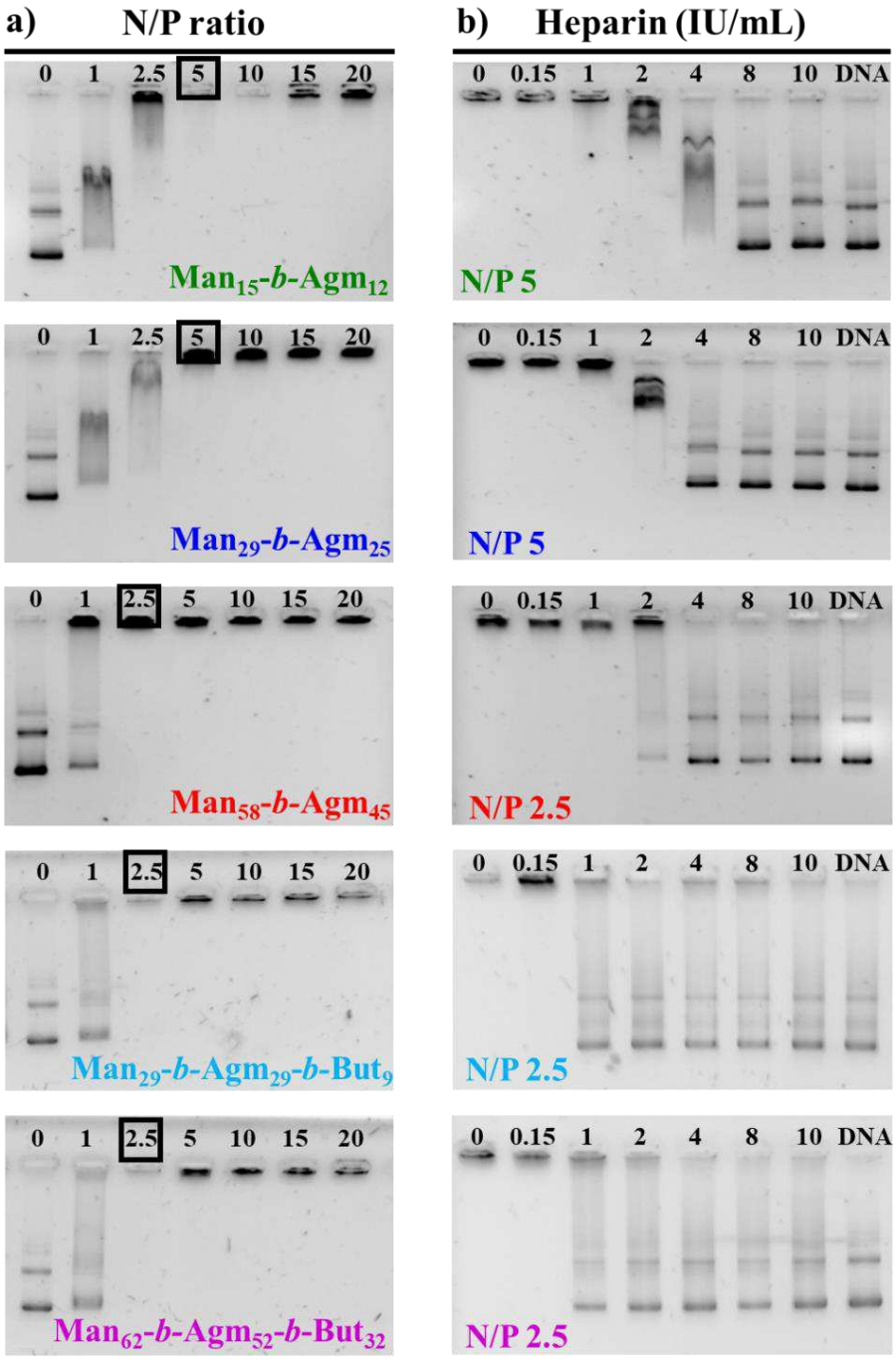

Figure 25. *(a) Agarose gel electrophoresis of, from top to bottom, Man₁₅-b-Agm₁₂/pEGFP, Man₂₉-b-Agm₂₅/pEGFP, Man₅₈-b-Agm₄₅/pEGFP, Man₂₉-b-Agm₂₉-b-But₉/pEGFP and Man₆₂-b-Agm₅₂-b-But₃₂/pEGFP. N/P ratios in the range 0-20 were tested with gel mobility assay. The ratios selected for all the following studies are encircled with a black rectangle. (b) GPPs were tested for stability by heparin displacement assay with electrophoresis. Polyplexes were prepared at the N/P ratios reported in the left bottom corner of each gel and heparin was used in a concentration range of 0-10 IU/mL. Free pDNA was used as positive control.*

The same N/P ratios identified to provide complete pEGFP complexation were also suitable for the complete complexation of ovalbumin-encoding plasmid (pOVA) with Man_{58}-*b*-Agm_{45}, Man_{29}-*b*-Agm_{29}-*b*-But_9 and Man_{62}-*b*-Agm_{52}-*b*-But_{32}, as shown in Figure 26.

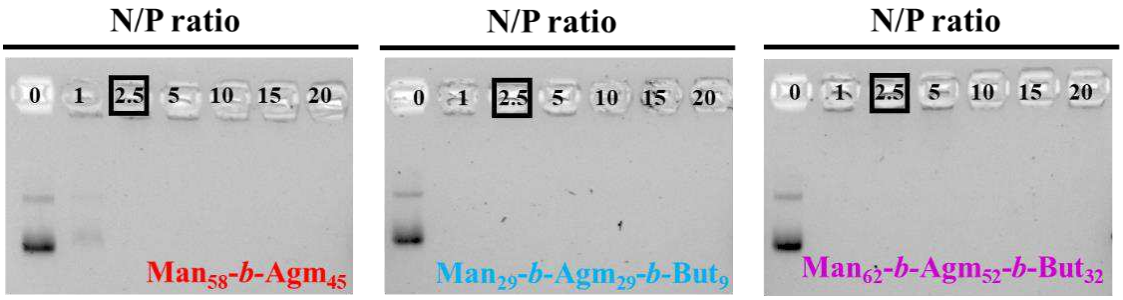

Figure 26. *Agarose gel electrophoresis of, from left to right, Man_{58}-b-Agm_{45}/pOVA, Man_{29}-b-Agm_{29}-b-But_9/pOVA and Man_{62}-b-Agm_{52}-b-But_{32}/pOVA. N/P ratios in the range 0-20 were tested with gel mobility assay. The ratios selected for the following in vitro and in vivo studies are encircled with a black rectangle.*

Premature or delayed intracellular release of DNA can also lead to inefficient gene transfer. The polyplexes unpackaging in presence of polyanionic molecules was also investigated using heparin sulfate (concentration range 0.15-10 IU/mL) that was found to displace more easily pDNA than ssDNA from the complexes (Figure 25, panel b). Indeed, a heparin sulfate concentration of 6.6- or 13-times (1 or 2 IU/mL) higher than the physiological value was enough to induce a partial pDNA competitive displacement from 1st and 2nd generation polymers, respectively. This could be explained again with a lower stability of polymer/pDNA GPPs ascribable to the fact that at the selected N/P ratios the nanoassemblies, despite they tend to assemble kinetically more efficiently, they may be more loosely structured as compared to the polymer/ssDNA GPPs, due to the different mechanism of assembling that take place depending on the DNA type and length. The different arrangement of the polyplexes at molecular level may reflect in a different morphology of the GPPs, which was observed by the TEM imaging that showed substantial differences in the ssDNA or pDNA encapsulating polyplexes (*vide infra,* paragraph 3.6).

3.6 Particles size and shape

Polyplexes size, shape and morphology are three of the more important features, that affect almost every aspect of particles colloidal and biopharmaceutical properties, including

biodistribution, uptake mechanism, payload release, intracellular trafficking, clearance and ultimately their therapeutic benefits. While intravenous administration (i.v.) of colloidal carriers requires more stringent conditions, particles up to 1 µm are suitable for the subcutaneous route (s.c.), the latter being the administration strategy for which our polyplexes were designed.

Polymers/ssDNA polyplexes were analyzed by Dynamic Light Scattering at the N/P ratios previously selected. Indeed, a complete complexation of the ssDNA is necessary to ensure the formation of stable and compact particles. Samples were prepared in PBS and the analysis were acquired considering the volume-based size (Figure 27). Notably, all the polymers were found to form colloidal structures with a low polydispersity index (PDI), ranging from 0.397 for the polyplexes obtained with the lowest MW polymer, i.e. Man_{15}-*b*-Agm_{12}/ssDNA, to 0.059 for Man_{58}-*b*-Agm_{45}/ssDNA. Regarding particles size, volume-based diameters of 25.1±5.9 nm, 23.6±2.9 nm, 45.2±0.7 nm, 43.5±1 nm and 52.9±0.5 nm were found for Man_{15}-*b*-Agm_{12}/ssDNA, Man_{29}-*b*-Agm_{25}/ssDNA, Man_{58}-*b*-Agm_{45}/ssDNA, Man_{29}-*b*-Agm_{29}-*b*-But_9/ssDNA and Man_{62}-*b*-Agm_{52}-*b*-But_{32}/ssDNA, respectively. More in detail, polymers with lower molecular weights (Man_{15}-*b*-Agm_{12} and Man_{29}-*b*-Agm_{25}) were found to complex ssDNA forming smaller particles with a size of about 25 nm, while polymers with higher molecular weights provide particles with slightly bigger dimension, in the range of 35-53 nm.

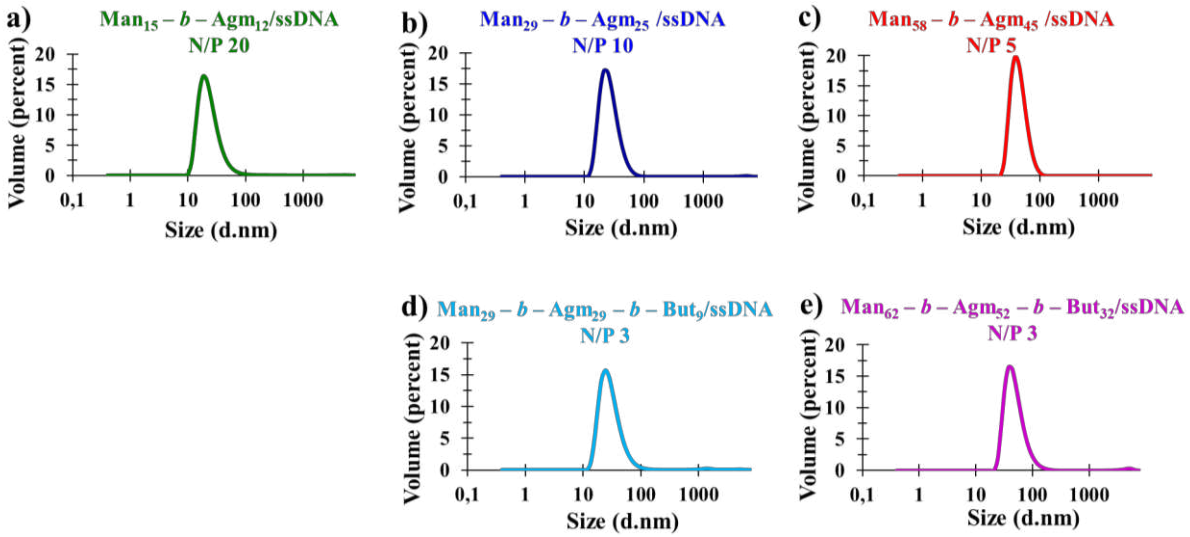

Figure 27. *DLS size profiles of Man_{15}-b-Agm_{12}/ssDNA (a), Man_{29}-b-Agm_{25}/ssDNA (b), Man_{58}-b-Agm_{45}/ssDNA (c), Man_{29}-b-Agm_{29}-b-But_9/ssDNA (d) and Man_{62}-b-Agm_{52}-b-But_{32}/ssDNA (e) polyplexes at N/P ratio 20, 10, 5, 3 and 3, respectively.*

GPPs underwent also Transmission Electron Microscopy analysis either to confirm DLS results and to get more detailed information about the particles shape and morphology (Figure 28). Samples were prepared in MilliQ water to avoid salts background noise in the image and were visualized by negative staining. Results were mostly in agreement with dimensions found by DLS except for Man_{58}-*b*-Agm_{45}/ssDNA and Man_{62}-*b*-Agm_{52}-*b*-But_{32}/ssDNA, that showed particles of smaller sizes (34.3±7.6 nm and 27.7±5.4, respectively) as compared to DLS results (45.2±0.7 nm and 52.9±0.5 nm, respectively). We can hypothesize that polymers with longer hydrophilic mannosylated block can form GPPs with a higher hydrodynamic volume, thus inducing an overestimation of the diameter by DLS respect to TEM, where the hydrophilic corona may not be clearly detectable. Furthermore, the polymers with higher MW can be more sensitive to the TEM vacuum condition which induce the removal of water and the shrinkage of the matrix, which may be more evident for polymers with a thicker hydrated corona. Moreover, spherical shape was observed for all polyplexes, with the exception of Man_{29}-*b*-Agm_{29}-*b*-But_{9}/ssDNA, that showed a higher heterogeneity of the particle population, with co-existence of spherical and rod-shaped particles, 27.7 nm-wide and 149.1 nm-long. This finding is consistent with the size detected by DLS for Man_{29}-*b*-Agm_{29}-*b*-But_{9}/ssDNA polyplex prepared in MilliQ water (data not shown) which resulted in a two populations sample with diameter of 251±100.9 nm and 1030.3±168.2 nm and a quite broad size distribution (PDI of 0.842). In this case, the choice of the solvent used for the sample preparation, that is MilliQ water, strongly affected the dimension and morphology of the glycopolyplex as compared to PBS. However, it is important to highlight that this behavior was not observed for all the other tested glycopolyplexes were a strong correspondence of DLS and TEM analyses was observed despite the solvent used. Further TEM analysis of GPPs prepared in PBS will be planned to deeply investigate the contribution of salts in the shape and morphology of the particles.

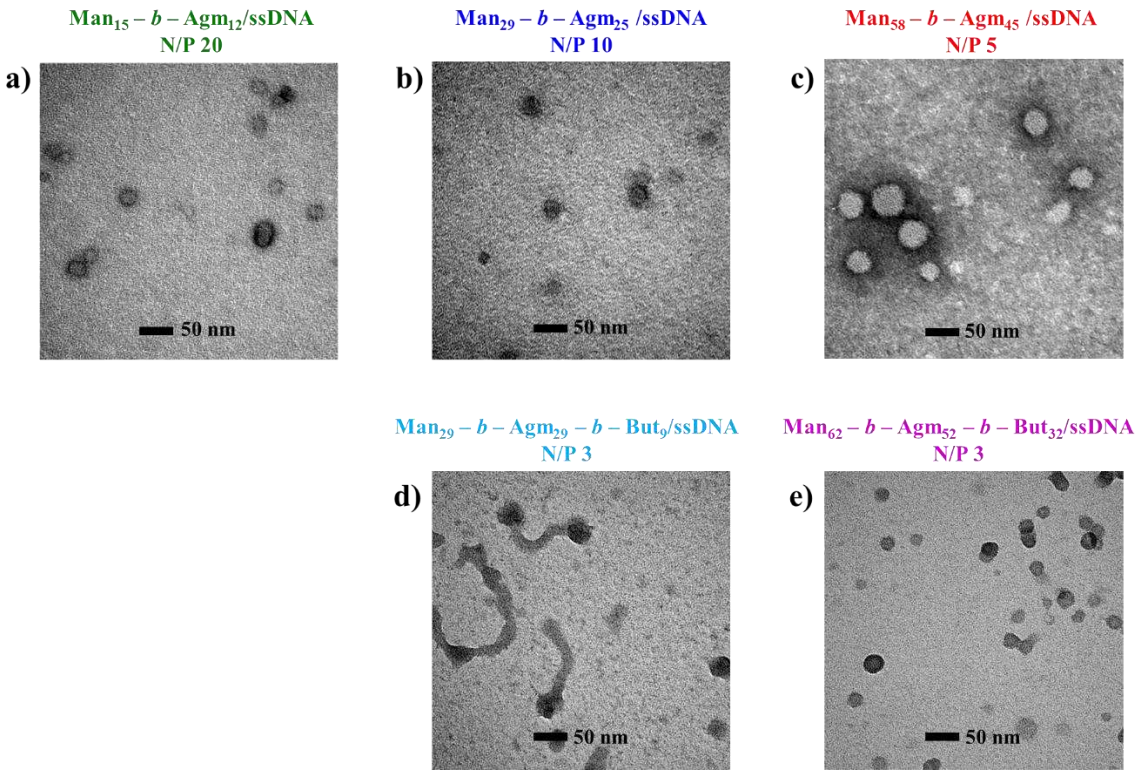

Figure 28. *TEM images of Man$_{15}$-b-Agm$_{12}$/ssDNA (a), Man$_{29}$-b-Agm$_{25}$/ssDNA (b), Man$_{58}$-b-Agm$_{45}$/ssDNA (c), Man$_{29}$-b-Agm$_{29}$-b-But$_9$/ssDNA (d) and Man$_{62}$-b-Agm$_{52}$-b-But$_{32}$/ssDNA (e) polyplexes at N/P ratio 20, 10, 5, 3 and 3, respectively. The average diameter of GPPs from TEM images was calculated using ImageJ software, by measuring 50 individual polyplexes.*

In parallel, size characterization was performed also on pEGFP-loaded polyplexes. Given the 500-times higher number of bases and the double stranded nature of pDNA, formation of larger glycopolyplexes was expected. As mentioned above, either nanometric or micrometric particles can fit for the s.c. route. Furthermore, since the aim is to deliver GPPs to the APCs, it must be taken into account that particles traffic to the draining lymph node (LN) in a size-dependent manner, with a drainage of small nanoparticles (20–200 nm) trafficking alone to the LN while large particles (500–2000 nm) traffic to the LN mostly transported by dendritic cells from the injection site.[90]

Firstly, polymers were complexed with pDNA at the lowest N/P ratio able to completely complex nucleic acid (see paragraph 3.5.2), that is N/P 5 for Man$_{15}$-*b*-Agm$_{12}$/pDNA and Man$_{29}$-*b*-Agm$_{25}$/pDNA and N/P 2.5 for Man$_{58}$-*b*-Agm$_{45}$/pDNA, Man$_{29}$-*b*-Agm$_{29}$-*b*-But$_9$/pDNA and Man$_{62}$-*b*-Agm$_{52}$-*b*-But$_{32}$/pDNA (Figure 29, solid lines). All the samples were found to form two main populations, one with larger size of about 1000 nm and a smaller one of about 100 nm. The polydispersity was in the range 0.380-0.500. Polyplexes were formulated also at higher N/P ratios (Figure 29, dotted lines) to assess if the excess of cationic

portion of the polymer could induce the formation of more tightly complexed particles. Particularly, Man_{15}-*b*-Agm_{12}/pDNA and Man_{29}-*b*-Agm_{25}/pDNA were formulated at an N/P ratio of 10, while Man_{58}-*b*-Agm_{45}/pDNA, Man_{29}-*b*-Agm_{29}-*b*-But_9/pDNA and Man_{62}-*b*-Agm_{52}-*b*-But_{32}/pDNA were prepared at an N/P ratio of 5. As shown in the DLS, all glycopolyplexes obtained with the higher excess of polymer showed a shift of the population distribution toward particles of smaller size (dotted profiles). Nevertheless, only the polymers with the higher molecular weights, that are Man_{58}-*b*-Agm_{45} and Man_{62}-*b*-Agm_{52}-*b*-But_{32}, formed one major homogeneous population of 94.04±3.7 nm and 83.78±12.38 nm, respectively.

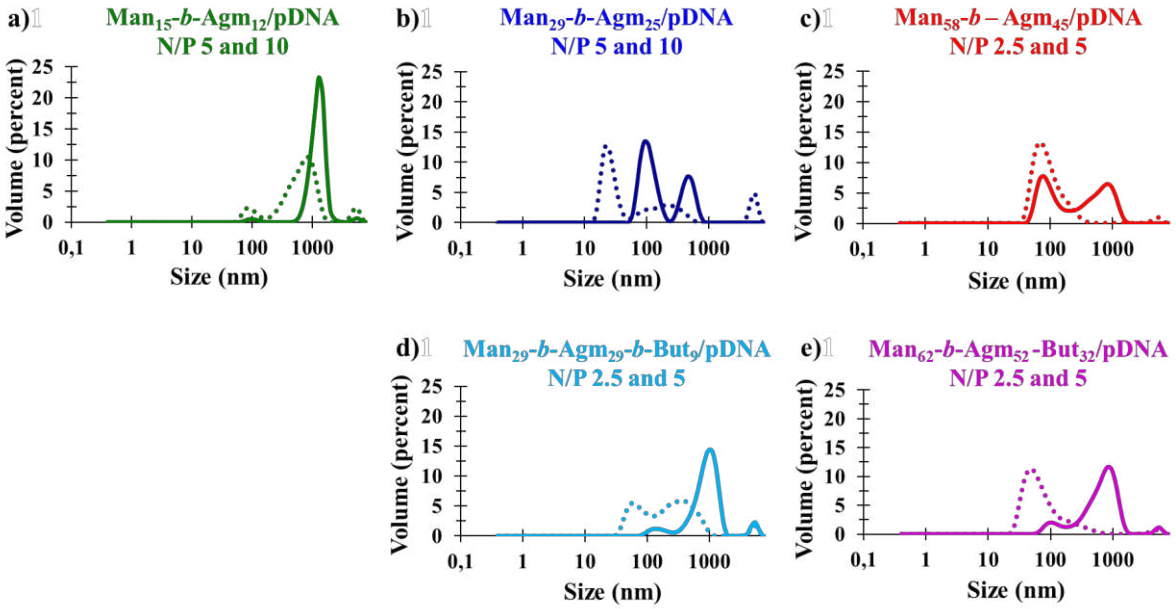

Figure 29. *DLS size profiles of Man_{15}-b-Agm_{12}/pDNA (a), Man_{29}-b-Agm_{25}/pDNA (b), Man_{58}-b-Agm_{45}/pDNA (c), Man_{29}-b-Agm_{29}-b-But_9/pDNA (d) and Man_{62}-b-Agm_{52}-b-But_{32}/pDNA (e) polyplexes at higher (dotted line) and lower (solid line) N/P ratios, as reported in figure.*

The different size, homogeneity and morphology of Man_{58}-*b*-Agm_{45}/pDNA, Man_{29}-*b*-Agm_{29}-*b*-But_9/pDNA and Man_{62}-*b*-Agm_{52}-*b*-But_{32}/pDNA GPPs at N/P 2.5 as compared to N/P 5 was clearly detectable by Transmission Electron Microcopy analysis (Figure 30). Indeed, diverse shapes were detected for glycopolyplexes at the N/P ratio of 2.5 in all samples (Figure 30, top panels), justifying the existence of different size populations in the DLS profiles. Toroidal shaped glycopolyplexes were found for Man_{58}-*b*-Agm_{45}/pDNA and Man_{29}-*b*-Agm_{29}-*b*-But_9/pDNA, while a bunch-like shape was detected for Man_{62}-*b*-Agm_{52}-*b*-But_{32}/pDNA glycopolyplexes. On the other hand, when GPPs were assembled at N/P ratio of 5, shape appeared more homogeneous, with very well-defined rod-like polyplexes for Man_{58}-*b*-Agm_{45}/pDNA and spherical for Man_{62}-*b*-Agm_{52}-*b*-But_{32}/pDNA. The TEM images were in

agreement with information from the DLS analysis, that displayed a single size population for these GPPs. Man$_{29}$-*b*-Agm$_{29}$-*b*-But$_{9}$/pDNA polyplexes at the N/P ratio of 5 still displayed highly heterogeneous populations with the co-existence of globular and worm-like polyplexes (Figure 30, bottom panels); this also confirmed the DLS analysis that detected two main peaks for Man$_{29}$-*b*-Agm$_{29}$-*b*-But$_{9}$/pDNA GPPs at this N/P ratio.

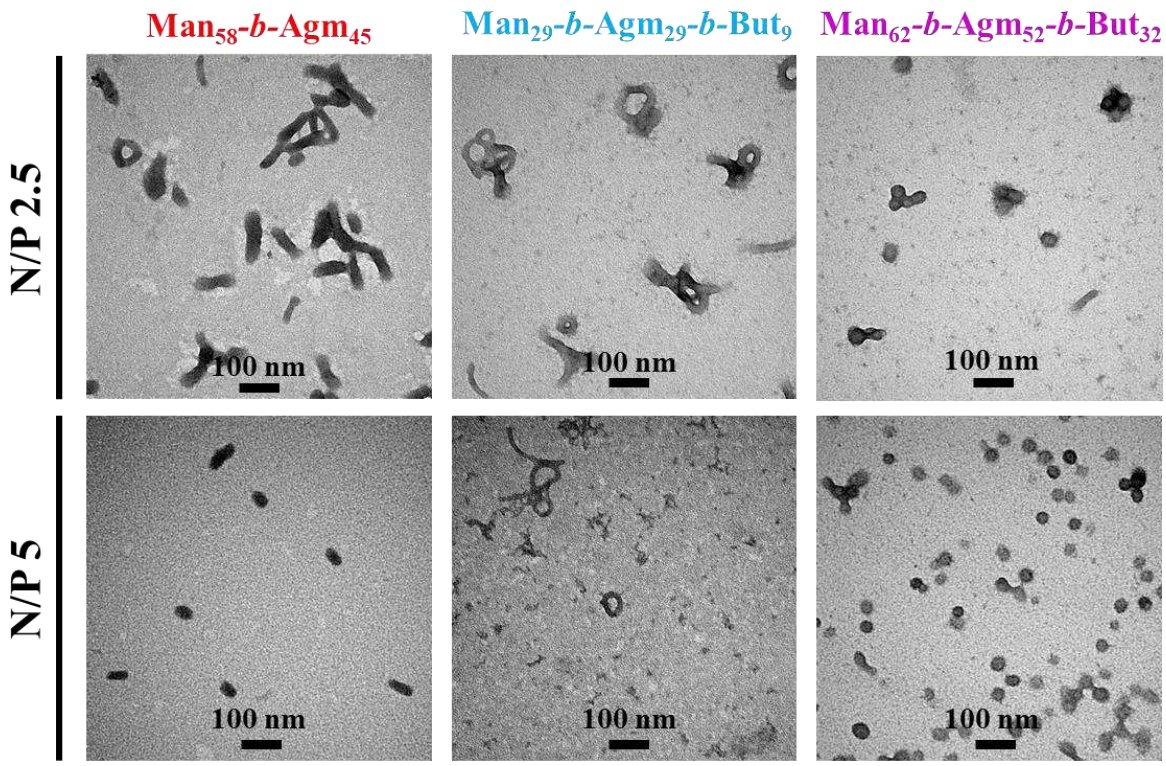

Figure 30. *TEM images of (from left to right) Man$_{58}$-b-Agm$_{45}$/pDNA, Man$_{29}$-b-Agm$_{29}$-b-But$_{9}$/pDNA and Man$_{62}$-b-Agm$_{52}$-b-But$_{32}$/pDNA at N/P 2.5 (above) and N/P 5 (below).*

The conditions and mechanisms underlying when and how pDNA organizes in multi-hierarchically ordered structures is still unclear, thought it has been widely debated in literature. pDNA forms various structures by undergoing folding, collapsing, or spooling of its strand, forming spherical, rod-shaped or toroidal particles, respectively. Golan *et al.*[91] reported an increased degree of condensation of pDNA with poly-Lysine-asialoorosomucoid protein (PLL-AsOR) as the N/P ratio increased or polymers with longer PLL were used, resulting in shorter rods or more compact toroids. Furthermore, several studies from Osada *et al.*[92] showed that with PEG-*b*-PLL-based gene delivery systems, the rod length was shortened with increased degree of polymerization of the PLL block or with decreased number or size of PEG chains displayed in the shell. The evidence seems to prove that our polymers behave similarly: glycopolyplexes shape shifted from an elongated toroids to a shorter shape structure

when the cationic block increase in length (from Man_{29}-*b*-Agm_{29}-*b*-But_{9}/pDNA to Man_{62}-*b*-Agm_{52}-*b*-But_{32}/pDNA). Furthermore, shorter rods resulted as the N/P ratio was increased as a result of higher de-structuration of the plasmid DNA when the cationic blocks intermingle the pDNA molecules; this was more remarkable for polymers with longer cationic blocks, namely Man_{58}-*b*-Agm_{45}/pDNA and Man_{62}-*b*-Agm_{52}-*b*-But_{32}/pDNA.

The shape of GPPs assemblies can have a remarkable effect on the therapeutic outcome. Toroid structures assumed by pDNA have gained attention owing to their relevance in the packaging mechanism of viruses. In agreement with our observations (Figure 30), Kwoh and coworkers reported a decrease in the number of polyplexes central holes at higher charge ratios.[93] Interestingly, in a work by Yanmin *et al.*,[94] carriers obtained by assembly of pDNA with PEGylated cationic polymers presenting toroidal packaging were able to both increase cell-free transcription/translation and to promote *in vivo* gene expression. In Figure 31 we have quantified percentages of round-/bunch-, rod-, and toroid-shaped particles observed in TEM images in our samples. Particularly, as mentioned above, the percentages of rods and toroids were found to decrease with increasing N/P ratios and with increasing DP of the cationic block.

It is worth to note that Li *et al.*[94] demonstrated that the NaCl concentration in polyplexes colloidal suspension influences the formation of toroids, with an increase in ring-shaped particles with the increment of sodium chloride in solution. Being our TEM samples prepared in MilliQ water to avoid salts background noise, the salt effect was not appreciable. Further investigation on GPPs shape at increasing NaCl concentration will be planned to assess the morphology of the particles in the physiological condition (0.9%w/v NaCl).

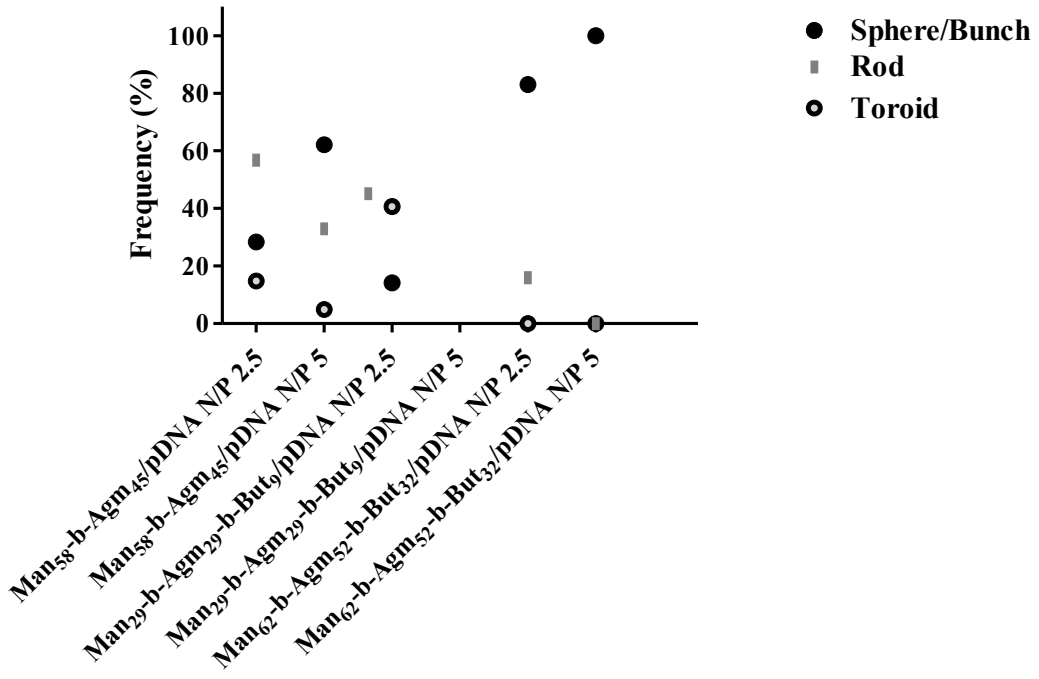

Figure 31. *Percentage of sphere/bunch (black circle), rods (grey bar) and toroids (black opened circle) for different GPPs at N/P ratios 2.5 and 5, as derived from TEM images. Results for* Man_{29}-b-Agm_{29}-b-But_9*/pDNA at N/P 5 were not reported because the background noise did not allow a simple counting.*

3.7 Zeta potential (ZP) before and after ssDNA complexation

The assembly of glycopolyplexes (GPPs) occurring by polymer/DNA electrostatic interaction was confirmed also by Zeta potential (ZP) analysis. The ZP of colloidal systems affects not only their stability, but also their uptake by cells, thus their therapeutic efficacy. Indeed, polyplexes are often formulated at N/P ratios close or above 1, which provide a slight positive Zeta potential that results in the electrostatic repulsion among positively charged particles. This reduces particles aggregation and changes of the size during time, as confirmed by the stability study reported in the next chapter. On the other hand, since cell membrane surface is slightly anionic, excess of positive charges on the polyplexes can cause non-specific binding and uptake by cells, which is an undesired drawback for selective targeting.

GPPs were assembled by mixing polymers with ssDNA at the N/P ratios encircled in Figure 24. Although the Zeta potential is by definition the potential difference between the dispersion medium and the stationary layer of fluid attached to a dispersed particle, as a proof of concept the resulting glycopolyplex ZPs were compared to those of the corresponding free polymers analyzed at identical concentration (0.1 mg/mL).

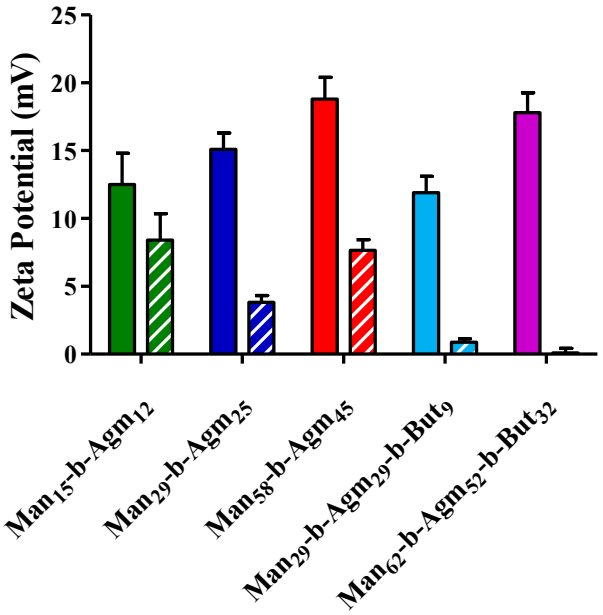

Figure 32. *Zeta potential values of free polymers (filled bars) and ssDNA-loaded glycopolyplexes (striped bars) in 5 mM HEPES. Man_{15}-b-Agm_{12}/ssDNA, Man_{29}-b-Agm_{25}/ssDNA, Man_{58}-b-Agm_{45}/ssDNA, Man_{29}-b-Agm_{29}-b-But_9/ssDNA and Man_{62}-b-Agm_{52}-b-But_{32}/ssDNA were formulated at N/P ratio of 20, 10, 5, 3 and 3, respectively.*

Figure 32 shows that before complexation all polymers possess a positive ZP in virtue of the cationic nature of guanidinium groups of the agmatine, with a ZP of 12.5 mV, 15.1 mV and 18.8 mV for Man_{15}-*b*-Agm_{12}, Man_{29}-*b*-Agm_{25}, Man_{58}-*b*-Agm_{45} and of 11.90 mV and 17.80 mV for Man_{29}-*b*-Agm_{29}-*b*-But_9 and Man_{62}-*b*-Agm_{52}-*b*-But_{32}, respectively. It is worth noting that, since the moles of agmatine in polymer solutions used in the analysis is almost the same for all the materials, also the Zeta potential values are very closed, independently from polymers molecular weight.

A remarkable decrease in the Zeta potential was found after complexation with ssDNA, with ZP values of 8.4 mV, 3.82 mV and 7.65 mV for Man_{15}-*b*-Agm_{12}/ssDNA, Man_{29}-*b*-Agm_{25}/ssDNA and Man_{58}-*b*-Agm_{45}/ssDNA and of 0.88 mV and 0.10 mV for Man_{29}-*b*-Agm_{29}-*b*-But_9/ssDNA and Man_{62}-*b*-Agm_{52}-*b*-But_{32}/ssDNA, respectively. It is noteworthy that the ZP decrease for Man_{15}-*b*-Agm_{12} after complexation with ssDNA was subtle, in agreement with the use of excess of polymer with respect to ssDNA (N/P ratio is 20), thus of a high excess of agmatines. Similarly, the close to zero ZP for both 2nd generation polymers after complexation with ssDNA can be justified by the N/P ratio of 3 chosen for GPPs formulation.

However, despite the overall ZP became almost zero after complexation for the 2nd generation polymers, the particles were found to be colloidally stable (*vide infra*) which proves that the flexible and hydrophilic polysaccharidic corona is exposed and responsible of the "stealth" properties of the systems.

The effect on Zeta potential of increasing the N/P ratio, thus the amount of polymer, for polyplexes assembly was not investigated. Indeed, being the GPPs actively targeted by mannose-based molecules, the formation of polyplexes at N/P ratio higher than the optimal value is not recommended, since a possibly neutral or only weakly positive ZP is preferable to avoid non-specific cell uptake and to ensure that association of particles is provided by the binding to mannose receptors and subsequent mannose receptor-mediated endocytosis.

3.8 GPPs stability in physiological media

The formulation stability during storage and in physiological conditions are two important parameters to assess before addressing *in vitro* and *in vivo* studies. To this aim, we investigated GPPs size changes over time, either at 4 °C in PBS or at 37 °C in presence of 10% FBS.

Polyplexes stability profile in storage conditions is reported in Figure 33. All the formulations were found to be stable at least for 8 days, with the higher molecular weight polymers performing very satisfactorily until day 14. The presence of the hydrophilic mannose block could probably prevent the formation of aggregates, promoting the stability. Particularly, Man_{15}-*b*-Agm_{12}/ssDNA started to aggregate after day 10, which may result from the lower compactness, thus stability, of polyplexes formed by shorter polymers. Indeed, shorter polymers have both short cationic blocks for complexation, and shorter polysaccharide blocks for surface coating. On the other hand, size was maintained stable by Man_{58}-*b*-Agm_{45}/ssDNA throughout the time scale of the experiment. Furthermore, 2nd generation polymers were found to form polyplexes with a certain variability in size compared to 1st generation polymers, although the percentage of secondary populations was quite subtle. We ascribed this trend to the lower compactness and so lower stability of Man_{29}-*b*-Agm_{29}-*b*-But_9/ssDNA and Man_{62}-*b*-Agm_{52}-*b*-But_{32}/ssDNA polyplexes, as showed also by heparin displacement studies.

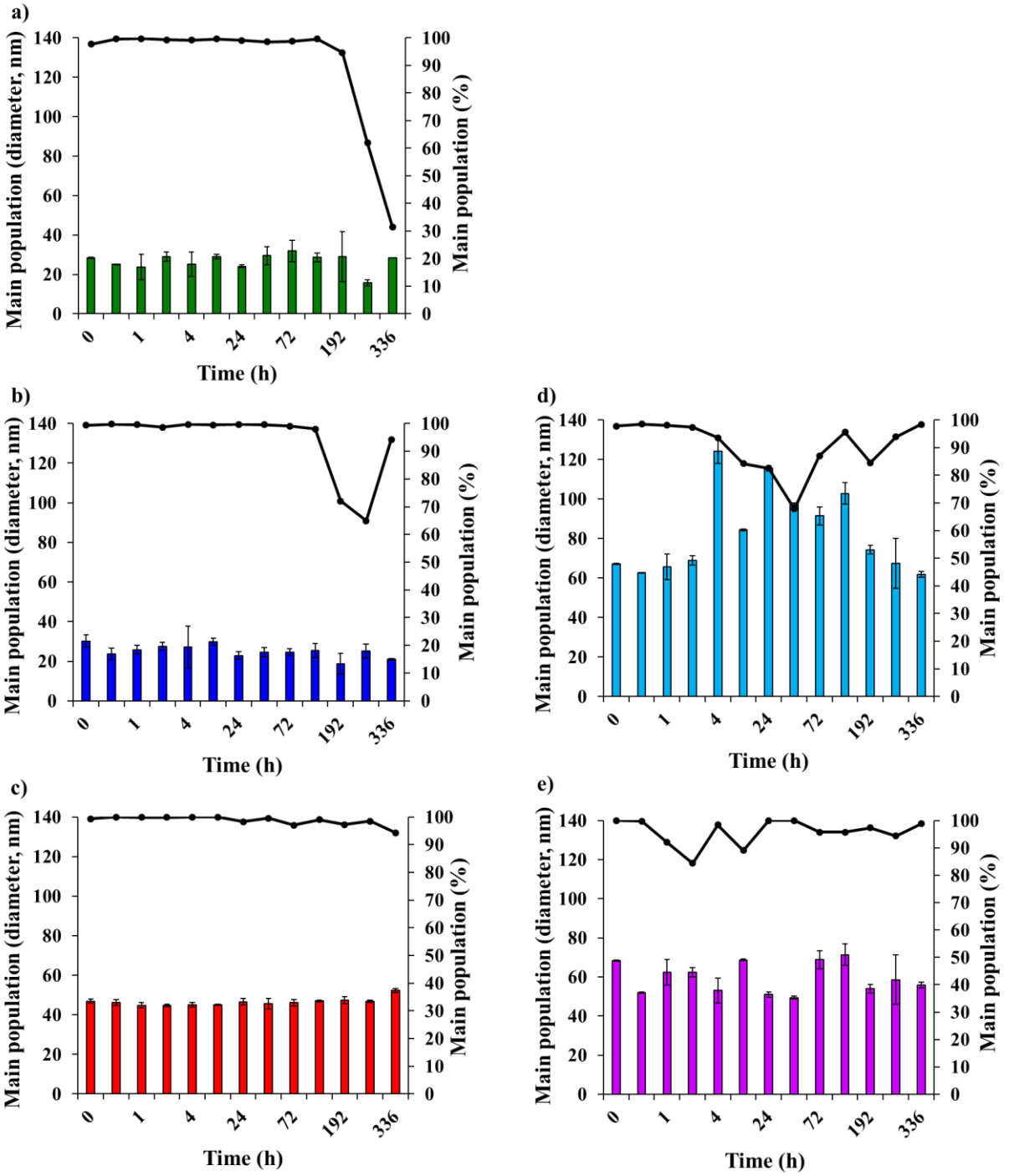

Figure 33. *Kinetic stability profile in PBS at storage conditions of Man_{15}-b-Agm_{12}/ssDNA N/P 20 (a), Man_{29}-b-Agm_{25}/ssDNA N/P 10 (b), Man_{58}-b-Agm_{45}/ssDNA N/P 5 (c), Man_{29}-b-Agm_{29}-b-But_{9}/ssDNA N/P 3 (d) and Man_{62}-b-Agm_{52}-b-But_{32}/ssDNA N/P 3 (e). Volume-based diameter (left axis) and percentage (right axis) of the main population are represented as bars and dots, respectively.*

Regarding the stability profiles under physiological condition mimicking-media, intensity-based diameters are reported instead of the volume-based to minimize the contribution of protein-derived scattering signals in the DLS profiles (Figure 34).

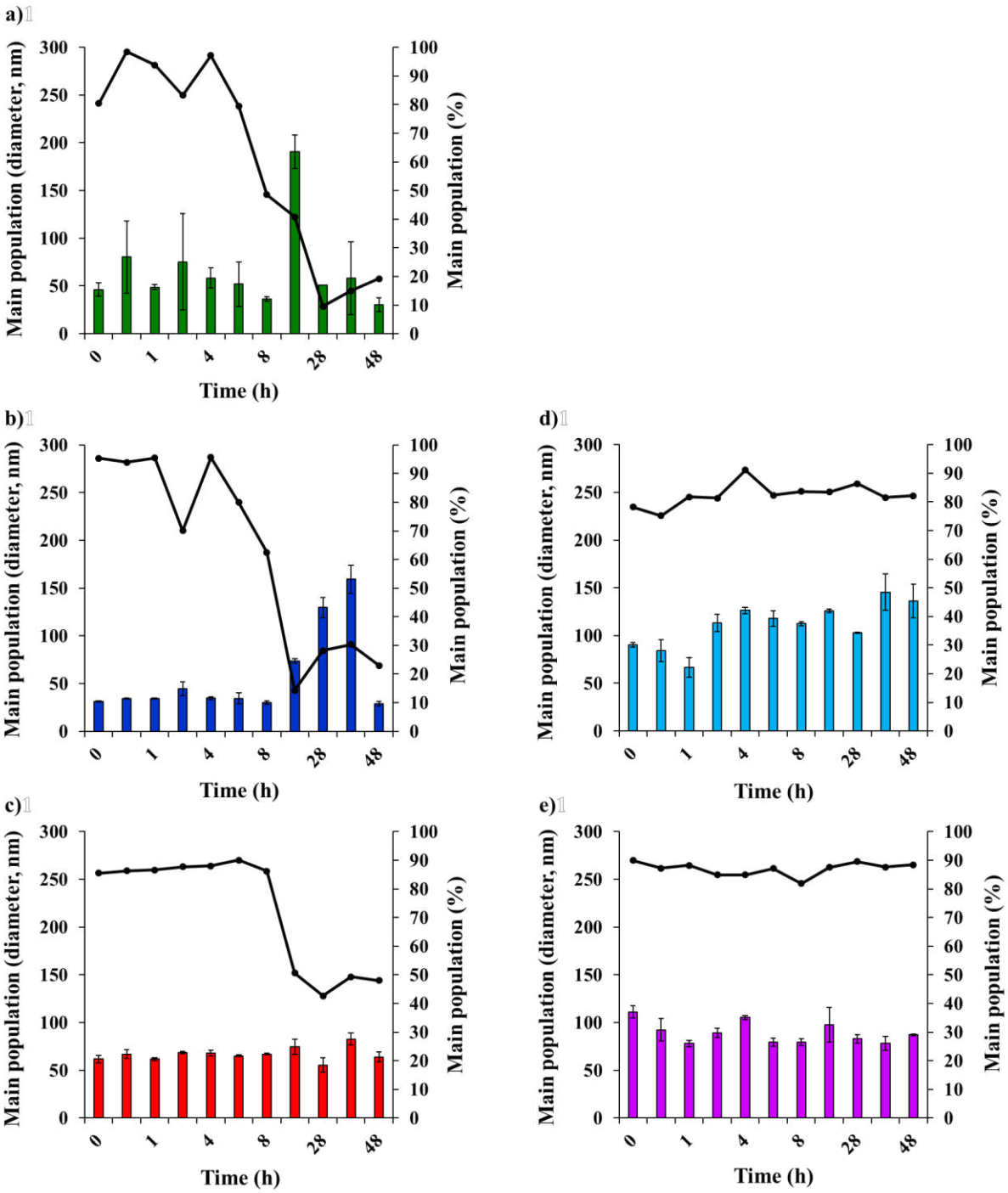

Figure 34. *Kinetic stability profile of Man_{15}-b-Agm_{12}/ssDNA N/P 20 (a), Man_{29}-b-Agm_{25}/ssDNA N/P 10 (b), Man_{58}-b-Agm_{45}/ssDNA N/P 5 (c), Man_{29}-b-Agm_{29}-b-But_{9}/ssDNA N/P 3 (d) and Man_{62}-b-Agm_{52}-b-But_{32}/ssDNA N/P 3 (e) incubated in PBS supplemented with 10% FBS at 37 °C. Intensity-based diameter (left axis) and percentage (right axis) of the main population are represented as bars and dots, respectively.*

All the polyplexes showed a good stability in presence of serum proteins at 37 °C for at least 8 hours. Particularly, 1st generation GPPs were found to maintain a size comparable to

that detected in PBS, even if a bias on the size evaluation was inserted by considering the intensity-based diameter. However, all these formulations underwent instability after 24 hours of incubation with FBS, with only Man_{58}-*b*-Agm_{45}/ssDNA maintaining a fairly good stability over time. The 2nd generation polymers showed to form glycopolyplexes with an increased size in serum-supplemented conditions, which could be due to protein adsorption on polyplexes surface because of either hydrophobic or electrostatic interactions between serum proteins and polymers.[95] However, GPPs resulted highly stable. We concluded that the hydrophobic butyl-bearing block can be partially exposed, thus enhancing the opsonization process right from the beginning, although the particle size remains then constant over time, with a diameter never higher than 150 nm. The stability of the GPPs containing the butyl-based block can be ascribed to the assembly strength, which is promoted by the interchain interaction of the butyl-bearing blocks. This was even more noticeable in the GPPs obtained with Man_{62}-*b*-Agm_{52}-*b*-But_{32} that possesses a longer butyl block. On the contrary, for 1st generation polyplexes the hydrophilicity of the mannosylated-block hindered the protein adsorption at first contact with serum, which instead took place later with a longer delay, driven mainly by electrostatic forces.

3.9 Polymers hemolytic activity

Endosomal release and intracellular delivery of therapeutics still remain a major barrier in achieving an efficient non-viral nucleic acid therapy. Drug delivery systems escape from endo-lysosomal vesicles is a requisite to avoid the degradation of the loaded therapeutic molecules by low pH and enzymes. To overcome this hurdle, drug delivery systems have been engineered to actively cross this intracellular barrier. A possible way to enhance endosomal escape is the use of cationic polymers with a pKa around or slightly below physiological pH, which allows to exploit what is called the “proton sponge” effect. Actually, polymers with buffering capacity are not always able to induce endosomal escape and to improve DDSs efficiency.[96] Another approach was adopted in this project by endowing 2nd generation polymers with a butyl-based block,[97] which is able to interact with endosome phospholipid bilayers in virtue of its hydrophobicity. To evaluate the endosomolytic activity of our materials, red blood cells (RBCs) were incubated with two different concentrations of glycopolymers (5-50 μg/mL final concentration) in endosome-mimicking conditions (pH 6)

(Figure 35). The degree of destabilization of RBCs cellular membrane, that causes the hemoglobin release, can be assumed as a predictor of endosomal escape ability.

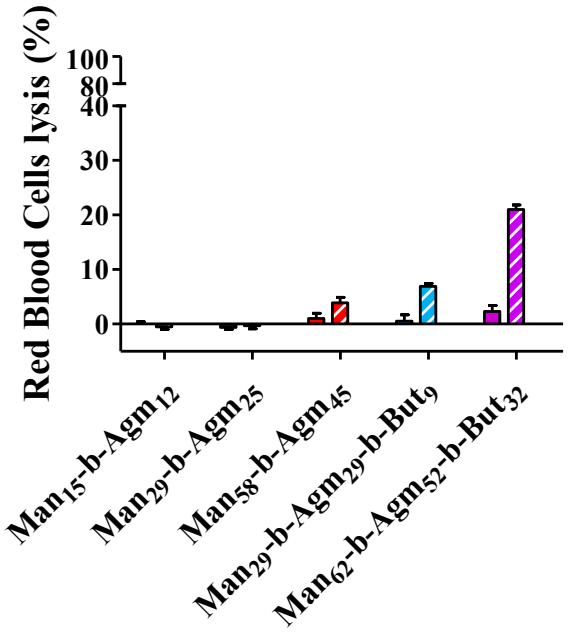

Figure 35. *RBC lysis evaluation of Man_{15}-b-Agm_{12} (■), Man_{29}-b-Agm_{25} (■), Man_{58}-b-Agm_{45} (■), Man_{29}-b-Agm_{29}-b-But_9 (■) and Man_{62}-b-Agm_{52}-b-But_{32} (■) either at 5 μg/mL (filled bars) or at 50 μg/mL (striped bars) concentration in PBS, pH=6. 1% Triton X-100 was used for normalization.*

As expected, the profile showed that Man_{29}-*b*-Agm_{29}-*b*-But_9 and Man_{62}-*b*-Agm_{52}-*b*-But_{32} glycopolymers possess high hemolytic activity due to the presence of butyl-based block and, particularly, Man_{62}-*b*-Agm_{52}-*b*-But_{32} was found to be the polymer with the highest hemolytic activity (21% of RBC lysis at 0.05 mg/mL concentration), in agreement with the presence of a longer hydrophobic block. On the other hand, 1st generation polymers were found to possess a hemolytic effect <4% at all concentrations, confirming our previous hypothesis. Thus, we can state that the effect of membrane destabilization is ascribable to the hydrophobic effect of the butyl chains, with only minor contribution by the high positively charged agmatine-block. Ongoing studies will clarify the hemolytic activity, that is endosomal escape efficiency, of GPPs, thus clarifying also if in the formation of polyplexes the hydrophobic blocks of 2nd generation polymers are completely shielded in the core of the particles or are exposed on the surface.

3.10 GPPs showed high *in vitro* biocompatibility

MTT viability assay was performed to assess the biocompatibility of our systems after 24 hours of incubation with wild type (CHO) and mannose receptor-expressing (CHO-MR$^+$) Chinese Hamster Ovary cell lines. The results (Figure 36) indicated great biocompatibility of both generation of glycopolyplexes at the concentration used in the uptake studies (125 nM ssDNA), either in CHO or CHO-MR$^+$ cells, without any significant difference, despite a different cell association and uptake was quantified for the two cell lines (see paragraph 3.11).

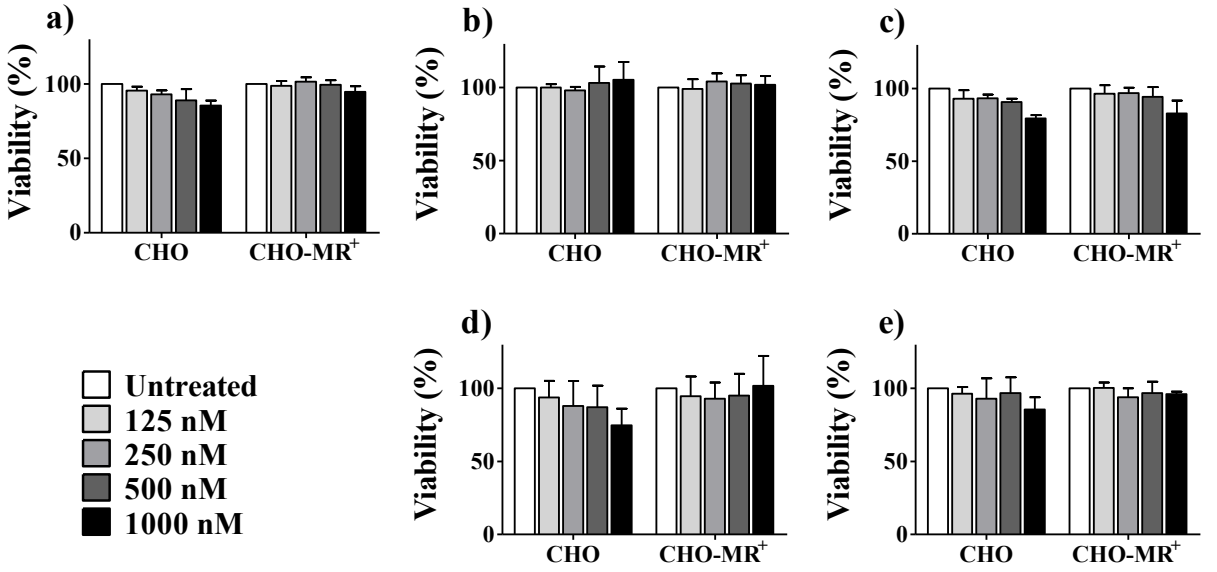

Figure 36. *MTT cell viability on CHO and CHO-MR$^+$ cells. Cells were incubated for 24 hours with Man_{15}-b-Agm_{12}/ssDNA N/P 20 (a), Man_{29}-b-Agm_{25}/ssDNA N/P 10 (b), Man_{58}-b-Agm_{45}/ssDNA N/P 5 (c), Man_{29}-b-Agm_{29}-b-But_9/ssDNA N/P 3 (d) and Man_{62}-b-Agm_{52}-b-But_{32}/ssDNA N/P 3 (e) at increasing concentration of ssDNA (0-1000 nM). Three independent experiments were performed in triplicate. Results are reported as mean±SD.*

Indeed, in both cell lines the viability was above 80% for almost all the formulations, even at the highest concentration tested. Only Man_{29}-*b*-Agm_{29}-*b*-But_9/ssDNA N/P 3 was found to have a slightly higher cytotoxicity, with a percentage of viability of 75% on CHO cells at 1000 nM ssDNA concentration. This effect could be ascribed to the higher heterogeneity in GPPs structure and to the rod shape of Man_{29}-*b*-Agm_{29}-*b*-But_9/ssDNA complexes, as observed by TEM analysis (see paragraph 3.6).

3.11 Polymer/ssDNA glycopolyplexes association to cells expressing MR

The active and selective association of the targeted systems by mannose receptor-expressing cells was studied by flow cytometric analysis on wild type CHO cells, used as negative control, and on CHO-MR$^+$ cells. In addition to this model cell line, murine dendritic cells DC2.4 underwent also cytofluorimetric analysis under the same conditions to screen polyplexes performances in an *in vitro* model that have closer phenotypic features with our target dendritic cells. Cyanine-3 (Cy3) labelled ssDNA (ssDNA-Cy3) was used for polyplexes formulation and glycopolyplexes association to cells was quantified by Cy3 fluorescence intensity on FL2 channel (488 nm excitation laser and 575 nm emission). GPPs were formulated as reported in paragraph 2.9, using a 125 nM concentration of ssDNA-Cy3 to ensure a condition of biocompatibility of the system.

Regarding the study on model cell lines (Figure 37), a highly selective association of glycopolyplexes to CHO-MR$^+$ cells was found for all the GPPs obtained with the 1st generation polymers, with up to 9-folds higher association to mannose receptor-expressing cells than to the control cell line for Man$_{15}$-*b*-Agm$_{12}$/ssDNA GPPs after 30 minutes incubation. Particularly, 1st generation polymers showed either a higher percentage of uptake (panel a) or a higher amount of particles per cell (read MFI, panel b). Instead, 2nd generation polymers showed a lower degree of selectivity respect to 1st generation ones.

Furthermore, increasing the incubation time to 1 hour, only Man$_{15}$-*b*-Agm$_{12}$/ssDNA and Man$_{29}$-*b*-Agm$_{25}$/ssDNA maintained a certain cell selectivity toward MR-expressing cells, even if without any significant increase in particles internalization with respect to the shorter incubation time. A quite high non-specific association was detected after 1 hour incubation for glycopolyplexes formulated with the higher molecular weight polymer Man$_{58}$-*b*-Agm$_{45}$, probably because the disposition of more agmatine units in the same polymer backbone determines an increased non-specific endocytosis due to stronger electrostatic interactions with the cellular membrane. Indeed, it is worth mentioning that, being Man$_{58}$-*b*-Agm$_{45}$/ssDNA glycopolyplexes prepared at N/P 5, the excess of cationic guanidine groups is even less than for Man$_{15}$-*b*-Agm$_{12}$/ssDNA and Man$_{29}$-*b*-Agm$_{25}$/ssDNA. Consequently, the reason for the non-specific endocytosis may be ascribable to polymer conformation and disposition within the glycopolyplexes rather than solely on the total number of positive groups or on the GPPs surface charge. Regarding 2nd generation polymers, massive and non-specific cell association was found after one hour incubation (panel c, d), which may be

ascribed to a degree of exposure of butyl moieties on polyplexes surface, which promotes interaction with cells membranes. Indeed, as for endosomal vesicles, hydrophobic chains could modify also cell membrane fluidity, giving rise to a huge, but not selective uptake. We can assume that this trend was not visible after 30 minutes incubation in virtue of the different kinetic of the non-receptor- and the receptor- mediated internalization process.[98]

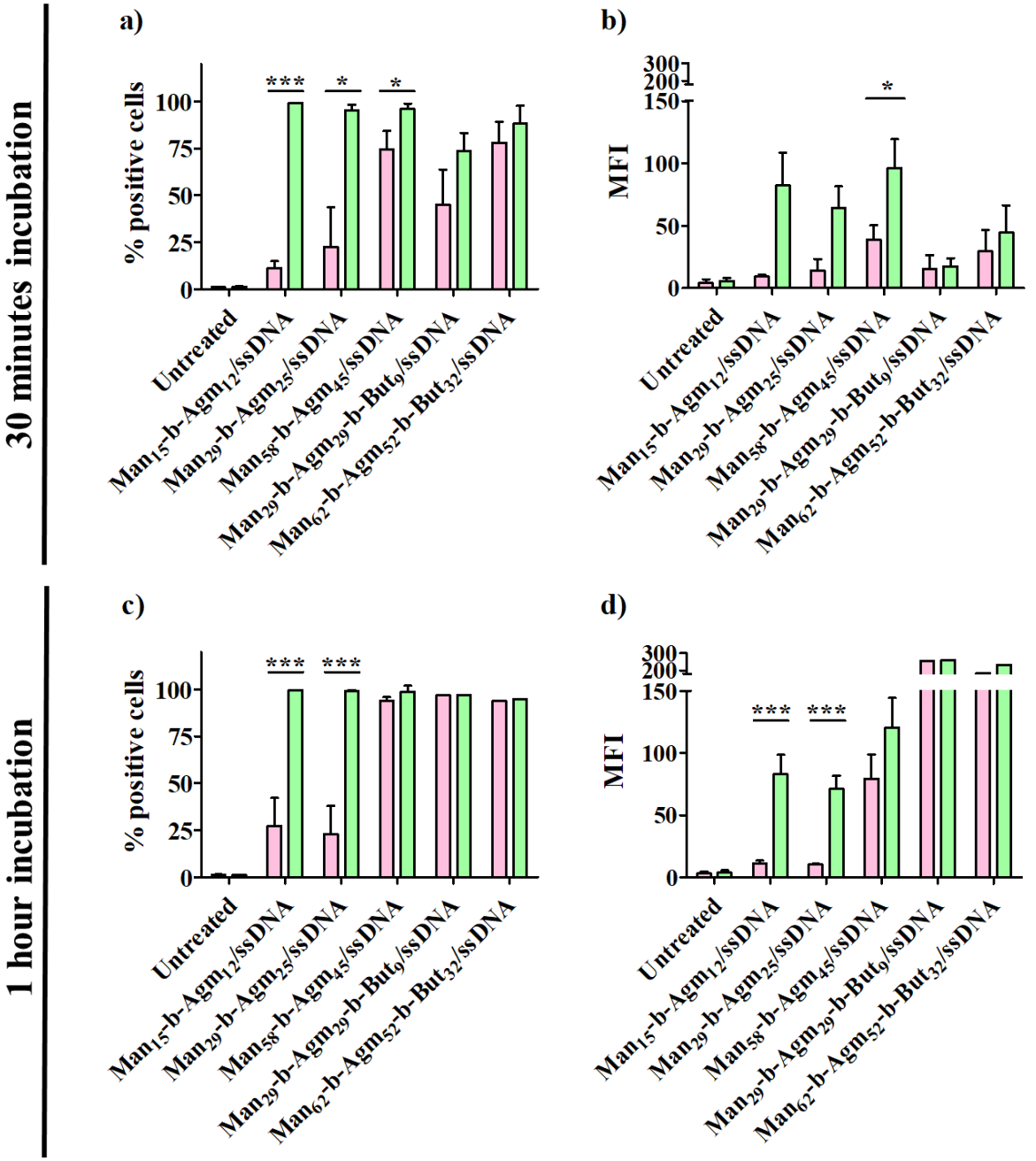

Figure 37. *GPPs association profile to CHO (□) and CHO-MR$^+$ (□) cells after 30 minutes (a, b) and 1 hour (c, d) incubation with Cy-3 labelled GPPs. The percentage of positive cells and the mean fluorescence intensity (MFI) values are reported on the left and on the right column, respectively. Data are presented as means ± SD (n = 2, *p < 0.05, **p < 0.01, ***p < 0.001).*

Interestingly, when the study was performed with DC2.4 dendritic cells (Figure 38), a significant higher association was observed for Man_{58}-*b*-Agm_{45}/ssDNA and for 2nd generation GPPs with respect to Man_{15}-*b*-Agm_{12}/ssDNA and Man_{29}-*b*-Agm_{25}/ssDNA, that showed only a negligible interaction with cells. In particular, Man_{15}-*b*-Agm_{12} and Man_{29}-*b*-Agm_{25} based glycopolyplexes required one hour of incubation to result in 17.5% and 50.1% of positive cells, respectively, while at the same time point Man_{58}-*b*-Agm_{45}/ssDNA, Man_{29}-*b*-Agm_{29}-*b*-But_9/ssDNA and Man_{62}-*b*-Agm_{52}-*b*-But_{32}/ssDNA showed internalization in almost the totality of the DC2.4 population. We can assume that a multivalent interaction with multiple mannose receptor on the cell surface could enhance GPPs MR-mediated cell association, which makes Man_{58}-*b*-Agm_{45} and Man_{62}-*b*-Agm_{52}-*b*-But_{32} more performing materials. Indeed, several research groups have synthesized multivalent mannosylated ligands and demonstrated higher *in vitro* binding affinity for mannose receptor than the monovalent mannosylated analogues.[84,85,99] The mean fluorescence intensity values found for DC2.4 cells are lower in comparison to those found in CHO-MR^+ cells, confirming that natural dendritic cells and macrophages may have a different level of expression of the MR and also a different internalization degree with respect to the engineered CHO cells.

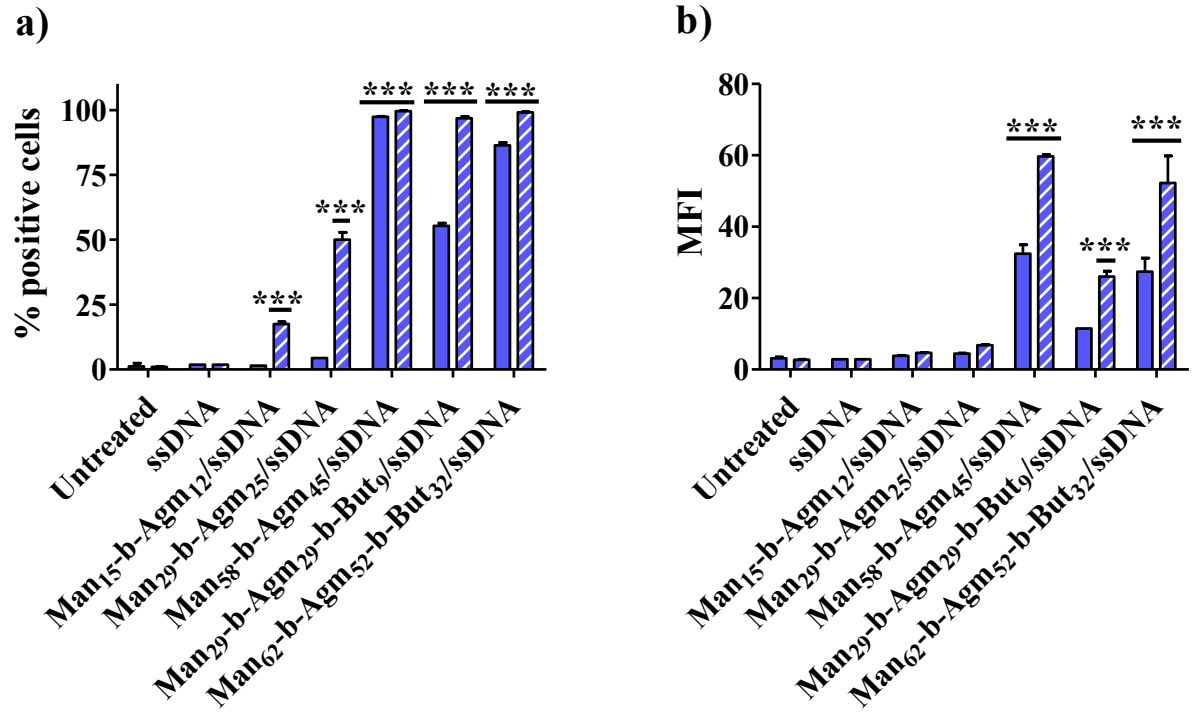

Figure 38. *GPPs association profile to DC2.4 cells after 30 minutes (filled bars) and 1 hour (striped bars) incubation with Cy-3 labelled GPPs. The percentage of positive cells (a) and the mean fluorescence intensity (MFI) values (b) are reported on the left and on the right column, respectively. Data are presented as means ± SD (n = 2, *p < 0.05, **p < 0.01, ***p < 0.001).*

In summary, glycopolyplexes association to cells was found to be higher for Man_{58}-*b*-Agm_{45}/ssDNA, Man_{29}-*b*-Agm_{29}-*b*-But_{9}/ssDNA and Man_{62}-*b*-Agm_{52}-*b*-But_{32}/ssDNA in all cell lines used with respect to Man_{15}-*b*-Agm_{12}/ssDNA and Man_{29}-*b*-Agm_{25}/ssDNA polyplexes. It is reasonable that the multivalency of polymers with longer mannose-bearing blocks is crucial to promote MR-mediated association to cells. However, we did not exclude a role of the positively charged block length in the internalization mechanism. The synthesis of polymers with equal number of agmatine monomers but increasing mannose units will be planned to further investigate the polymer composition that guarantees for the highest cell association.

3.12 Evaluation of GPPs endosomal escape properties by Förster Resonance Energy Transfer

As reported in paragraph 3.9, glycopolyplexes escape from endo-lysosomal vesicles is a pre-requisite to avoid degradation of the nucleic acid induced by nucleases of the compartment and to ensure the nucleic acid payload localization in the right subcellular compartment (e.g. cytoplasm or nucleus). The ssDNA intracellular release was also evaluated by fluorescence resonance energy transfer (FRET).[100] Man_{58}-*b*-Agm_{45} was co-loaded with ssDNA labelled either with the donor dye cyanine 3 (Cy3-ssDNA) or with the acceptor dye cyanine 5 (Cy5-ssDNA), thus allowing the energy transfer from Cy3 to Cy5 before ssDNA is released from endosomes and polyplexes. CHO-MR^+ cells were incubated for 2 hours with Man_{58}-*b*-Agm_{45}/Cy3-5-ssDNA, then incubated for additional 2, 6 or 24 hours with fresh medium. Cy3-ssDNA and Cy5-ssDNA emission before (panels above) and after (panels below) the acceptor (Cy5) photobleaching is reported in Figure 39 for the different time points. Particularly, a defined area, namely region of interest (ROI), was bleached and the donor fluorescence intensities before (D_{pre}, upper panels) and after (D_{post}, bottom panels) acceptor photobleaching were compared.[101] The energy transfer efficiency (Eff_{FRET}) was quantified as:

$$Eff_{FRET} = (D_{post}-D_{pre})/D_{post}$$

If FRET is present, i.e. the two probes are colocalized in endo-lysosomal compartment, Cy3 donor fluorescence increase will occur on photo bleaching of the Cy5 acceptor.

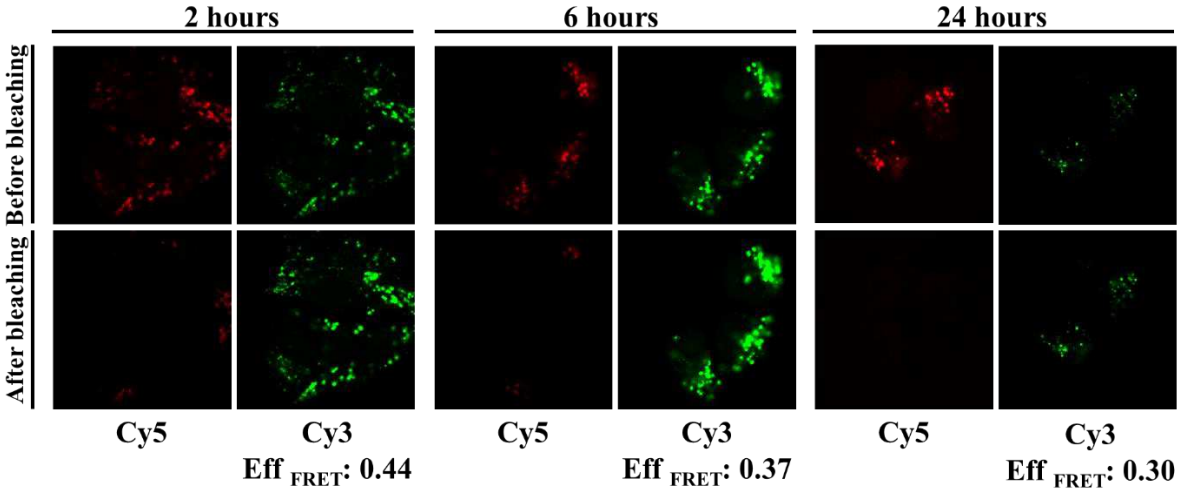

Figure 39. *Confocal images of Cy3-ssDNA and Cy5-ssDNA emission before (panels above) and after (panels below) the acceptor photobleaching. The energy transfer efficiency values after 2, 6 and 24 hours incubation are reported in the line below.*

Particularly, a decrease in the energy transfer efficiency from 0.44 to 0.30 was found over 24 hours, confirming glycopolyplexes release from endosomes during time. Nevertheless, a certain degree of colocalization is still detectable after 24 hours.

The test was performed on Man_{58}-*b*-Agm_{45}/ssDNA glycopolyplexes as a proof of concept, but an extensive screening will be performed on all GPPs, thus comparing the effect of butyl-based block insertion on endosome escape properties of these systems.

3.13 Cell transfection studies with model plasmid DNA: pEGFP

The transfection efficiency of our systems was extensively evaluated by flow cytometry. While the results reported in paragraph 3.11 are representative of the cell entry capacity of targeted polyplexes, pEGFP delivery and transcription in the nucleus are necessary conditions for enhanced green fluorescence protein detection. Indeed, pDNA needs both to translocate into the nucleus and to be released by the vector to be translated.

Here, CHO and CHO-MR^+ model cell lines and DC2.4 dendritic cells were treated for 6 hours with Man_{15}-*b*-Agm_{12}/pEGFP and Man_{29}-*b*-Agm_{25}/pEGFP formulated at N/P 5 and Man_{58}-*b*-Agm_{45}/pEGFP, Man_{29}-*b*-Agm_{29}-*b*-But_9/pEGFP and Man_{62}-*b*-Agm_{52}-*b*-But_{32}/pEGFP formulated at N/P 2.5. The transfection was evaluated after further 24 hours of incubation. The lower N/P ratios that guarantee for complete pDNA complexation were selected (see

paragraph 3.5.2) to avoid a massive and non-specific uptake due to the excess of positive charges. Furthermore, as mentioned in chapter 3.6, many authors reported superior biological activity of toroid pDNA packaging,[94,102] which is the case of Man_{58}-*b*-Agm_{45}/pEGFP and Man_{29}-*b*-Agm_{29}-*b*-But_{9}/pEGFP at N/P 2.5 as shown by the TEM analysis.

A remarkable higher transfection was observed for Man_{58}-*b*-Agm_{45}/pEGFP and for 2nd generation GPPs, while Man_{15}-*b*-Agm_{12}/pEGFP and Man_{29}-*b*-Agm_{25}/pEGFP did not induce any improvement on the transfection when compared to pEGFP alone (Figure 40 and Figure 41). Particularly, 11, 7 and 10% of CHO-MR^+ and 4, 7 and 11% of DC2.4 cells were found to be transfected with Man_{58}-*b*-Agm_{45}/pEGFP, Man_{29}-*b*-Agm_{29}-*b*-But_{9}/pEGFP and Man_{62}-*b*-Agm_{52}-*b*-But_{32}/pEGFP, respectively. Considered the difficulty of non-viral transfection of dendritic cells described by a number of authors,[103,104] our results can be considered promising.

Despite the internalization studies had shown a certain uptake also for Man_{15}-*b*-Agm_{12}/Cy3-ssDNA and Man_{29}-*b*-Agm_{25}/Cy3-ssDNA (see paragraph 3.11), we cannot certainly hypothesize that the smaller polymers are able to deliver nucleic acid into MR-expressing cells but are not so efficient in transfection. Indeed, polymers are able to complex ssDNA and pDNA at different N/P ratios, forming polyplexes with different shapes and physico-chemical characteristics, that could present different internalization rate or pathway and could have different endosomal escape efficiency. Future studies with fluorescently-labelled pDNA will compare the internalization trend of pDNA-based glycopolyplexes depending on the cationic polymer used.

Furthermore, it is worth to underline that the use of agmatine as cationic pendant group could be the added value of our systems with respect to other polymer-based gene delivery systems. Indeed, Kim *et al.* [66] ascribed the better transfection efficiency of arginine-grafted polyplexes as compared to the plain system to a good nuclear localization ability of arginine groups. Furthermore, an effect of the alkyl spacer length on the subcellular localization of non peptidic- guanidine-capped dendrimers was found by Huang *et al.*,[67] with dendrimer with an ethyl- or a hexyl- spacer between the core and the guanidine groups concentrating nucleic acid in the nucleus and in the cytosol, respectively.

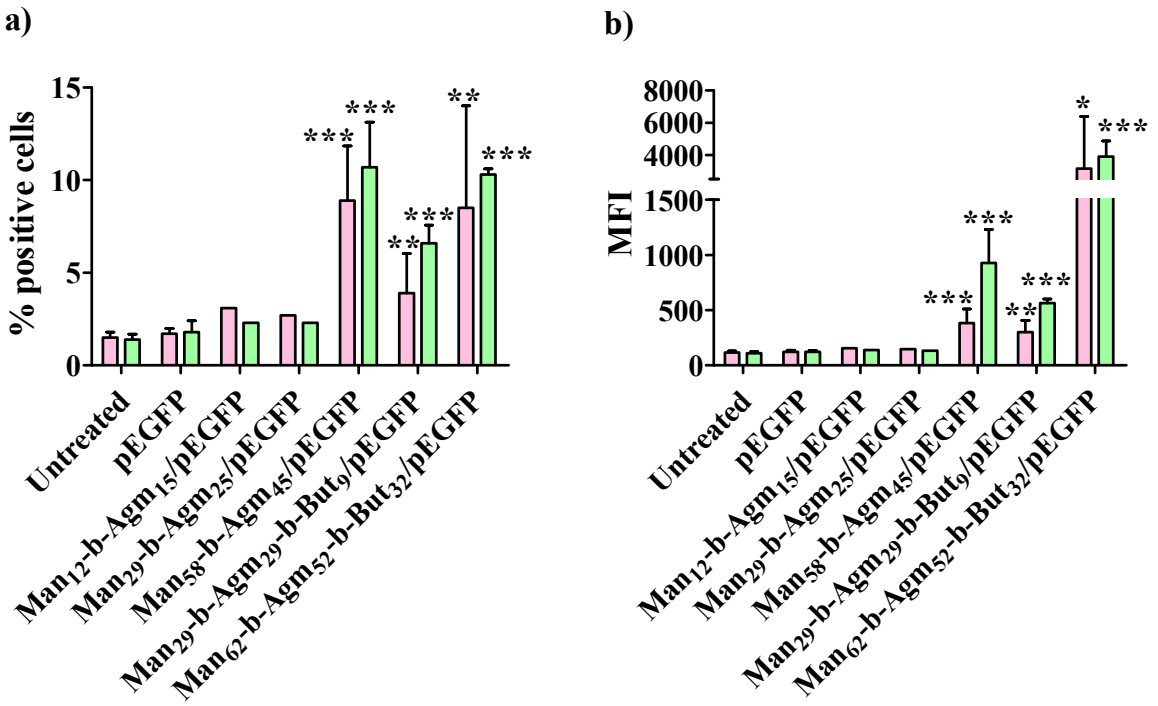

Figure 40. *GPPs transfection efficiency on CHO (□) and CHO-MR$^+$ (□) cells after 6 hours incubation with pEGFP-loaded GPPs and additional 24 hours of post transfection incubation. The percentage of positive cells (a) and the mean fluorescence intensity (MFI) (b) values are reported. Data are presented as means ± SD (n = 2, **p < 0.01).*

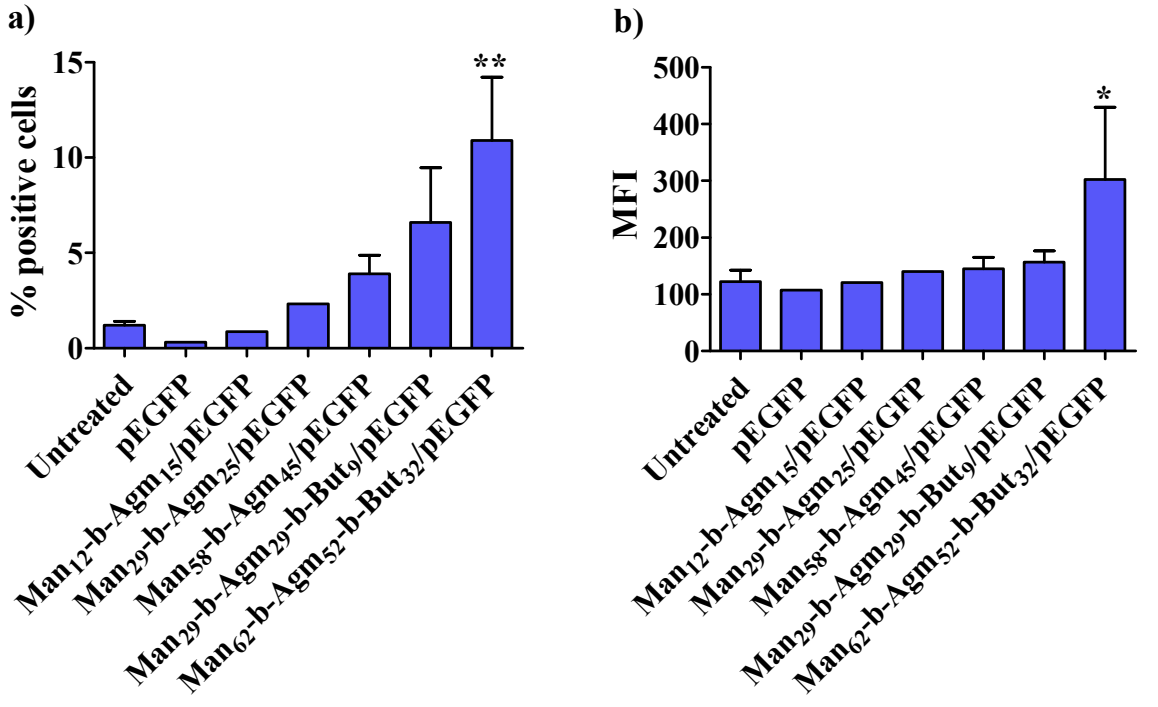

Figure 41. *GPPs transfection efficiency on DC2.4 cells after 6 hours incubation with pEGFP-loaded GPPs and additional 24 hours of post transfection incubation. Percentage of positive cells (a) and the mean fluorescence intensity (MFI) values (b). Data are presented as means ± SD (n = 2, *p < 0.05, **p < 0.01).*

Notably, the hydrophobic butyl block in Man_{29}-*b*-Agm_{29}-*b*-But_9 and Man_{62}-*b*-Agm_{52}-*b*-But_{32} was found to enhance the transfection efficiency in all the cell lines in comparison to the corresponding 1st generation polymers, Man_{29}-*b*-Agm_{25} and Man_{58}-*b*-Agm_{45}. On the other hand, as reported in the association studies, a non-specific cell transfection was observed for wild type CHO cell line, further confirming the role of the butyl moieties on polyplexes access in the cell, reducing the MR-mediated specificity, and on their endosomal escape.

Preliminary results by confocal microscopy analysis were generated using Man_{58}-*b*-Agm_{45}/pEGFP GPPs. CHO and CHO-MR^+ cells were seeded in 24-well plates containing glass dishes and incubated for 6 hours with Man_{58}-*b*-Agm_{45}/pEGFP and then washed twice with PBS and further incubated for 24 hours. Figure 42 shows the higher transfection efficiency of this GPPs on MR-expressing with respect to wild type CHO cells, confirming the selectivity on uptake and transfection efficiency of the high molecular weight 1st generation polymer.

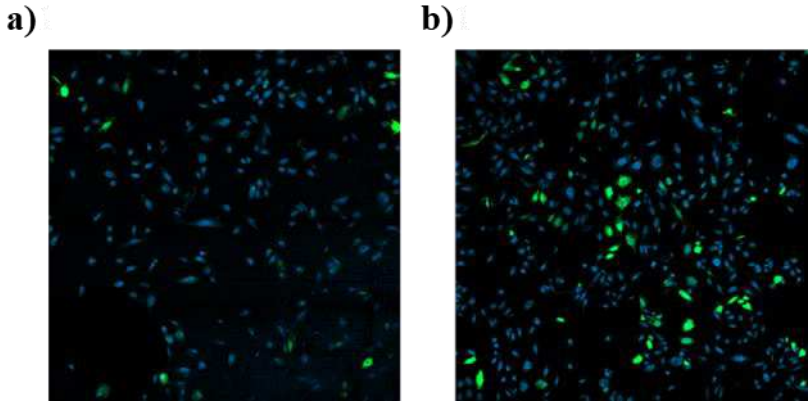

Figure 42. *Confocal microscopy images of CHO (a) and CHO-MR^+ (b) cell lines transfected with Man_{58}-b-Agm_{45}/pEGFP. Nuclei and EGFP protein are represented in blue and in green, respectively.*

3.14 Dendritic cells activation and cross presentation experiment induced by polymer/pOVA glycopolyplexes

GPPs that showed the highest *in vitro* transfection efficacy were selected for more specific studies, that were conducted in collaboration with the University of Helsinki in the ImmunoViroTherapy laboratory of Professor Vincenzo Cerullo. Particularly, 1st generation Man_{58}-*b*-Agm_{45}, and 2nd generation Man_{29}-*b*-Agm_{29}-*b*-But_9 and Man_{62}-*b*-Agm_{52}-*b*-But_{32} were complexed with an ovalbumin-encoding plasmid (pOVA) and investigated for their ability to activate dendritic cells *in vitro* and to induce antigen cross-presentation by Major

Histocompatibility Complex I (MHC I). Indeed, ovalbumin (OVA), the major protein constituent of chicken egg whites, is a glycoprotein that is sufficiently large and complex to be mildly immunogenic. To date, OVA remains a key model protein for vaccine investigation and development in virtue of its existing well consolidated characterization and to the plethora of research tools for its detection and study.

Murine dendritic cells JAWS II were incubated with Man_{58}-*b*-Agm_{45}/pOVA, Man_{29}-*b*-Agm_{29}-*b*-But_{9}/pOVA and Man_{62}-*b*-Agm_{52}-*b*-But_{32}/pOVA at N/P 2.5 according to the same transfection protocol reported in paragraph 3.13 (6 hours incubation + 24 hours post transfection). Complexes of pOVA with polyethylenimine (PEI) (N/P 10) were used as positive control. Cells were gently detached with a non-enzymatic method (EDTA) to preserve cell surface receptors and proteins, and stained with an antibody panel in order to detect $CD11c^+$, $CD86^+$ and H-$2K^b$-bound-$SIINFEKL^+$ cells.

As reported in Figure 43, JAWS II cells were found to express a high level of the lineage DC marker in all the treatment conditions and, more importantly, the expression of the costimulatory clusters of differentiation CD86, necessary for T cell activation, was increased by Man_{58}-*b*-Agm_{45}/pOVA and Man_{62}-*b*-Agm_{52}-*b*-But_{32}/pOVA treatments as compared to the control and to the free polymers. Particularly, 2^{nd} generation Man_{62}-*b*-Agm_{52}-*b*-But_{32}/pOVA GPPs enhanced the CD86 expression more than the corresponding 1^{st} generation Man_{58}-*b*-Agm_{45}/pOVA, confirming previous findings on the better *in vitro* efficacy of butyl-bearing polymers.

Moreover, these two GPPs were found to efficiently transfect JAWS II cells, inducing the presentation of the SIINFEKL ovalbumin antigenic epitope by MHC I complex, with a slightly higher presentation by Man_{62}-*b*-Agm_{52}-*b*-But_{32}/pOVA (2.5%) with respect to Man_{58}-*b*-Agm_{45}/pOVA. This result was obtained by cell staining with a monoclonal antibody designed to react with the ovalbumin-derived peptide SIINFEKL bound to H-$2K^b$ of MHC class I, but not with unbound H-$2K^b$, or H-$2K^b$ bound with other peptides.

It is worth to highlight that for T cells activation, proliferation and differentiation, both antigen presentation by MHC molecule to T cell receptor (TCR) and the binding of CD80/CD86 to CD28 on the surface of T cells are required.[105] We can state that T cells could acquire effector functions after APC treatment with Man_{58}-*b*-Agm_{45}/pOVA and Man_{62}-*b*-Agm_{52}-*b*-But_{32}/pOVA. Thus, these more promising glycopolyplexes were selected for *in vivo* studies, as reported in the next chapter.

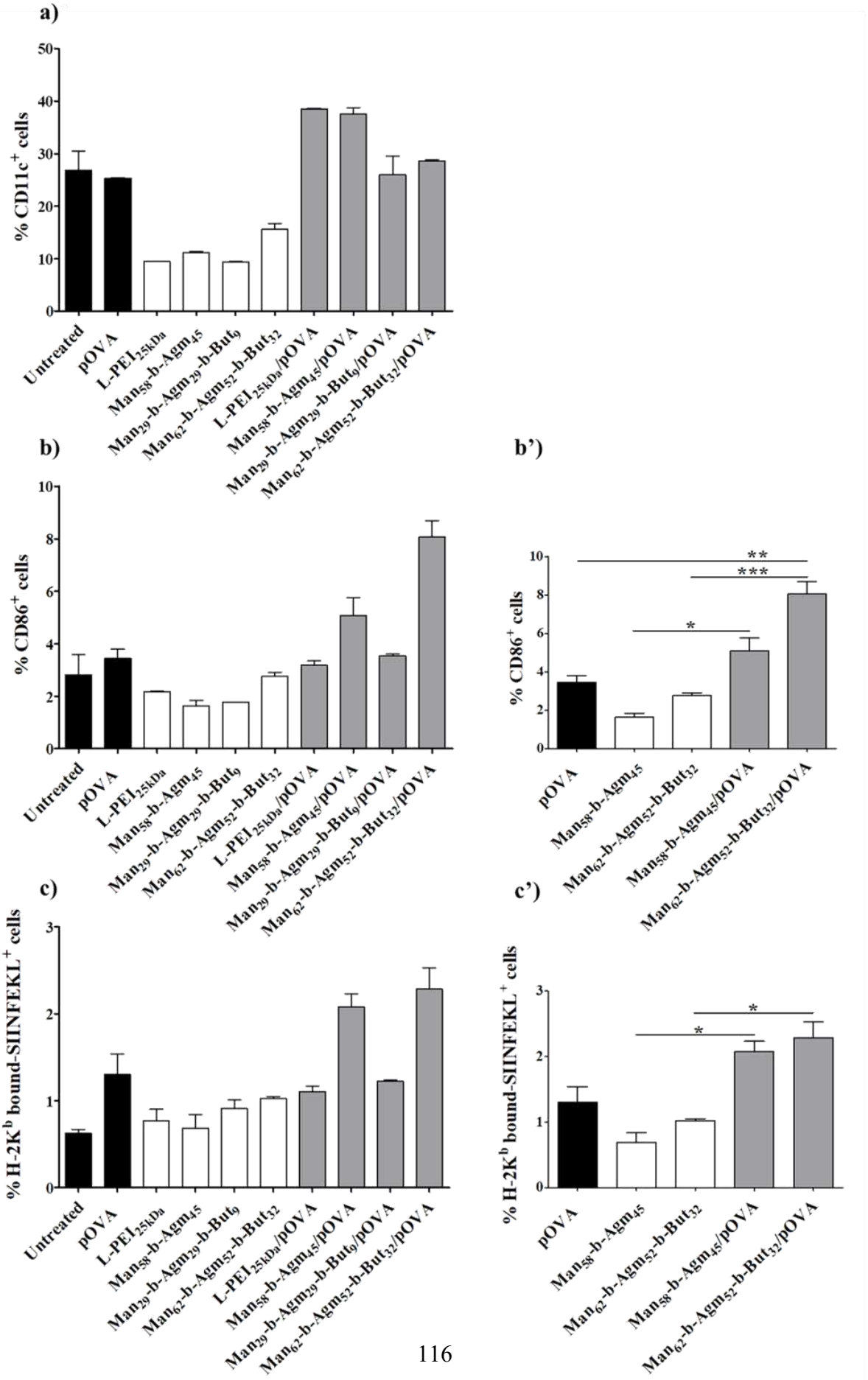
a)
% CD11c+ cells
0
10
20
30
40
50
Untreated
pOVA
L-PEI25kDa
Man58-b-Agm45
Man29-b-Agm29-b-But9
Man62-b-Agm52-b-But32
L-PEI25kDa/pOVA
Man58-b-Agm45/pOVA
Man29-b-Agm29-b-But9/pOVA
Man62-b-Agm52-b-But32/pOVA
b)
% CD86+ cells
0
2
4
6
8
10
Untreated
pOVA
L-PEI25kDa
Man58-b-Agm45
Man29-b-Agm29-b-But9
Man62-b-Agm52-b-But32
L-PEI25kDa/pOVA
Man58-b-Agm45/pOVA
Man29-b-Agm29-b-But9/pOVA
Man62-b-Agm52-b-But32/pOVA
b')
% CD86+ cells
0
2
4
6
8
10
**
***
*
pOVA
Man58-b-Agm45
Man62-b-Agm52-b-But32
Man58-b-Agm45/pOVA
Man62-b-Agm52-b-But32/pOVA
c)
% H-2Kb bound-SIINFEKL+ cells
0
1
2
3
Untreated
pOVA
L-PEI25kDa
Man58-b-Agm45
Man29-b-Agm29-b-But9
Man62-b-Agm52-b-But32
L-PEI25kDa/pOVA
Man58-b-Agm45/pOVA
Man29-b-Agm29-b-But9/pOVA
Man62-b-Agm52-b-But32/pOVA
c')
% H-2Kb bound-SIINFEKL+ cells
0
1
2
3
*
*
pOVA
Man58-b-Agm45
Man62-b-Agm52-b-But32
Man58-b-Agm45/pOVA
Man62-b-Agm52-b-But32/pOVA

Figure 43. *The ability of different pOVA-loaded GPPs to induce CD11c (a) and CD86 (b) expression on dendritic cells is reported in the first and second raws, respectively. In the third raw, SIINFEKL presentation by MHC class I after JAWS II transfection with pOVA-loaded GPPs is shown (c). A zoom-in on $CD86^+$ (b') and H-$2K^b$-bound-$SIINFEKL^+$ (c') cells after treatment with the most efficient materials is reported. Controls, polymers alone and GPPs are represented with black, white and grey bars, respectively. Data are presented as means ± SD (n = 2, *p < 0.05, **p < 0.01, ***p < 0.001).*

3.15 *In vivo* studies

Based on the *in vitro* results, the antitumor efficacy of Man_{58}-*b*-Agm_{45}/pOVA and Man_{62}-*b*-Agm_{52}-*b*-But_{32}/pOVA was evaluated *in vivo* in C57BL/6 mice. Our novel platforms were screened for their efficacy in cancer immunotherapy either as prophylactic vaccination or as therapeutic treatment to activate the immune system selective attack against developing tumor.

Murine B16-OVA cells (i.e. an OVA-transfected clone derived from the murine melanoma cell line B16 and over-expressing chicken ovalbumin) were used as subcutaneous melanoma tumor model. Consequently, pOVA-loaded polyplexes were used in these proof-of-concept studies to induce an immune response against ovalbumin, thus allowing tumor prevention or eradication. Given the wide range of treatment schedule reported in literature,[106-109] the pDNA injected dose and the experiment schedule were selected merging published protocols for polymeric gene delivery systems. Anyway, the mice body weight (Figure 44) and wellbeing were constantly monitored during all the experiments and no significant alterations were observed, confirming the safety and the good tolerability of the systems at the selected dose.

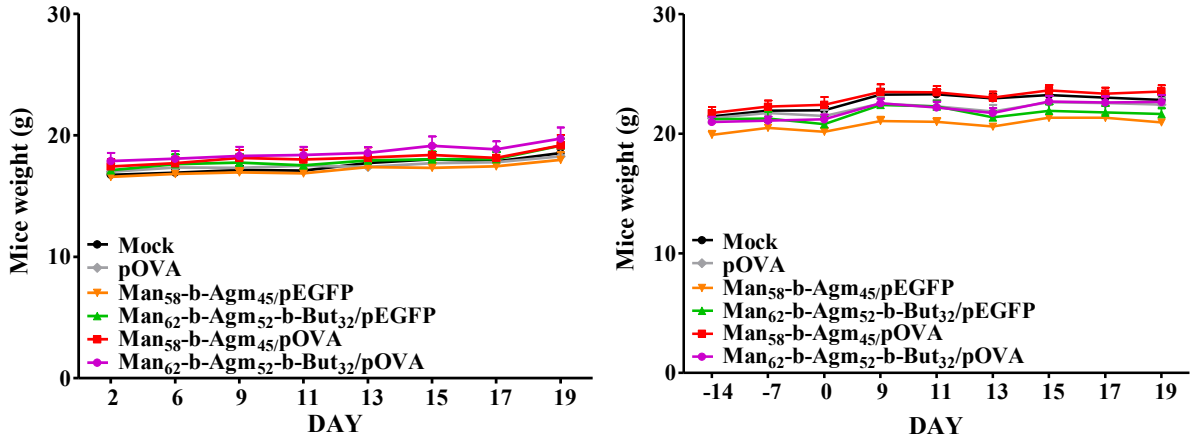

Figure 44. *Animal body weight monitoring during the therapeutic (panel left) and the prophylactic (panel right) treatment approach.*

3.15.1 *In vivo* prophylactic approach: prime and boost

In the prophylactic model, the mice were vaccinated with pOVA, free or complexed with polymers, and then challenged with the tumor cells. pEGFP complexes with the same polymers at the same N/P ratios were used as negative control. Particularly, each mouse was subcutaneously injected in the right flank at day -14, -13 (prime) and -7 (boost) before tumor implantation with 12.5 µg of pDNA for the treated groups or with PBS, as reported in Figure 45.

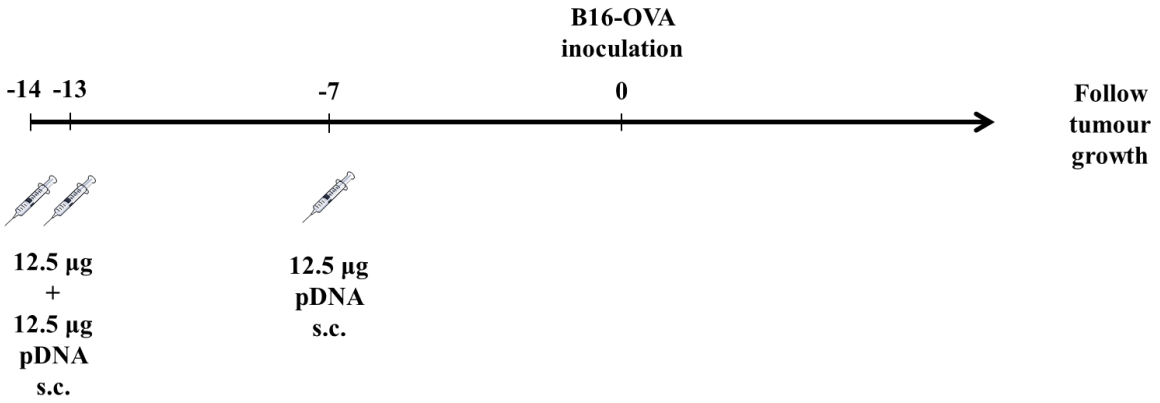

Figure 45. *Mice treatment schedule for the prophylactic vaccination approach.*

The analysis of the tumor volume, reported in Figure 46, demonstrated that Man_{58}-*b*-Agm_{45}/pOVA treated mice developed 3.3-fold smaller tumor mass at day 19 after tumor implantation as compared to pOVA treated mice. The small tumor volume showed for the untreated group (mock) can be ascribed to the development of big ulcerations in their tumors, with the resulting voiding of the mass; these mice were sacrificed once their wellbeing did not fulfill the requirements. Furthermore, it is worth to note that big tumors quickly developed in Man_{62}-*b*-Agm_{52}-*b*-But_{32}/pOVA treated mice. This result is different than expected according to the *in vitro* studies, that showed the high molecular weight 2nd generation polymer as the best performing, both for transfection (Figure 41) and for DCs activation (Figure 43) efficiency. Since tumor volume in the corresponding Man_{62}-*b*-Agm_{52}-*b*-But_{32}/pEGFP control group was found to be similar to the other control groups, a tolerogenic effect was hypothesized for Man_{62}-*b*-Agm_{52}-*b*-But_{32}/pOVA treatment. Consequently, an alternative vaccination schedule or dosage will be proposed to re-evaluate *in vivo* the potentialities showed by the 2nd generation polymer *in vitro*.

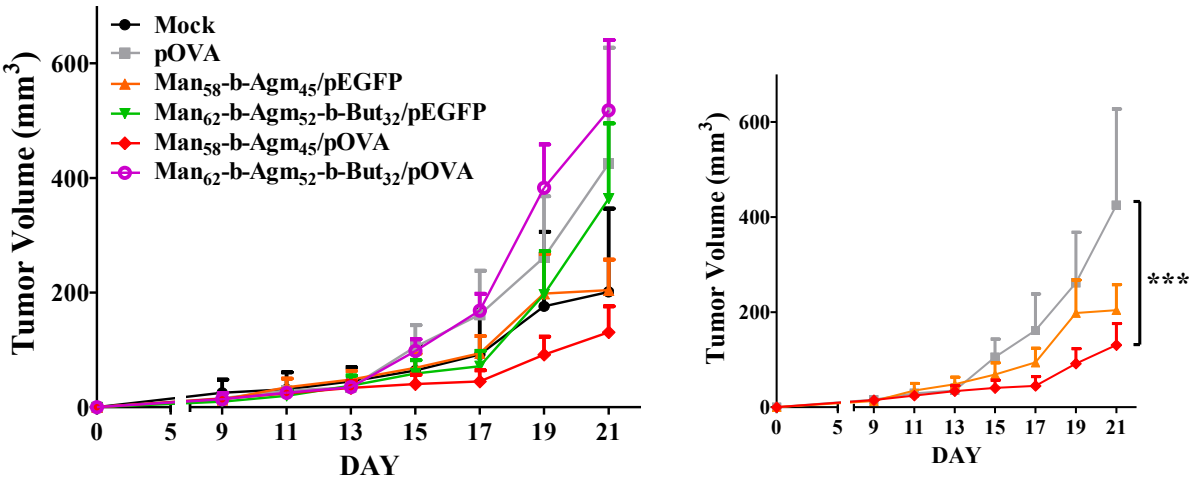

Figure 46. *In vivo antitumor prophylactic efficacy of PBS (-), pOVA (-), Man_{58}-b-Agm_{45}/pEGFP (-), Man_{62}-b-Agm_{52}-b-But_{32}/pEGFP (-), Man_{58}-b-Agm_{45}/pOVA (-) and Man_{62}-b-Agm_{52}-b-But_{32}/pOVA (-). The tumor volume after subcutaneous injection of the treatments is reported in the left panel for all the formulations. A zoom in on the effective treatment Man_{58}-b-Agm_{45}/pOVA is reported on the right panel. Results are reported as mean ± SEM (n = 7-10, ***p < 0.001).*

3.15.2 *In vivo* therapeutic approach

In the therapeutic approach, B16-OVA tumors were implanted in both flank of the mice and subsequently the mice were treated with pOVA, free or complexed with polymers. pEGFP complexes with the same polymers at the same N/P ratios were used as negative control. Particularly, each mouse was subcutaneously or peritumorally injected in the right and in the left flank at day 2 (s.c.), 6 (s.c.), 10 (i.t.) and 16 (i.t.) with 25 µg of pDNA for the treated groups or with PBS for the untreated group, as reported in Figure 47. The same treatment schedule was adopted also for control mice bearing B16-F1 tumors.

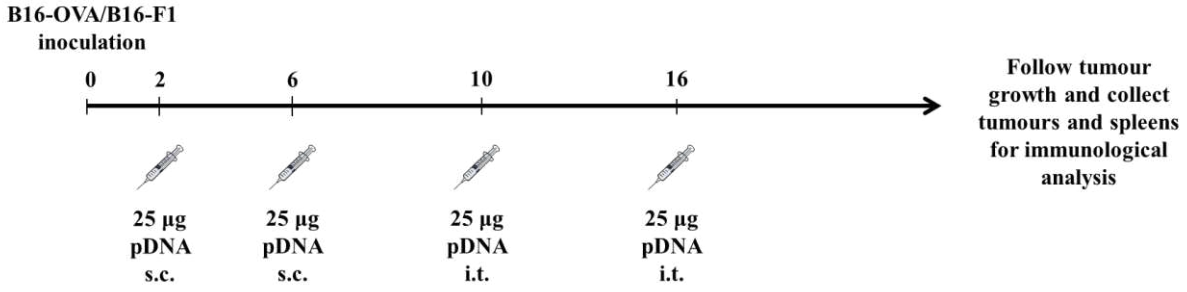

Figure 47. *Mice treatment schedule for the therapeutic vaccination approach.*

In Figure 48, panel a, the percentage of tumor growth for B16-OVA tumor bearing mice is reported for all the treatment groups, with a focus on the best performing formulation on the right panel. Indeed, in the therapeutic approach Man_{58}-*b*-Agm_{45}/pOVA was again found to better control the tumor development. A 3.2-fold higher percentage of tumor growth was found in pOVA-treated mice with respect to Man_{58}-*b*-Agm_{45}/pOVA ones. Interestingly, the anticancer effect is attributable to the efficient delivery of the pDNA encoding ovalbumin, as demonstrated either by the null effect of pEGFP-loaded polyplexes (negative control) or by the failing of Man_{58}-*b*-Agm_{45}/pOVA in B16-F1 tumor growth control (data not shown).

Since the results regarding the percentage of tumor growth were not as striking as expected, we investigated the immunological features and the specific activation against ovalbumin of tumor-infiltrating and splenic T cells.

The immunological analysis performed on tumors (Figure 48, panel b) and spleens (Figure 48, panel c) collected after mice euthanasia were in agreement with previous findings. Indeed, T-cell activation against SIINFEKL antigenic peptide was checked on tumor infiltrating T cells by flow cytometry and on splenic T cells by ELISpot analysis. Particularly, both $CD8^+$ and $CD4^+$ T cells were found to infiltrate more the tumors of B16-OVA mice treated with Man_{58}-*b*-Agm_{45}/pOVA in comparison to all the other treatments. Furthermore, $CD8^+$ cells on that group was found to efficiently recognize SIINFEKL-MHC I complex, thus being statistically more prone to be activated against that antigenic epitope and to trigger a cell-mediated immune response against ovalbumin (2.43% of SIINFEKL-MHC I positive T-cells for Man_{58}-*b*-Agm_{45}/pOVA, respect to 0.66% and 0.3% of SIINFEKL reactive T-cells for pOVA and Man_{58}-*b*-Agm_{45}/pEGFP treatment conditions). Regarding splenic T cells, their IFN-γ production after stimulation with SIINFEKL peptide was evaluated; MHC-I restricted gp100 antigenic peptide was used to evaluate T cells unspecific activation. In agreement with all the previously reported results, splenic T-cells of Man_{58}-*b*-Agm_{45}/pOVA treated mice were found to produce 10-fold higher amount of IFN-γ than the other treatment groups after stimulation with the MHC-I restricted ovalbumin antigenic peptide.

As expected, B16-F1 tumors were found to have low T-cells infiltration in all the treatment groups and splenic T-cells were found to not be activated after stimulation with SIINFEKL peptide (data not shown).

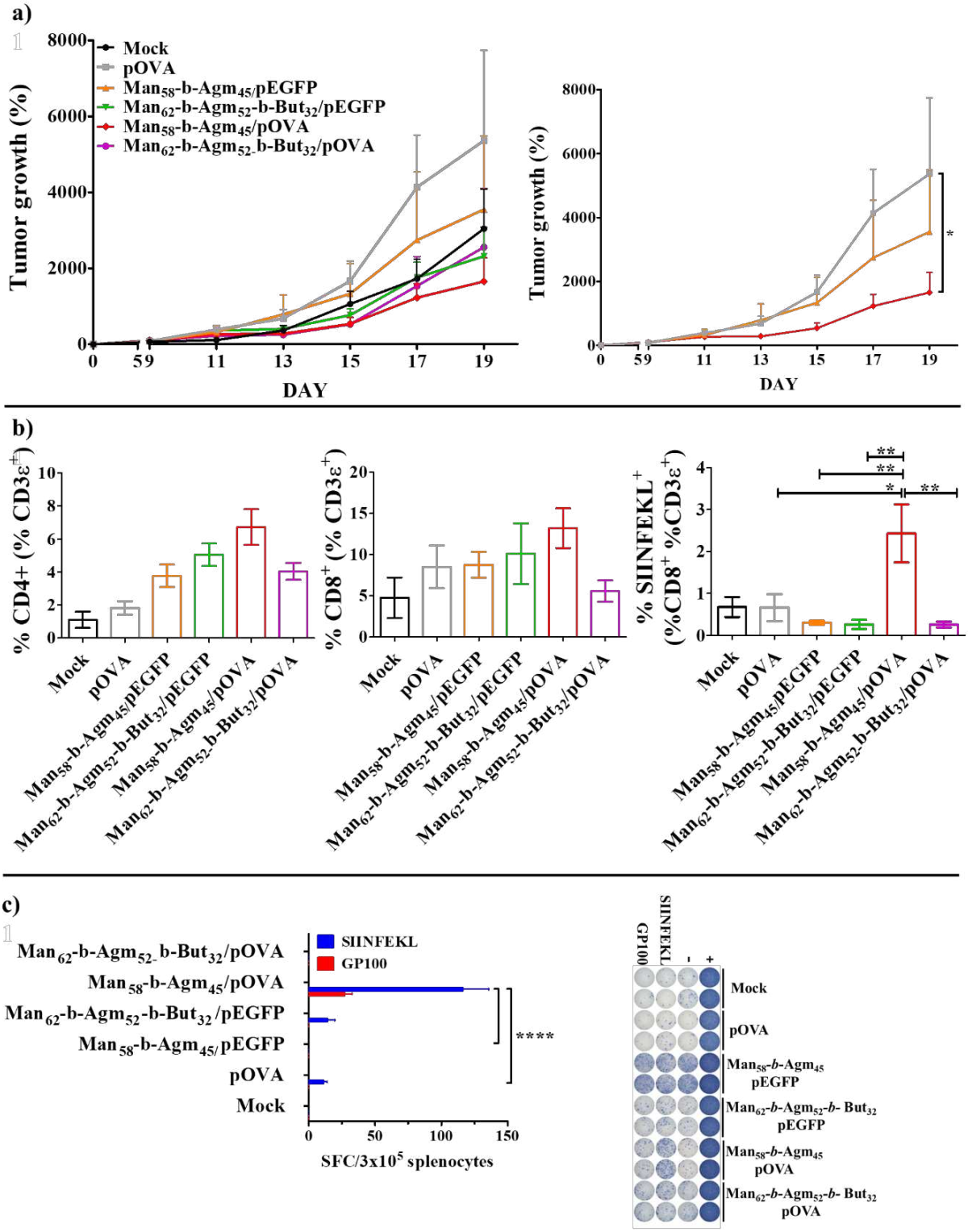

Figure 48. *In vivo antitumor therapeutic efficacy of PBS (-), pOVA (-), Man_{58}-b-Agm_{45}/pEGFP (-), Man_{62}-b-Agm_{52}-b-But_{32}/pEGFP (-), Man_{58}-b-Agm_{45}/pOVA (-) and Man_{62}-b-Agm_{52}-b-But_{32}/pOVA (-). a) The percentage of tumor growth after subcutaneous or peritumoral injection of the treatments is reported in the left panel for all the formulations. A zoom in on the effective treatment Man_{58}-b-Agm_{45}/pOVA is reported on the right panel. b) Immunological analysis of T-cells population in the tumor mass. T-cells were analyzed for their expression of $CD8^+$ or $CD4^+$ molecules on the surface and for their ability to specifically recognize SIINFEKL bound to the MHC I molecule. c) IFN-γ*

*production by splenic T-cells after their stimulation with SIINFEKL (blue bars) or gp100 (red bars) peptides and original picture of the ELISpot plate. Results are reported as mean ± SEM (a) or mean ± SD (n = 4, *p < 0.05, **p < 0.01, ***p < 0.001, ****p < 0.0001).*

The immunological results showed that the T cells are efficiently and selectively activated against ovalbumin by the Man_{58}-b-Agm_{45}/pOVA treatment. However, the therapeutic outcome is a result of the efficient infiltration of the immune cells in the tumor mass and in the cancer cells distant from the blood vessels and of the immunogenicity of the specific treated tumor. Indeed, B16 melanoma model has classically been described as a low-immunogenic tumor, thus it is useful to keep in mind that a therapeutic regimen that is effective in other tumor models may not work for B16 melanoma model.[110] It is conceivable that the therapeutic treatment with nanocarriers loaded with TAAs-encoding pDNA has to be combined with other synergistic therapies, such as immune checkpoint inhibitors, to support effector T-cells stimulation and an efficient therapeutic outcome, i.e. melanoma tumor eradication.

CONCLUSION

Triggering immune cells response and long-term memory against tumor through the active delivery of pDNA-encoding TAAs to antigen presenting cells (APCs) have emerged as a new powerful tool in cancer treatment. Indeed, the tumor-specific immune response is associated to the activation of APCs, which initiate $CD4^+$ and $CD8^+$ T cell response by capturing, endocytosing and processing delivered mRNA or pDNA encoding tumor-associated antigens. Since nucleic acids are negatively charged biomacromolecules, their ability to enter into cells is very low. Several strategies have been adopted by researchers to efficiently deliver genetic material into cells and to elicit their therapeutic effects, ranging from the use of viral vector to lipid-based or polymer-based carriers.

In this work, we successfully synthesized and extensively characterized AB di-block and ABC tri-block cationic glycopolymers. Co-polymers with the general formula Man_x-*b*-Agm_y (1^{st} generation) or Man_x-*b*-Agm_y-*b*-But_z (2^{nd} generation) were obtained by a multi-step one-pot synthesis using the RAFT polymerization technique. Polymers were designed starting from vinyl-based mannose, agmatine and butyl monomers and maintaining the same monomer feed ratio but increasing the final degree of polymerization. These novel materials were able to efficiently complex either a model 19 bases oligonucleotide or pDNA, as confirmed by gel retardation assays. Particularly, the optimum N/P ratio to achieve complete complexation was found to be lower in the case of pDNA polyplexes, even if in the competitive displacement assay polymers showed to retain better ssDNA than pDNA at a certain heparin concentration. Spherical and stable particles in the dimension range 25-55 nm were detected by DLS and TEM for ssDNA-loaded polyplexes, while pDNA-loaded GPPs resulted in rod- and toroidal- shaped complexes with a size in the range 100-1000 nm.

Cell viability assay showed that polyplexes were devoid of cytotoxicity, resulting in a high biocompatibility. Although the *in vitro* encouraging data on the safety of these new materials, more detailed information on the nanotoxicology of these delivery systems will be investigated to better understand the hemolytic effect of the 2^{nd} generation polymers.

Flow cytometry studies with Cy3-ssDNA on CHO and CHO-MR^+ cells confirmed glycopolyplexes selectivity for mannose receptor-expressing cells, particularly for Man_{15}-*b*-

Agm_{12}/ssDNA and Man_{29}-*b*-Agm_{25}/ssDNA, confirming the relevant potential of mannose as targeting agent to the selective delivery to dendritic cells. It is worth to note that the addition of the hydrophobic block on 2nd generation polymers caused a decrease in the selectivity for CHO-MR^+ cells. Furthermore, Man_{29}-*b*-Agm_{29}-*b*-But_9/pEGFP, Man_{62}-*b*-Agm_{52}-*b*-But_{32}/pEGFP and Man_{58}-*b*-Agm_{45}/pEGFP complexes were found to be the best performing *in vitro* for transfection both on CHO-MR^+ model cell line and on immortalized dendritic cells, although a decrease in the selectivity for MR-expressing cells was observed for polymers endowed with the butyl-based block. These high transfecting materials were complexed with ovalbumin-encoding plasmid (pOVA) to further investigate their ability to induce an *in vitro* immune response against ovalbumin. In particular, Man_{58}-*b*-Agm_{45}/pOVA and Man_{62}-*b*-Agm_{52}-*b*-But_{32}/pOVA treatments efficiently stimulated the expression on DCs of the costimulatory clusters of differentiation CD86 and the presentation of the SIINFEKL ovalbumin antigenic epitope by MHC I complex. Finally, Man_{58}-*b*-Agm_{45}/pOVA was confirmed as the more promising candidate for cancer vaccine development, since it was able to control the tumor growth or reduce the tumor volume in prophylactic and therapeutic *in vivo* mice vaccination, and to efficiently induce the priming and the T cells specific activation against SIINFEKL antigenic peptide. The evidence showed that, despite glycopolyplexes based on Man_{62}-*b*-Agm_{52}-*b*-But_{32} may have better performances *in vitro* as a result of their endosomal escape efficiency, their *in vivo* therapeutic outcome may be quenched by the lack of specificity for MR-expressing cells and by the subsequent internalization by cells that are not competent in immune system and T-cells activation.

Ongoing studies will elucidate the uptake and endosomal escape mechanisms of glycopolyplexes through confocal microscopy investigations. Thus, new findings at the molecular mechanistic level will help to design new 2nd generation polymers by tuning monomer units of each block in order to maintain their high transfection efficiency and reestablish the mannose receptor selectivity which was possessed by the 1st generation polymers.

REFERENCES

1. Hanagata, N. Structure-dependent immunostimulatory effect of CpG oligodeoxynucleotides and their delivery system. *International journal of nanomedicine* **7**, 2181 (2012).
2. Khan, K.H. DNA vaccines: roles against diseases. *Germs* **3**, 26 (2013).
3. Moad, G., Rizzardo, E. & Thang, S.H. Radical addition–fragmentation chemistry in polymer synthesis. *Polymer* **49**, 1079-1131 (2008).
4. Keler, T., Ramakrishna, V. & Fanger, M.W. Mannose receptor-targeted vaccines. *Expert opinion on biological therapy* **4**, 1953-1962 (2004).
5. Ragelle, H., Danhier, F., Préat, V., Langer, R. & Anderson, D.G. Nanoparticle-based drug delivery systems: a commercial and regulatory outlook as the field matures. *Expert Opinion on Drug Delivery* **14**, 851-864 (2017).
6. Li, Z., Tan, S., Li, S., Shen, Q. & Wang, K. Cancer drug delivery in the nano era: An overview and perspectives. *Oncology reports* **38**, 611-624 (2017).
7. Hanahan, D. & Weinberg, R.A. The hallmarks of cancer. *cell* **100**, 57-70 (2000).
8. Hanahan, D. & Weinberg, R.A. Hallmarks of cancer: the next generation. *cell* **144**, 646-674 (2011).
9. Chen, D.S. & Mellman, I. Oncology meets immunology: the cancer-immunity cycle. *Immunity* **39**, 1-10 (2013).
10. Moura, L.I.*, et al.* Functionalized Branched Polymers: Promising Immunomodulatory Tools for the Treatment of Cancer and Immune Disorders. *Materials Horizons* (2019).
11. Vanneman, M. & Dranoff, G. Combining immunotherapy and targeted therapies in cancer treatment. *Nature reviews cancer* **12**, 237 (2012).
12. Barenholz, Y.C. Doxil®—the first FDA-approved nano-drug: lessons learned. *Journal of controlled release* **160**, 117-134 (2012).
13. Autio, K.A.*, et al.* Safety and efficacy of BIND-014, a docetaxel nanoparticle targeting prostate-specific membrane antigen for patients with metastatic castration-resistant prostate cancer: a phase 2 clinical trial. *JAMA oncology* **4**, 1344-1351 (2018).
14. Couzin-Frankel, J. Cancer immunotherapy. (American Association for the Advancement of Science, 2013).
15. Coley, W.B. The treatment of inoperable sarcoma by bacterial toxins (the mixed toxins of the Streptococcus erysipelas and the Bacillus prodigiosus). *Proceedings of the Royal Society of Medicine* **3**, 1-48 (1910).
16. Khalil, D.N., Smith, E.L., Brentjens, R.J. & Wolchok, J.D. The future of cancer treatment: immunomodulation, CARs and combination immunotherapy. *Nature reviews Clinical oncology* **13**, 273 (2016).
17. Cheung, A.S. & Mooney, D.J. Engineered materials for cancer immunotherapy. *Nano today* **10**, 511-531 (2015).
18. Park, J.A. & Cheung, N.-K.V. Limitations and opportunities for immune checkpoint inhibitors in pediatric malignancies. *Cancer treatment reviews* **58**, 22-33 (2017).
19. Finn, O.J. Cancer vaccines: between the idea and the reality. *Nature Reviews Immunology* **3**, 630 (2003).
20. Pardoll, D.M. Cancer vaccines. *Nature medicine* **4**, 525 (1998).

21. Butterfield, L.H. Cancer vaccines. *Bmj* **350**, h988 (2015).
22. Kantoff, P.W.*, et al.* Sipuleucel-T immunotherapy for castration-resistant prostate cancer. *New England Journal of Medicine* **363**, 411-422 (2010).
23. Banchereau, J. & Palucka, K. Immunotherapy: Cancer vaccines on the move. *Nature reviews Clinical oncology* **15**, 9 (2018).
24. Sahin, U.*, et al.* Personalized RNA mutanome vaccines mobilize poly-specific therapeutic immunity against cancer. *Nature* **547**, 222 (2017).
25. Mitomo, K.*, et al.* Toward gene therapy for cystic fibrosis using a lentivirus pseudotyped with Sendai virus envelopes. *Molecular Therapy* **18**, 1173-1182 (2010).
26. Lozier, J. Gene therapy of the hemophilias. in *Seminars in hematology*, Vol. 41 287-296 (Elsevier, 2004).
27. Dellorusso, C.*, et al.* Functional correction of adult mdx mouse muscle using gutted adenoviral vectors expressing full-length dystrophin. *Proceedings of the National Academy of Sciences* **99**, 12979-12984 (2002).
28. Cavazzana-Calvo, M.*, et al.* Gene therapy of human severe combined immunodeficiency (SCID)-X1 disease. *Science* **288**, 669-672 (2000).
29. Ginn, S.L., Amaya, A.K., Alexander, I.E., Edelstein, M. & Abedi, M.R. Gene therapy clinical trials worldwide to 2017: An update. *The journal of gene medicine* **20**, e3015 (2018).
30. Pezzoli, D. & Candiani, G. Non-viral gene delivery strategies for gene therapy: a "ménage à trois" among nucleic acids, materials, and the biological environment. *Journal of nanoparticle research* **15**, 1523 (2013).
31. Weide, B., Garbe, C., Rammensee, H.-G. & Pascolo, S. Plasmid DNA-and messenger RNA-based anti-cancer vaccination. *Immunology letters* **115**, 33-42 (2008).
32. Stewart, M.P.*, et al.* In vitro and ex vivo strategies for intracellular delivery. *Nature* **538**, 183 (2016).
33. James, E.N., Ulery, B.D. & Nair, L.S. Biomaterials for Therapeutic Gene Delivery. *Biomaterials Science: Processing, Properties and Applications II: Ceramic Transactions* **237**, 191-211 (2012).
34. Bao, S., Thrall, B.D. & Miller, D.L. Transfection of a reporter plasmid into cultured cells by sonoporation in vitro. *Ultrasound in medicine & biology* **23**, 953-959 (1997).
35. Lehrman, S. Virus treatment questioned after gene therapy death. (Nature Publishing Group, 1999).
36. Islam, M.A.*, et al.* Biomaterials for mRNA delivery. *Biomaterials science* **3**, 1519-1533 (2015).
37. Jorritsma, S., Gowans, E., Grubor-Bauk, B. & Wijesundara, D. Delivery methods to increase cellular uptake and immunogenicity of DNA vaccines. *Vaccine* **34**, 5488-5494 (2016).
38. Xu, Y. & Szoka, F.C. Mechanism of DNA release from cationic liposome/DNA complexes used in cell transfection. *Biochemistry* **35**, 5616-5623 (1996).
39. Zuhorn, I.S.*, et al.* Nonbilayer phase of lipoplex–membrane mixture determines endosomal escape of genetic cargo and transfection efficiency. *Molecular therapy* **11**, 801-810 (2005).
40. Cornelis, S., Vandenbranden, M., Ruysschaert, J.-M. & Elouahabi, A. Role of intracellular cationic liposome–DNA complex dissociation in transfection mediated by cationic lipids. *DNA and cell biology* **21**, 91-97 (2002).
41. Hassett, K.J.*, et al.* Optimization of lipid nanoparticles for intramuscular administration of mrna vaccines. *Molecular Therapy-Nucleic Acids* **15**, 1-11 (2019).

42. Hattori, Y., Kawakami, S., Nakamura, K., Yamashita, F. & Hashida, M. Efficient gene transfer into macrophages and dendritic cells by in vivo gene delivery with mannosylated lipoplex via the intraperitoneal route. *Journal of Pharmacology and Experimental Therapeutics* **318**, 828-834 (2006).
43. De Smedt, S.C., Demeester, J. & Hennink, W.E. Cationic polymer based gene delivery systems. *Pharmaceutical research* **17**, 113-126 (2000).
44. Farber, F.E., Melnick, J.L. & Butel, J.S. Optimal conditions for uptake of exogenous DNA by Chinese hamster lung cells deficient in hypoxanthine-guanine phosphoribosyltransferase. *Biochimica et Biophysica Acta (BBA)-Nucleic Acids and Protein Synthesis* **390**, 298-311 (1975).
45. Wu, G.Y. & Wu, C.H. Receptor-mediated in vitro gene transformation by a soluble DNA carrier system. *Journal of Biological Chemistry* **262**, 4429-4432 (1987).
46. Tietz, P.S., Yamazaki, K. & Larusso, N.F. Time-dependent effects of chloroquine on pH of hepatocyte lysosomes. *Biochemical pharmacology* **40**, 1419-1421 (1990).
47. Itaka, K.*, et al.* In situ single cell observation by fluorescence resonance energy transfer reveals fast intra-cytoplasmic delivery and easy release of plasmid DNA complexed with linear polyethylenimine. *The Journal of Gene Medicine: A cross-disciplinary journal for research on the science of gene transfer and its clinical applications* **6**, 76-84 (2004).
48. Thomas, M. & Klibanov, A.M. Enhancing polyethylenimine's delivery of plasmid DNA into mammalian cells. *Proceedings of the National Academy of Sciences* **99**, 14640-14645 (2002).
49. Ogris, M., Brunner, S., Schüller, S., Kircheis, R. & Wagner, E. PEGylated DNA/transferrin–PEI complexes: reduced interaction with blood components, extended circulation in blood and potential for systemic gene delivery. *Gene therapy* **6**, 595 (1999).
50. Lee, C.C., MacKay, J.A., Fréchet, J.M. & Szoka, F.C. Designing dendrimers for biological applications. *Nature biotechnology* **23**, 1517 (2005).
51. Pack, D.W., Hoffman, A.S., Pun, S. & Stayton, P.S. Design and development of polymers for gene delivery. *Nature reviews Drug discovery* **4**, 581 (2005).
52. Borchard, G. Chitosans for gene delivery. *Advanced drug delivery reviews* **52**, 145-150 (2001).
53. Forrest, M.L., Koerber, J.T. & Pack, D.W. A degradable polyethylenimine derivative with low toxicity for highly efficient gene delivery. *Bioconjugate chemistry* **14**, 934-940 (2003).
54. Gosselin, M.A., Guo, W. & Lee, R.J. Efficient gene transfer using reversibly cross-linked low molecular weight polyethylenimine. *Bioconjugate chemistry* **12**, 989-994 (2001).
55. Zhou, X.*, et al.* Controlled release of PEI/DNA complexes from mannose-bearing chitosan microspheres as a potent delivery system to enhance immune response to HBV DNA vaccine. *Journal of Controlled Release* **121**, 200-207 (2007).
56. He, C., Hu, Y., Yin, L., Tang, C. & Yin, C. Effects of particle size and surface charge on cellular uptake and biodistribution of polymeric nanoparticles. *Biomaterials* **31**, 3657-3666 (2010).
57. Khalil, I.A., Kogure, K., Akita, H. & Harashima, H. Uptake pathways and subsequent intracellular trafficking in nonviral gene delivery. *Pharmacological reviews* **58**, 32-45 (2006).

58. Bettinger, T., Remy, J.-S. & Erbacher, P. Size reduction of galactosylated PEI/DNA complexes improves lectin-mediated gene transfer into hepatocytes. *Bioconjugate chemistry* **10**, 558-561 (1999).
59. Zatloukal, K.*, et al.* Transferrinfection. A Highly Efficient Way to Express Gene Constructs in Eukaryotic Cells. *Annals of the New York Academy of Sciences*, 136-153 (1992).
60. Akinc, A., Thomas, M., Klibanov, A.M. & Langer, R. Exploring polyethylenimine-mediated DNA transfection and the proton sponge hypothesis. *The Journal of Gene Medicine: A cross-disciplinary journal for research on the science of gene transfer and its clinical applications* **7**, 657-663 (2005).
61. Li, W., Nicol, F. & Szoka Jr, F.C. GALA: a designed synthetic pH-responsive amphipathic peptide with applications in drug and gene delivery. *Advanced drug delivery reviews* **56**, 967-985 (2004).
62. Bremner, K.H., Seymour, L.W., Logan, A. & Read, M.L. Factors influencing the ability of nuclear localization sequence peptides to enhance nonviral gene delivery. *Bioconjugate chemistry* **15**, 152-161 (2004).
63. Wong, S.Y., Pelet, J.M. & Putnam, D. Polymer systems for gene delivery—past, present, and future. *Progress in Polymer Science* **32**, 799-837 (2007).
64. Sève, A.-P.*, et al.* Analysis of sugar-binding sites in mammalian cell nuclei by quantitative flow microfluorometry. *Proceedings of the National Academy of Sciences* **83**, 5997-6001 (1986).
65. Roche, A.*, et al.* Glycofection: facilitated gene transfer by cationic glycopolymers. *Cellular and Molecular Life Sciences CMLS* **60**, 288-297 (2003).
66. Kim, T.-i., Ou, M., Lee, M. & Kim, S.W. Arginine-grafted bioreducible poly (disulfide amine) for gene delivery systems. *Biomaterials* **30**, 658-664 (2009).
67. Huang, K., Voss, B., Kumar, D., Hamm, H.E. & Harth, E. Dendritic molecular transporters provide control of delivery to intracellular compartments. *Bioconjugate chemistry* **18**, 403-409 (2007).
68. Stahl, P.D. & Ezekowitz, R.A.B. The mannose receptor is a pattern recognition receptor involved in host defense. *Current opinion in immunology* **10**, 50-55 (1998).
69. Boskovic, J.*, et al.* Structural model for the mannose receptor family uncovered by electron microscopy of Endo180 and the mannose receptor. *Journal of Biological Chemistry* **281**, 8780-8787 (2006).
70. Martinez-Pomares, L. The homeostatic properties of the mannose receptor in health and disease. *Inmunología* **27**, 132-140 (2008).
71. Gody, G., Maschmeyer, T., Zetterlund, P.B. & Perrier, S.b. Pushing the limit of the RAFT process: multiblock copolymers by one-pot rapid multiple chain extensions at full monomer conversion. *Macromolecules* **47**, 3451-3460 (2014).
72. Chiefari, J.*, et al.* Living free-radical polymerization by reversible addition− fragmentation chain transfer: the RAFT process. *Macromolecules* **31**, 5559-5562 (1998).
73. Moad, G., Rizzardo, E. & Thang, S.H. Living radical polymerization by the RAFT process. *Australian journal of chemistry* **58**, 379-410 (2005).
74. Gody, G., Maschmeyer, T., Zetterlund, P.B. & Perrier, S. Rapid and quantitative one-pot synthesis of sequence-controlled polymers by radical polymerization. *Nature communications* **4**, 2505 (2013).
75. Sandler, S.R., Karo, W., Bonesteel, J. & Pearce, E.M. *Polymer synthesis and characterization: a laboratory manual*, (Elsevier, 1998).

76. Truong, N.P., Dussert, M.V., Whittaker, M.R., Quinn, J.F. & Davis, T.P. Rapid synthesis of ultrahigh molecular weight and low polydispersity polystyrene diblock copolymers by RAFT-mediated emulsion polymerization. *Polymer Chemistry* **6**, 3865-3874 (2015).
77. Obata, M.*, et al.* Synthesis, characterization and cellular internalization of poly(2-hydroxyethyl methacrylate) bearing α-d-mannopyranose. *Polymer Chemistry* **2**, 651-658 (2011).
78. Mattias Algotsson, P.B., Nicolas Thevenin. Method for synthesis of acrylamide derivatives. in *United States Patent*, Vol. US 7,294,743 B2 4 (GE Healthcare Bio-Sciences AB, United States, 2007).
79. Evans, B.C.*, et al.* Ex vivo red blood cell hemolysis assay for the evaluation of pH-responsive endosomolytic agents for cytosolic delivery of biomacromolecular drugs. *JoVE (Journal of Visualized Experiments)*, e50166 (2013).
80. Mosmann, T. Rapid colorimetric assay for cellular growth and survival: application to proliferation and cytotoxicity assays. *Journal of immunological methods* **65**, 55-63 (1983).
81. Ghadban, A., Reynaud, E., Rinaudo, M. & Albertin, L. RAFT copolymerization of alginate-derived macromonomers–synthesis of a well-defined poly (HEMAm)-graft-(1→ 4)-α-l-guluronan copolymer capable of ionotropic gelation. *Polymer Chemistry* **4**, 4578-4583 (2013).
82. Lächelt, U. & Wagner, E. Nucleic acid therapeutics using polyplexes: a journey of 50 years (and beyond). *Chemical reviews* **115**, 11043-11078 (2015).
83. Pissuwan, D., Boyer, C., Gunasekaran, K., Davis, T.P. & Bulmus, V. In vitro cytotoxicity of RAFT polymers. *Biomacromolecules* **11**, 412-420 (2010).
84. Espuelas, S., Thumann, C., Heurtault, B., Schuber, F. & Frisch, B. Influence of ligand valency on the targeting of immature human dendritic cells by mannosylated liposomes. *Bioconjugate chemistry* **19**, 2385-2393 (2008).
85. Raviv, L., Jaron-Mendelson, M. & David, A. Mannosylated polyion complexes for in vivo gene delivery into CD11c+ dendritic cells. *Molecular pharmaceutics* **12**, 453-462 (2015).
86. Valdebenito, A. & Encinas, M.V. Effect of solvent on the free radical polymerization of N, N-dimethylacrylamide. *Polymer International* **59**, 1246-1251 (2010).
87. Jiang, X.*, et al.* Molar-mass characterization of cationic polymers for gene delivery by aqueous size-exclusion chromatography. *Pharmaceutical research* **23**, 595-603 (2006).
88. Blakney, A.K., Yilmaz, G., McKay, P.F., Becer, C.R. & Shattock, R.J. One size does not fit all: The effect of chain length and charge density of poly (ethylene imine) based copolymers on delivery of pDNA, mRNA, and RepRNA polyplexes. *Biomacromolecules* **19**, 2870-2879 (2018).
89. Engelberg, H. & Dudley, A. Plasma heparin levels in normal man. *Circulation* **23**, 578-581 (1961).
90. Manolova, V.*, et al.* Nanoparticles target distinct dendritic cell populations according to their size. *European journal of immunology* **38**, 1404-1413 (2008).
91. Golan, R., Pietrasanta, L.I., Hsieh, W. & Hansma, H.G. DNA toroids: stages in condensation. *Biochemistry* **38**, 14069-14076 (1999).
92. Osada, K. Versatile DNA folding structures organized by cationic block copolymers. *Polymer Journal*, 1 (2019).

93. Kwoh, D.Y.*, et al.* Stabilization of poly-L-lysine/DNA polyplexes for in vivo gene delivery to the liver. *Biochimica et Biophysica Acta (BBA)-Gene Structure and Expression* **1444**, 171-190 (1999).
94. Li, Y.*, et al.* Toroidal packaging of pDNA into block ionomer micelles exerting promoted in vivo gene expression. *Biomacromolecules* **16**, 2664-2671 (2015).
95. Filice, M. & Ruiz-Cabello, J. *Nucleic Acid Nanotheranostics: Biomedical Applications*, (Elsevier, 2019).
96. Funhoff, A.M.*, et al.* Endosomal escape of polymeric gene delivery complexes is not always enhanced by polymers buffering at low pH. *Biomacromolecules* **5**, 32-39 (2004).
97. Adolph, E.J.*, et al.* Enhanced performance of plasmid DNA polyplexes stabilized by a combination of core hydrophobicity and surface PEGylation. *Journal of Materials Chemistry B* **2**, 8154-8164 (2014).
98. Behzadi, S.*, et al.* Cellular uptake of nanoparticles: journey inside the cell. *Chemical Society Reviews* **46**, 4218-4244 (2017).
99. Biessen, E.A.*, et al.* Lysine-based cluster mannosides that inhibit ligand binding to the human mannose receptor at nanomolar concentration. *Journal of Biological Chemistry* **271**, 28024-28030 (1996).
100. Martens, T.F., Remaut, K., Demeester, J., De Smedt, S.C. & Braeckmans, K. Intracellular delivery of nanomaterials: how to catch endosomal escape in the act. *Nano Today* **9**, 344-364 (2014).
101. Karpova, T.*, et al.* Fluorescence resonance energy transfer from cyan to yellow fluorescent protein detected by acceptor photobleaching using confocal microscopy and a single laser. *Journal of microscopy* **209**, 56-70 (2003).
102. Osada, K.*, et al.* Quantized folding of plasmid DNA condensed with block catiomer into characteristic rod structures promoting transgene efficacy. *Journal of the American Chemical Society* **132**, 12343-12348 (2010).
103. Irvine, A.S.*, et al.* Efficient nonviral transfection of dendritic cells and their use for in vivo immunization. *Nature biotechnology* **18**, 1273 (2000).
104. Awasthi, S. & Cox, R.A. Transfection of murine dendritic cell line (JAWS II) by a nonviral transfection reagent. *Biotechniques* **35**, 600-604 (2003).
105. Alegre, M.-L., Frauwirth, K.A. & Thompson, C.B. T-cell regulation by CD28 and CTLA-4. *Nature Reviews Immunology* **1**, 220 (2001).
106. Chen, J.*, et al.* Charge-conversional zwitterionic copolymer as pH-sensitive shielding system for effective tumor treatment. *Acta biomaterialia* **26**, 45-53 (2015).
107. Kasturi, S.P.*, et al.* Prophylactic anti-tumor effects in a B cell lymphoma model with DNA vaccines delivered on polyethylenimine (PEI) functionalized PLGA microparticles. *Journal of Controlled Release* **113**, 261-270 (2006).
108. Ma, Y.-F. & Yang, Y.-W. Delivery of DNA-based cancer vaccine with polyethylenimine. *European Journal of Pharmaceutical Sciences* **40**, 75-83 (2010).
109. Velluto, D., Thomas, S.N., Simeoni, E., Swartz, M.A. & Hubbell, J.A. PEG-b-PPS-b-PEI micelles and PEG-b-PPS/PEG-b-PPS-b-PEI mixed micelles as non-viral vectors for plasmid DNA: tumor immunotoxicity in B16F10 melanoma. *Biomaterials* **32**, 9839-9847 (2011).
110. Overwijk, W.W. & Restifo, N.P. B16 as a mouse model for human melanoma. *Current protocols in immunology* **39**, 20.21. 21-20.21. 29 (2000).